Jül-4270

Institut für Neurowissenschaften und Biophysik (INB)
Zelluläre Biophysik (INB-1)

Structural and functional studies of a prokaryotic cyclic nucleotide-gated channel

Abhishek Cukkemane

Mitglied der Helmholtz-Gemeinschaft

JÜLICH
FORSCHUNGSZENTRUM

Structural and functional studies of a prokaryotic cyclic nucleotide-gated channel

Abhishek Cukkemane

Berichte des Forschungszentrums Jülich ; 4270
ISSN 0944-2952
Institut für Neurowissenschaften und Biophysik (INB)
Zelluläre Biophysik (INB-1) Jül-4270
D 38 (Diss., Köln, Univ., 2007)

Zu beziehen durch: Forschungszentrum Jülich GmbH · Zentralbibliothek, Verlag
D-52425 Jülich · Bundesrepublik Deutschland
☎ 02461 61-5220 · Telefax: 02461 61-6103 · E-Mail: zb-publikation@fz-juelich.de

Zusammenfassung

Zyklisch Nukleotid-gesteuerte Ionenkanäle spielen eine entscheidende Rolle in kardialer und neuronaler Erregbarkeit sowie in der Signaltransduktion primärer Sinneszellen. Die direkte Bindung zyklischer Nukleotide aktiviert die Kanäle und führt zu einer erhöhten Membranleitfähigkeit der Zelle. Obwohl viel über die Funktion dieser Ionenkanäle bekannt ist, sind die molekularen Ereignisse, die von der Ligandenbindung zur Kanalöffnung führen, weitgehend unbekannt.

Ich habe mich in meiner Arbeit mit der Ligandenbindung prokaryotischer zyklisch Nukleotid-gesteuerter Ionenkanäle beschäftigt. Einer dieser Ionenkanäle, der zyklisch Nukleotid-gesteuerte Ionenkanal des stickstofffixierenden Bakteriums *Mesorhizobium loti* (mlCNG), eignete sich besonders gut für biophysikalische Untersuchungen. Eine der Hauptfragestellungen, an denen ich arbeitete, war, in welcher Weise sich das Schaltverhalten des Ionenkanals auf die Ligandenbindung auswirkt. Ich habe Bindungsstudien sowohl an dem tetrameren mlCNG-Kanal als auch an der isolierten ligandenbindenden Domäne (CNBD) durchgeführt. Die Affinität der zyklischen Nukleotide zum mlCNG-Kanal sowie zur CNBD wurde mit spektroskopischen Methoden bestimmt. Beide Proteine, der tetramere Ionenkanal und die isolierte CNBD binden cAMP nicht-kooperativ mit sehr ähnlicher Affinität. Diese Ergebnisse deuten an, dass entweder nur ein sehr geringer Teil der Bindungsenergie für die Aktivierung benötigt wird, oder aber, dass die Konformationsänderungen, die innerhalb der CNBD stattfinden, schon den eigentlichen Aktivierungsschritt des Ionenkanals darstellen.

Ich habe Kristallographieansätze für den mlCNG-Kanal durchgeführt. Ich konnte zweidimensionale Proteinkristalle züchten, die in einem quadratischen Gitter angeordnet waren. Die Proteine zeigten eine tetramere Symmetrie und waren antiparallel angeordnet. Der Kristall beugte zu etwa 15 Å. Dies ist eine gute Ausgangsposition für weitere Arbeiten, um schließlich die Struktur des Ionenkanals in atomarer Auflösung zu erhalten.

Abstract

Ion channels gated by cyclic nucleotides have crucial roles in cardiac and neuronal excitability and in signal transduction of sensory neurons. On binding cyclic nucleotides these channels are activated, which results an increase in membrane conductance. Although a lot of information is available on the function of these channel proteins, the molecular events that relay ligand binding to channel activation is not well understood.

Here, I studied ligand binding of prokaryotic cyclic nucleotide-activated K^+ channels. One of them, the mlCNG channel from the nitrogen-fixing bacterium *Mesorhizobium loti* was suitable for biophysical characterization. One of the key questions that I worked on was how gating of the channel affects its ligand binding properties? I performed ligand binding studies on the tetrameric mlCNG protein and its isolated cyclic nucleotide-binding domain (CNBD). Affinity of cyclic nucleotides to the full-length mlCNG protein and to the CNBD was determined using spectroscopic methods. Both, the mlCNG channel and the CNBD bind cAMP in a non-cooperative manner with similar binding affinity. These results indicate that either no appreciable binding energy is required for activation, or the conformational change in the CNBD is the activation step itself.

Crystallography experiments were performed on the mlCNG channel. Two-dimensional crystals were obtained in which the channel proteins were ordered in a square lattice. The channel proteins were assembled as tetramers and were arranged in a head-to tail fashion. The crystal diffracts to 15 Å. This is an excellent starting condition for future work to eventually obtain a structure at atomic resolution.

Contents

Abbreviations

ε	Absorption coefficient
λ	wavelength
Å	Angstrom
Amp	Ampicillin
Br-	Bromo-
°C	Degrees Celsius
BSA	bovine serum albumin
CD	circular dichroism
CaM	Calmodulin
cAMP	adenosine cyclic-3´, 5´-monophosphate
CAP c	catabolite activator protein
CHAPS	3-[(3-Cholamidopropyl)dimethylammonio]-1-propansulfonat
cGMP	guanosine cyclic-3´, 5´-monophosphate
CNBD	cyclic nucleotide-binding domain
CNG	cGMP-gated cation channel
cNMP	cyclic nucleotides
CPT-	4-Chlorophenylthio-
Da	Dalton
DDM	Dodecyl-Maltopyranoside
DM	Decyl-Maltopyranoside
DNA	deoxyribonucleic acid
DNase	deoxyribonuclease
E. coli	*Escherichia coli*
EDTA	ethylenediaminetatraacetic acid
e.g.	for example
EPAC	exchange protein directly activated by cAMP
FPLC	fast protein liquid chromatography
GF	gel filtration
GST	glutathione S-transferase
h	hours

HCN	Hyper polarization activated Cyclic Nucleotide gated Ion channel
HEPES	N-2-hydroxyethyl peperazine-N´-2-ethanesulfonic acid
His	Histidine
HMW	high molecular weight
HPLC	high-performance liquid chromatography
i.e.	that is
IPTG	isopropyl-β-D-thiogalactoside
k	Kilo-
Kav	partition coefficient of gel filtration
kDa	kilodalton
l	Litre
LB	Luria-Bertani
LDAO	***N,N*-Dimethyldodecylamine *N*-oxide**
LMW	low molecular weight
m	Metre
M	Molar
mAU	milli absorbance units
MES	2-(N-Morpholino)ethansulfonsäure
min	minute
MPD	2-methyl 2,4-Pentanediol
MS	mass spectrometry
M_W	molecular weight
NBD-	((2-((7-Nitro-4-benzofurazanyl)amino)ethyl)thio)-
OD	optical density
OGP	O-gluco pyranoside
OTGP	O-thiogluco pyranoside
PAGE	polyacrylamide gel electrophoresis
PBC	phosphate binding cassette
PBS	phosphate buffered saline
PCR	polymerase chain reaction
PEG	polyethylene glycol

pI	isoelectric point
PKA	protein kinase A
PKG	protein kinase G
PVDF	polyvinylidene difluoride
RP-HPLC	reversed phase high-performance-liquid-chromatography
s	seconds
SDS	sodium dodecylsulfate
SEC	size exclusion chromatography
Sinapinic acid	3.5-dimethoxy-4-hydroxy cinnamic acid
TE	Tris-EDTA
TFA	trifluoroacetic acid
TNB	5-thio-2-nitrobenzoic acid
Tris	Tris(hydroxymethyl)-aminomethane
UV	Ultraviolet
v/v	volume by volume
w/v	weight by volume

Abbreviation of Amino acid residues

A	Alanine	Ala
R	Arginine	Arg
N	Asparagine	Asn
D	Aspartate	Asp
C	Cysteine	Cys
E	Glutamate	Glu
Q	Glutamine	Gln
G	Glycine	Gly
H	Histidine	His
I	Isoleucine	Ile
L	Leucine	Leu
K	Lysine	Lys
M	Methionine	Met
F	Phenylalanine	Phe
P	Proline	Pro
S	Serine	Ser
T	Threonine	Thr
W	Tryptophan	Trp
Y	Tyrosine	Tyr
V	Valine	Val

1 Introduction

Relating ligand binding to channel activation: Two sides of a coin

Ion-channels that are gated by cyclic nucleotides (cNMPs) come in two flavours, the *c*yclic *n*ucleotide-*g*ated (CNG) channels and the *h*yperpolarization-activated and *c*yclic *n*ucleotide-gated (HCN) channels. Both channel types belong to the superfamily of voltage-gated ion channels. CNG channels play key roles in signal transduction of sensory neurons. HCN channels play important roles in cardiac and neuronal excitability. A common feature of the two channel types is their ability to bind cyclic nucleotides. Both channel types harbour a C-terminal cyclic nucleotide-binding domain. Two notable differences, however distinguish CNG channels from HCN channels. CNG channels require cNMP to open and show cooperativity in channel opening (Kaupp *et al* 1989) while HCN channels open on hyperpolarization and their activity is modulated by cNMP (DiFrancesco and Tortora 1991). The channel types differ with respect to their ligand selectivity and sensitivity. CNG channels select cGMP over cAMP while HCN channels show greater sensitivity for cAMP. The molecular basis that sets apart ligand affinity and selectivity are not fully understood because of binding ligand has not been directly measured but rather inferred from electrophysiological studies for both channel types. Because binding and gating events are intimately coupled, it is difficult to dissect one from the other.

Here, I studied the ligand binding of a *pro*karyotic *c*yclic *n*ucleotide-*g*ated (pro-CNG) K^+ channel from *Mesorhizobium loti* and its isolated cyclic nucleotide-binding domain (CNBD). The channel and the binding domain bind cAMP with similar affinity in a non-cooperative fashion. The cAMP sensitivities of binding and activation coincide. Thus, each subunit in the tetrameric channel acts independently. The binding and gating properties of the bacterial channel are distinctively different from those of eukaryotic CNG channels.

1.1 Cyclic nucleotide-gated (CNG) channels

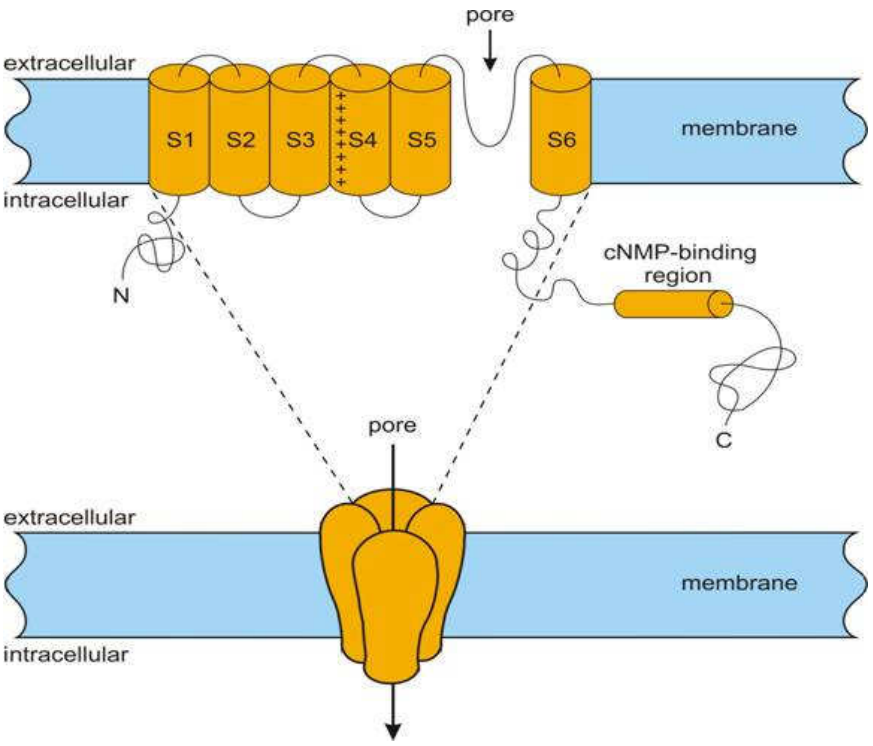

Figure 1.1: A pictorial representation of a cyclic nucleotide regulated channel. The channels embody six transmembrane segments (S1–S6).They are composed of four subunits. The channel carries a pore loop between the S5 and the S6 segment, a S4 domain carrying positive charges and a cyclic nucleotide binding-domain in the C-terminal region.

Eukaryotic CNG channels are non-selective cation channels first identified in retinal photoreceptors. CNG channels like other members of the superfamily of voltage-gated ion channels embody six transmembrane (TM) domains, named S1-S6. They are arranged in a tetrameric fashion (See Figure 1.1). CNG channels carry a C-terminal CNBD and are directly gated by cNMPs. Channel activation steeply dependent on cNMP concentration and has a Hill coefficient between 2 and 3. This suggests that at least three cNMPs molecules are required to open the channel (Kaupp *et al* 1989). CNG channels are weakly voltage sensitive, although they carry a voltage-sensor motif like their cousins from the family of voltage-gated ion channels. The voltage sensor motif, S4 (in a 6TM domain channel) is characterized by the presence of basic residues regularly interspersed between three amino acid residues. A voltage-sensor motif may carry 5-8 basic residues (Bezanilla 2000; Yellen 1998). So far, four different types of A subunits and two different types of B subunits have been identified (Kaupp and Seifert 2002). In contrast to A1, A2 and A3 subunits, the B subunits and the A4 subunit do not form functional channels when heterologously expressed alone. The stoichiometry of CNG channels was a matter of longstanding debate. Co-expression of A and B subunits results in channels with novel properties that resemble the ones observed in the

native system. It has now been shown that the native channels from photoreceptors and olfactory sensory neurons arrange in 3A and 1B stoichiometry. The rod CNG channel comprises A1:B1a in the ratio 3:1 (Weitz 2002, Figure 1.2). The olfactory CNG channel is arranged as A2:A4:B1b in the ratio 2:1:1 (Zheng and Zagotta 2004)). It is believed that a trimer forming C-terminal leucine-zipper motif found only in the A subunits is a prerequisite for the formation of a 3:1 stoichiometry (Zhong *et al* 2002).

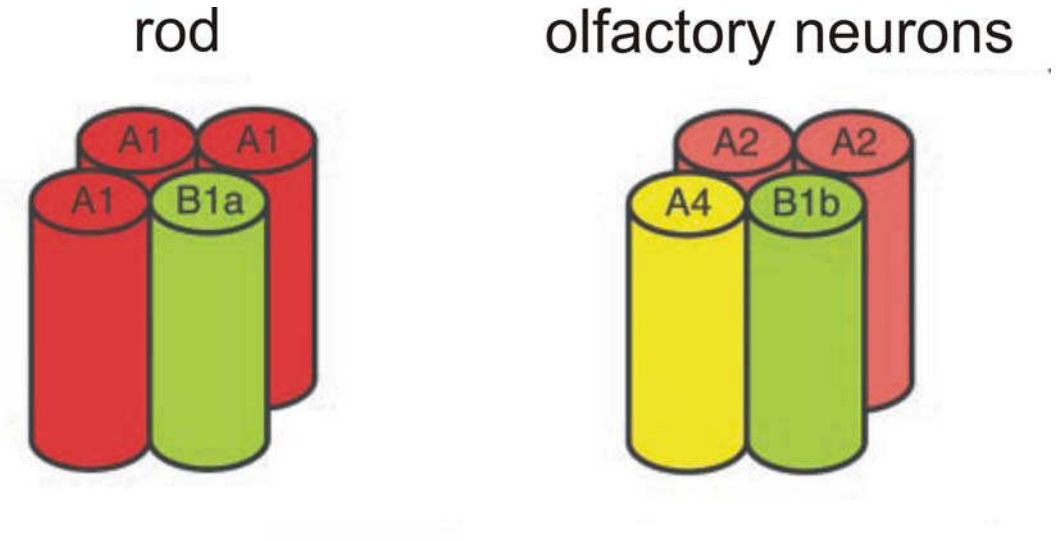

Figure 1.2: Pictorial representation of the subunit arrangement of CNG channels from rod photoreceptors (left) and olfactory sensory neurons (right). This figure is adapted from Kaupp and Seifert 2002.

1.2 Hyperpolarization-activated and cyclic nucleotide-gated (HCN) channels

Currents carried by hyper polarization-activated and cyclic nucleotide-gated (HCN) channels were first characterized in *s*ino-*a*trial *n*ode (SAN) cells, in photoreceptor cells, and in hippocampal pyramidal neurons. Currents are activated on hyperpolarization of the cell membrane. The voltage dependence of activation can be shifted towards more positive voltages by binding of cNMPs, resulting in higher channel activity (for reviews see Kaupp and Seifert 2001; Robinson and Siegelbaum 2003).

Four isoforms of HCN channels have been identified in mammals (HCN 1-4). It is commonly believed that HCN channels assemble as homotetramers (Figure 1.7). Recent evidence shows that HCN may form heterotetramers in thalamus and neocortex. HCN1 and HCN2 are found in thalamus and neocortex. Heterologous expression of HCN1 and HCN2 results in HCN channels with novel properties (Chen *et al* 2001). The resulting currents are similar to those observed in thalamus and neocortex. Similarly, heterotetramers of HCN4 and HCN2 have been proposed to form functional pacemaker channels in SAN (Whitaker *et al* 2007).

1.3 Prokaryotic CNG (Pro-CNG) channels

The prokaryotic CNG (pro-CNG) channels are the latest addition to the repertoire of cNMP binding channels. Six channel isoforms have been identified so far. The prokaryotic CNG channels have been named according to the bacterial source from which the channel gene was cloned, e.g mlCNG stands for the CNG channel cloned from *Mesorhizobium loti*. The sequence of all the six pro-CNG channels are shown in the appendix (section 6.1). These channels harbour a C-terminal CNBD and 6TM domains. All pro-CNG channels carry a pore sequence characteristic for K^+ selectivity. The first study on a prokaryotic CNG channel (mlCNG) was reported by Nimigean *et al* (2004). The channel was shown to be K^+ selective and was activated by cAMP. Recently, another channel belonging to the pro-CNG channel family (mmCNG, source *Magnetospirillum magnetotacticum*) was shown to be activated by cAMP and was a K^+ selective inward rectifier (Kuo *et al* 2007). The six bacterial channels carry 6 TM domains but none of them carry the proto-typical voltage-sensor motif. Absence of a typical voltage sensor does not rule out the possibility that the channels may be voltage sensitive. K^+-conducting channels carrying S4 domain similar to the prokaryotic CNG channel were shown to be voltage sensitive (Seoh *et al* 1996; Aggarwal and MacKinnon 1996), though to a lesser extent in comparison to the wild type Shaker K^+ channel .

None of the prokaryotic CNG channels carry large N-terminal domains and loops between transmembrane segments. Furthermore, these channels carry a very short C-linker segment (~ 20 amino acid residues). These channels offer the chance of studying binding and gating from a strucutral perspective.

1.4 Similarities and differences

The following section discusses the similarites and differences between CNG, HCN, and pro-CNG channels regarding the permeation pathway and the C-terminal region.

1.4.1 Permeation properties

CNG channels are non-selective cation channels that poorly discriminate between monovalent and divalent ions. Recently, the crystal structure of a NaK channel was solved (Shi *et al* 2006). The pore region of NaK channels is homologus to the selectivity filter of the CNG channels and both the channels may employ a similar mechanism for the passage of ions.

The non-selective cation pore of the NaK channel is arranged in a four-fold symmetry similar to the pore of the K^+-selective KcsA (Doyle *et al* 1998). However, the selectivity filter of the

NaK channel shows striking differences to the K^+-selective pore of KcsA (Figure 1.3). The extracellular region of NaK binds divalent ions. This not only leads to the passage of divalent ions like Ca^{2+} but also results in blockage by Mg^{2+}. Within the pore region only the last few residues (marked 3 and 4 in Figure 1.3 B) of the intracellular side contribute to ion binding, unlike KcsA where all the carbonyl groups (numbered 1-4 in Figure 1.3 A) of the amino acids contribute to ion binding. An interesting finding was that the structure of the pore region of NaK was virtually the same when the K^+ was replaced by Na^+ ions in the crystallization solution. Ion-omit maps calculated from the data of crystals grown in NaCl or KCl show that ions bind at the same site of the pore, i.e. Na^+ ions were observed in site 3 and 4. This feature is disticnt from a channel containing a sequence characteristic of a K^+ selective pore; in these channel Na^+ ions were never observed in analogous positions. The structure of the NaK channel pore provides insight into the binding sites of divalent and monovalent ions in the pore region of non-selective cation channels.

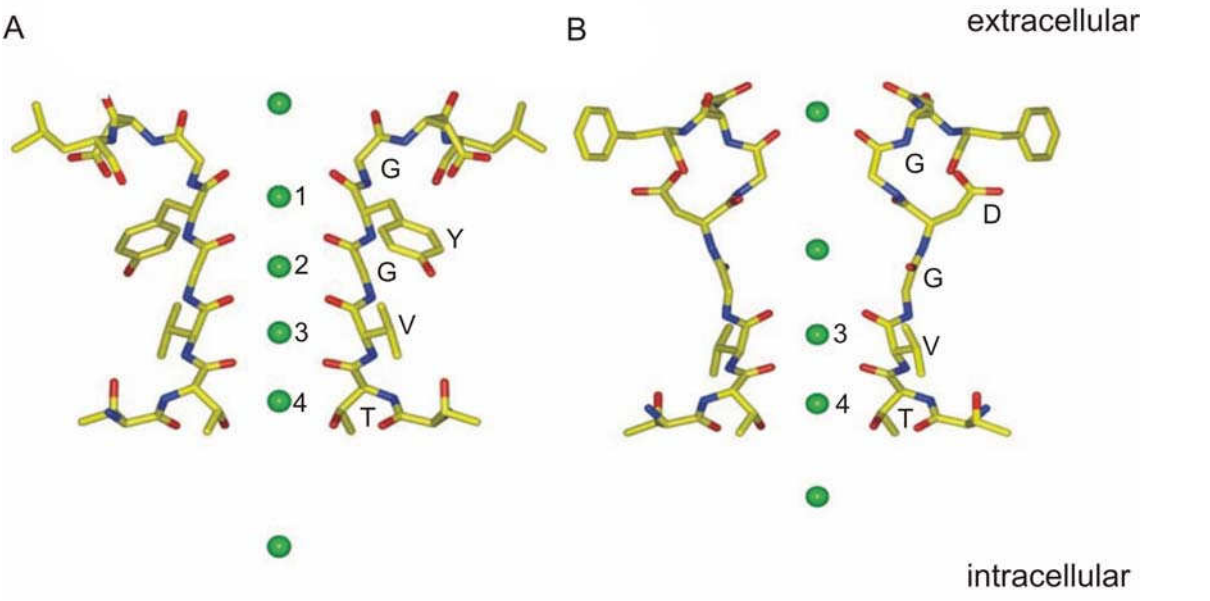

Figure 1.3: Structure of pore region of KcsA (A) and NaK (B). Ions are represented in green. The K+ binding sites in KcsA are numbered from 1-4. The analogous position in NaK have also been numbered. This figure is adapted from Shi *et al*, 2006.

HCN channels and the pro-CNG channels both carry a pore sequence characteristic of K^+ channel (G Y/F G, Heginbotham et al 1992). While two of the pro-CNG channels have been shown to be exclusively K^+-selective (Nimigean *et al* 2004; Kuo *et al* 2007), HCN channels carry a mixed current of K^+ and Na^+ ions (the permeability ratio of conducting Na^+:K^+ is 1:3). The structural determinant that results in a reduced K^+ selectivity in HCN channels remains unknown, although it is widely assumed that amino-acid residues that form the pore helix could be responsible (Kaupp and Seifert, 2001).

1.4.2 C-terminal region

The C-terminal part of the channels can be subdivided into the C-linker region and the CNBD. I will be discussing the following section in two parts: one exclusively dealing with the C-linker region and the other part deals the CNBD.

1.4.2.1 C-linker region

The C-linker region relays the event of ligand binding to the opening of the channel. It is located between the CNBD and the S6 TM domain. Hypothesis on the role of the C-linker region in the eukaryotic channel types was influenced by the availability of the crystal structure of the C-terminal region of HCN2 (Zagotta *et al* 2002). The sequence of the C-linker of CNG channels and HCN channels shows high homology. The C-linker region contains six α helices designated A' to F' (~70 amino acid residues). The CNBD immediately succeeds the C-linker region. It provides most of the contact points for the tetrameric arrangement. Most interactions between subunits occur due to A' and B' of the C-linker region from one subunit interacting with C' and D' of a neighbouring subunit. These interactions are mediated by several hydrophobic residues and a salt bridge between L472 of B' and E502 of D'. It has been shown that mutating these residues in HCN2 and analogous residues in CNGA1 results in constitutively active channels (Craven and Zagotta 2004).

In addition to relay ligand binding, the C-linker region also serves regulatory functions. The C-linker region of the A4 and B subunits carries a Ca^{2+}-Calmodulin binding motif (Weitz *et al* 1998). Calmodulin has been shown to associate with the olfactory CNG channel and to regulate channel activity (Bradley *et al* 2004). The homotetrameric A subunits are shown to be either potentiated (Gordon and Zagotta 1995a) or inhibited (Gordon and Zagotta 1995b) by Ni^{2+}, at low concentration on A1 and A2 subunits. This effect is due to the presence of a single His residue (H420 in A1, 396 in A2) preceeding S6 in the respective channel subunits. These residues do not occupy analogous positions and indicate subunit-specific regulation.

In another study it was shown that three amino acids (tri-peptide sequence, Q X R/K) are sufficient to delineate the differences between the functional CNG channels (A1, A2 and A3 subunits) and HCN channels versus the non-functional CNG channels (A4, B1 and B3, when expressed alone heterologously). Replacing the tri-peptide sequence of HCN2 (QEK) with the tri-peptide sequence of CNG A4 (FPN) resulted in dimers of HCN 2-CNBD in presence of cAMP and tetramers in absence of cAMP. From the crystal structure and equilibrium sedimentation experiments it was shown that HCN2-CNBD is predominantly tetrameric in

the presence of cAMP (Zagotta *et al* 2002). The crystal structure also suggests that the tetramerization of the CNBDs was a result of interaction between linker regions A' and B' of one domain to C' and D' of neighbouring domain (Figure 1.4). The tri-peptide sequence is located in the A' linker region and is crucial for tetramerization. Replacing the tri-peptide could prevent tetramerization. This points in the direction that the non-functional CNG subunits may be a result of hampered subunit contacts between the C-linker region.

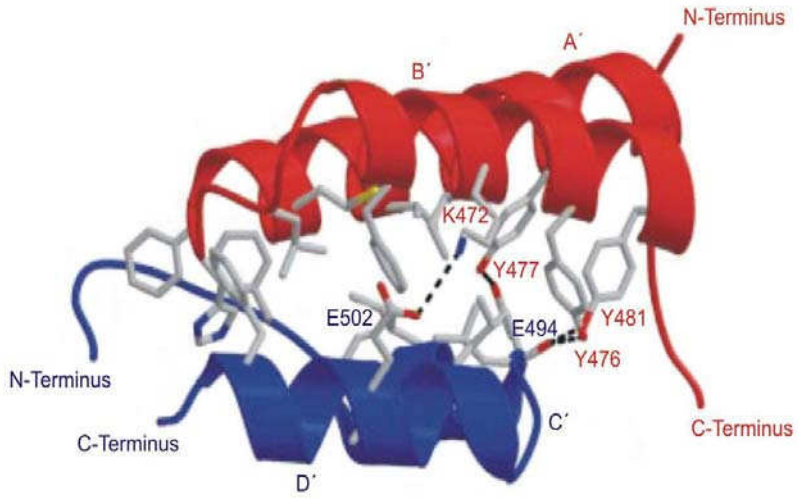

Figure 1.4: C-linker interactions observed in the HCN2-CNBD structure that promotes tetramerization. The A' and B' of one protomer interacts with C' and D' of another. This figure is adapted from Zagotta *et al* (2002).

Unlike the CNG and the HCN channels, the prokaryotic CNG channels carry a short C-linker region (~ 20 amino acids residues). Yet, from the crystal structure of the dimeric CNBD, the short C-linker region was proposed to be involved in inter-subunit contact.

1.4.2.2 Cyclic nuclotide-binding domain (CNBD)

All CNG channels harbour a C-terminal CNBD. Structural data is available on CNBD from several other proteins which include the catabolite activator protein (CAP) from *E.coli* (Mckay and Steitz 1981), protein kinase A (PKA, Su *et al* 1995), the CNBD from the HCN2 channel (Zagotta *et al* 2001) and the CNBD from mlCNG channel (Clayton *et al* 2004; See Appendix section 6.2 for the sequence alignment of CNBD of the above mentioned proteins. Please refer to Berman *et al* 2005, where similarity and differences of CNBDs from various proteins has been discussed in length). The crystal structures of the cNMP-bound CNBD proteins reveal a similar arrangement. The cAMP-binding site of HCN2 comprises of three α-helices (A, B, and C) and eight β-strands (β1 to β8), which served as template for cNMP-binding domains of other proteins. The β-strands form a flattened β-barrel consisting of two antiparallel β-sheets, each with four strands, connected in jelly-roll topography. The three

helices are connected to the ends of the β-jelly roll. The A helix is N-terminal of the β-jelly roll, whereas the B helix, immediately followed by the C helix, is C-terminal of the β-jelly roll. The cyclic nucleotide is bound within the binding site through a network of polar and hydrophobic interactions. The phosphate and the ribose ring of cAMP interact with the protein through several hydrogen bonds and electrostatic interactions. These contacts involve residues in the loop linking β6 and β7 which is known as the phosphate-binding cassette (PBC). PBC harbours the GEI tripeptide in the short helix between β6 and β7 that interacts with the ribofuranose, while the residues RRTAAT/S in the β7 interact with the phosphoryl moiety (Figure 1.5). The adenine ring interacts primarily through hydrophobic and stacking interactions with residues in and near the C helix. The CNBD structures from the mlCNG protein and the HCN2 channel carry an Arg residue in the C-helix (R348 in mlCNG and R632 in HCN 2) that has been shown to interact with the cyclic nucleotide by directly stacking over its ribose ring.

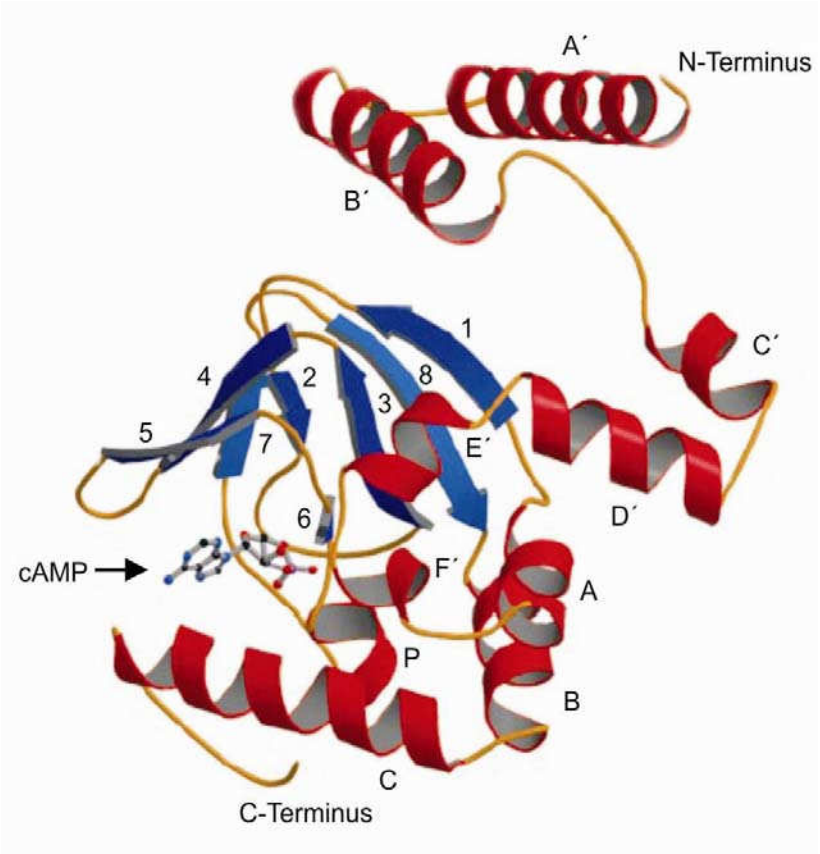

Figure 1.5: Ribbon representation of the C-linker and CNBD of HCN2 bound to cAMP. The six helices of C-linker region are marked A'-F', the β-jelly roll like structure with the eight strands are numbered from 1 - 8 and the three helices comprising the CNBD as A, B, and C and a short helix P between strands 6 and 7. This figure is adapted form Zagotta *et al* (2002)

From structural data and mutagenesis experiments, several amino acids have been identified that are crucial for ligand binding. The CNBD of HCN2 channel binds both cAMP and cGMP. Cyclic AMP activates HCN channels at lower concentrations than cGMP. The structure of CNBD of HCN2 was solved in the presence of either ligand. The residues ^{581}GEI^{583} bind to the C2'-OH of the ribose. R591 and T592 in β7 interact with the phosphate. These residues comprise the PBC. The major difference in the interaction of the two cyclic nucleotides with the the CNBD of HCN2 arises from the conformation of the bound cyclic nucleotide. Cyclic AMP binds to CNBD in the *anti* configuration, while cGMP binds to the CNBD in the *syn* configuration. R632 mediates a stacking interaction to the cNMPs It directly interacts with the N6 position of cAMP and indirectly with the N2 position of cGMP through a water molecule. Apart from interacting with the phosphate group, T592 is one of the important determinants of cGMP binding.

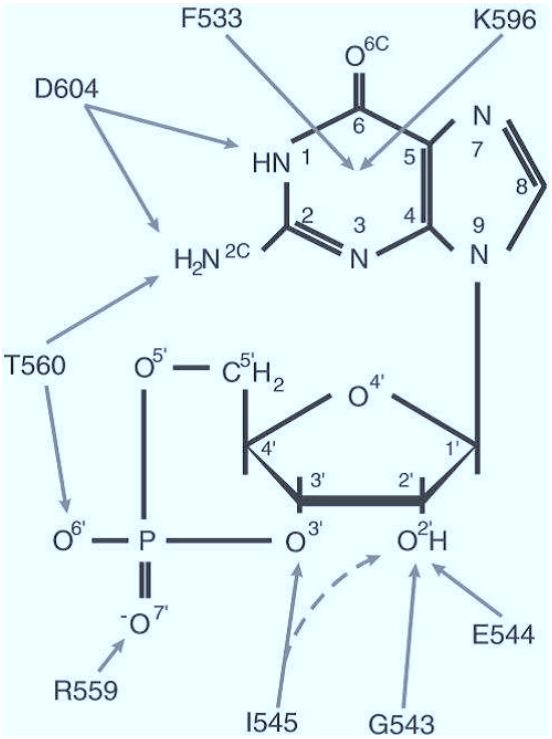

Figure 1.6: Interaction of amino acid residues of the CNGA1 CNBD with cGMP in the *syn*-conformation. This figure is adapted from Kaupp and Seifert 2002.

The selectivity of CNBD for cGMP over cAMP has been attributed to several residues. From mutation studies on bovine CNGA1 some of these residues are T560 (Altenhofen *et al* 1991), D604, F533 and K596 (Kaupp and Seifert 2002; Figure 1.6). Of the above mentioned residues, T560 is the only residue within the PBC (analogous to the position T592 in HCN2). D604 and K596 are found on the C-helix and F533 precedes the PBC.

Mutational studies on residues of CNBD from other proteins also reveal a similar trend:

1. At the respective position of T560 in both CNBDs of the regulatory subunit of PKA (Shabb *et al* 1991) is an Ala. Replacing Ala to Thr (A210T and A334T, PKA RI- α) results in cGMP binding of PKA.
2. Cyclic GMP is a partial agonist for an invertebrate HCN channel, SpHCN1 (Gauss *et al* 1998). Recently, a crystal structure of the CNBD of the SpHCN1 channel was solved with cGMP bound. Replacing V621 in the PBC to Thr, and additionally, mutating I665 to Asp (analogous to positions T560 and D604 in CNGA1, respectively) resulted in a CNBD with bound cGMP. These mutations on the full-length channel resulted in a cGMP-gated SpHCN1 channel.
3. The HCN2 channel binds almost equally well cAMP and cGMP. It contains the T in PBC which is required for cGMP binding. Mutation of residue I636D (analogous to D604 in CNG A1) results in an CNBD of HCN2 exclusively binding cGMP.

To appreciate the conformational change in CNBD, comparisons of the structure of cNMP-bound CNBD with that of ligand-free CNBD is a must. The cAMP-bound state of the CNBD from mlCNG and HCN2 show similar topology and interactions. The mlCNG-CNBD structure was solved in the presence and absence of cAMP (Figure 1.7). CNBD displays a high affinity for cAMP (Clayton *et al* 2004). When the CNBD is purified, cAMP co-purifies with the CNBD and even after extensive dialysis, cAMP is found to be associated with the CNBD. To obtain a cAMP-free CNBD, a critical residue R348 was mutated to Ala. This residue is analogous to the R632 from the HCN2 channel.

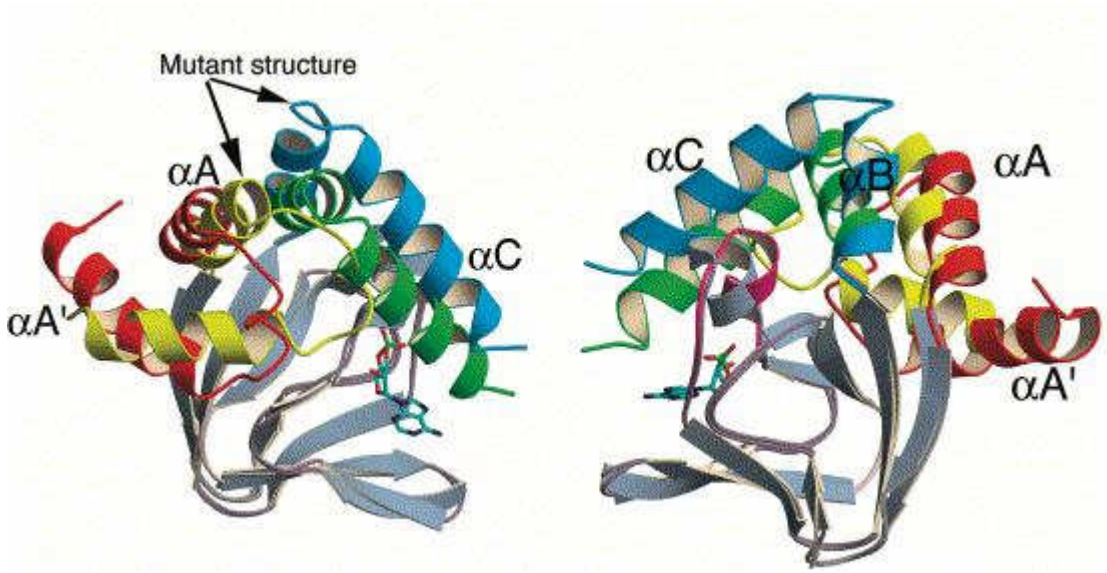

Figure 1.7: Comparison of the crystal structures of the cAMP bound and the cAMP free state of the CNBD from mlCNG. Two different views are shown: the mutant CNBD (R348A) has been marked with arrows and the helices are coloured in yellow and blue. Hardly any difference is observed in the structure of β-jelly roll like structure. cAMP bound CNBD shows repositioning of both the N and the C-terminal helices. The short helix (shown in magenta) between β6 and β7 also shows repositioning on cAMP binding.

Interesting differences are revealed when comparing the cAMP-bound and cAMP-free structure of the CNBD. Large changes are observed in the position of all three helices and the short helix constituting the PBC. Virtually no change in the β-jelly roll-like structure is observed. On binding cAMP, the B helix (hinge) repositions relative to the C helix (lid) to cap the mouth of the cavity, where R348 stacks over the cAMP. It still remains unclear as to how ligand binding is relayed to the A helix (channel gating). A large conformational change in the CNBD was expected, as in another study on the EPAC protein, which was crystallized in absence of cAMP. The crystals cracked when cAMP was added to it (Rehmann *et al* 2003). This is in line with the results obtained for the cAMP-free R348A structure.

1.5 Binding and gating in channels activated by cyclic-nucleotides

The CNG channels closely resemble haemoglobin (Hb) in several aspects. Both proteins are tetrameric and carry one binding site per protomer. Both show positive cooperativity with a Hill coefficient of 2-3. Although Hb shows positive cooperativity for binding, it was not clear until recently if the cooperativity in CNG arose due to binding or gating, therefore my attempt to study. Like for Hb, Monod, Wyman and Changeux's model (MWC or the concerted model) and its adaptations have been widely used to comprehend gating events in CNG channels. The MWC model assumed that an allosteric protein exists in two states R (relaxed state - active) and T (tensed state - inactive) which are under equilibrium (Li *et al*

1997). Binding of a ligand to the R state is more favourable than to the T state although the free energy associated with ligand binding would be the same. An allosteric ligand binds to an active receptor with an affinity K_R and binds to the inactive receptor with an affinity K_T ($K_R = f^*K_T$, where '*f*' is the ratio of the affinity of the ligand to the two states). Addition of the ligand to a system where the two states of a protein are in equilibrium would drive the reaction to the R state.

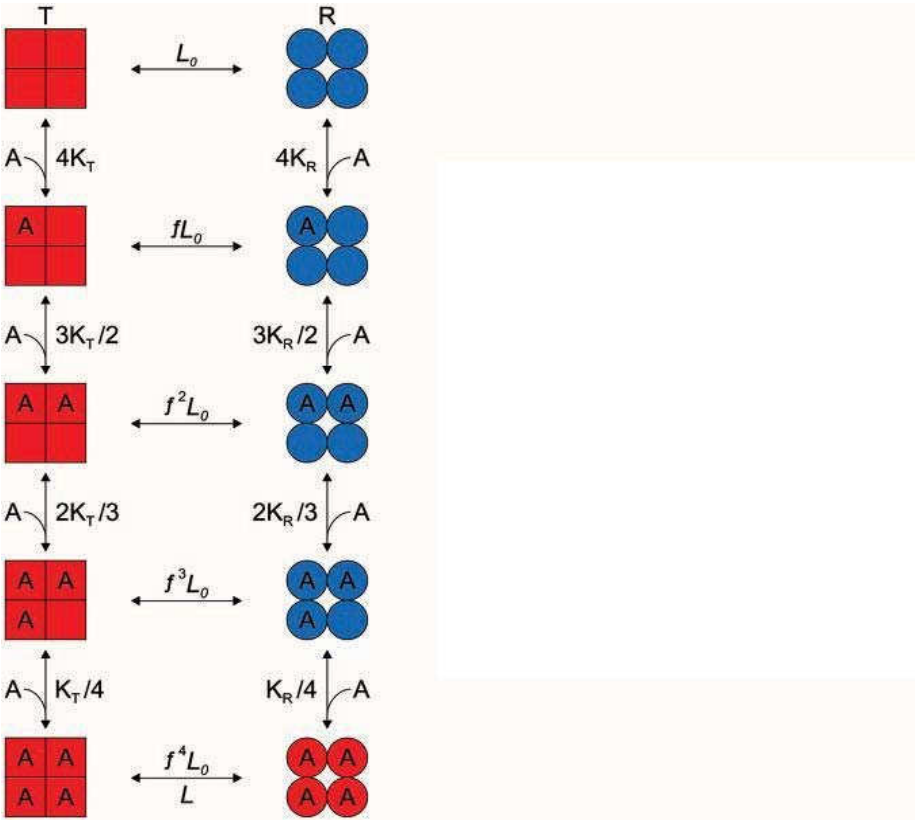

Figure 1.8: Monod *et al* 's concerted model : Subunits can exist in the inactive ("tense") conformation (T, squares) or the active ("relaxed") conformation (R, circles). K_T and K_R are the equilibrium constants for binding of the agonist A to the T and R states, respectively; L_0, equilibrium gating constant between the unliganded T and R states; *L*, equilibrium gating constant between T_{4A} and R_{4A} in the sequential model (red); *f* is a multiplicative factor, $f = K_R/K_T$. This figure is adapted from Kaupp, and Seifert 2002.

In a multi-subunit protein, binding of the ligand promotes T state to R state. The model predicts that the system would flip between T and R states in a concerted manner (Figure 1.8). The allosteric factor that would be required for the flip from T state to R state is denoted by *L* (*L* = [active]/[inactive]). As binding of the ligand is favourable to the R state, subsequent binding events would be enhanced by a factor *f*. Thus, binding of the ligand to an active protein is favoured by a factor f^n*L where 'n' is the number of subunits. The model predicted very well the binding and structural events of Hb and several other proteins.

One of the first few models on ligand binding on the CNG channels was inspired from the Del Castillo and Katz (1957) scheme. It was proposed by Gordon and Zagotta (1995b) and Varnum *et al* 1995 that binding of the ligand results in an inactive channel which requires the allosteric transition factor *L* to open. This scheme was put forth as:

$$C \xleftrightarrow{2K} C \xleftrightarrow{K/2} C \xleftrightarrow{L} O$$

where *C* represents the closed state, *O* represents the open state and *K* the ligand affinity.

From their analysis made on macroscopic currents from rod CNGA1 and olfactory CNGA2, it was proposed that both cNMPs bind to the channel with similar affinities but differ in inducing the allosteric transition *L*, to promote the closed channel to the open state. Cyclic GMP greatly promotes *L* in both channel types and cAMP has lower *L* in comparison to cGMP in the olfactory CNG channel. Cyclic AMP is a partial agonist for the rod CNG. This model was later discarded when it came to light from single-channel measurements (Li and Lester 1999) that the binding affinities for the cNMPs to the olfactory channel differed by a factor of 1000 and the allosteric transition only by a factor of 2. The other important finding was that the second binding event largely produced the sigmoidicity of the dose-response relation, indicating that the second binding event is crucial in promoting the gating event.

Another popular model is the coupled-dimer model (CD model or the dimer-of-dimers model, Liu *et al* 1998), which is a modification of the concerted model by considering that the binding domain forms a dimer (like CAP), and the two dimers behave independently. The channel opens only after both dimers are activated.

By far the most convincing data on ligand binding and activation was recently presented by Biskup *et al* (2007) wherein they measure ligand binding and channel activation simultaneously. The approach was to use a fluorescent ligand. When the fluorescent ligand bound to the channel the fluorescence intensity is enhanced in comparison to the background. The channel current was measured simultaneously. Biskup *et al* observed that the channel activation kinetics had a Hill coefficient of 2. The normalized activation and binding isotherm when plotted together have a crossover point. At ligand concentrations lower than the crossover point the relative percentage of ligand binding precedes the percentage of channel activation. The vice versa was observed at ligand concentrations above the crossover point. In a nutshell, it demonstrates that binding of 2 or 3 ligands drives the channel to the open state with the second binding event being the crucial step (a result also demonstrated by Li and Lester's single-channel measurements), while the third and the fourth binding stabilizes the

open state. This idea is very intriguing as the olfactory channel under native conditions is composed of two A2 subunits and the two other subunits serve a regulatory purpose. It will be fascinating to see how the rod channel behaves in similar experiments as it is composed of three A1 subunits.

Although these results represent a huge leap in understanding kinetics involved in channel activation on ligand binding it does not address the reverse question, namely the influence of activated channel to ligand binding. Furthermore, it will also be interesting to see how mutations in sites outside the binding domain influence channel binding and activation, e.g. several mutants of CNGA3 channel carrying single amino-acid substitution in the pore region were shown to have altered gating kinetics (Tränkner *et al* 2004).

Unlike the CNG channels, the HCN channels do not show any cooperativity in binding of cNMP and have a Hill coefficient of ~ 1. The I-V (current-voltage) profile of HCN channel can be fit by a Boltzmann equation (Seifert *et al* 1999). It has been difficult to dissect the activation kinetics of HCN channels as the channel shows an interplay of voltage dependency and ligand binding.

The lack of ligand-binding studies on CNG and HCN channels has been a major setback in ligand activation of these channels. The bottle neck in performing binding experiments on channel proteins has been the limited availability of protein. Proteins like Hb, phosphofructokinase, aspartate transcarbamylase etc. were abundant, which facilitated studies on binding and activity, in addition to obtaining structures. Heterologous expression of eukaryotic proteins in *E.coli* has been proven difficult. Therefore, I decided to study pro-CNG channels.

My work focuses on studying ligand binding kinetics on the pro-CNG channel mlCNG, in order to answer the fundamental question, ***how is binding related to gating?***

2. Materials and Methods

2.1 *Escherichia coli* (*E. coli*) cell culture and basic molecular biology

2.1.1 *E.coli* strains and plasmid/vectors

E. coli strains XL1-blue was used for DNA amplification and BL-21 (DE3) and its derivatives were used for protein expression. The detailed genotypes of the bacterial strains used are listed in the Table.

	E.coli strain (manufacturer)	Properties (Genotype)	Purpose
1	XL1-Blue (Stratagene)	*E.coli* K-12, recA1 endA1 gyrA96 thi-1 hsdR17 supE44 relA1 lac [F´proAB lacIqZΔM15 Tn10 (Tet^r)]	DNA amplification
2	BL-21 (DE3)-pLysE (Novagen)	*E.coli* B, F^- dcm ompT hsdS (rB^- mB^-) gal λ (DE3) [pLysE (Cam^r)]	protein expression
3	Rosetta (DE3) (Novagen)	*E.coli* B, F^- ompT hsdSB(rB^- mB^-) gal dcm lacY1 (DE3) pRARE [(argU, argW, ileX, glyT, leuW, proL) (Cam^r)]	protein expression
4	BL-21 (DE3)-CodonPlus-RIL (Stratagene)	*E.coli* B, F^- ompT hsdS (rB^- mB^-) dcm^+ Tet^r gal λ(DE3) endA Hte [argU ileY leuW (Cam^r)]	protein expression
5	BL-21 (DE3)-CodonPlus-RP (Stratagene)	*E.coli* B, F^- ompT hsdS(rB^- mB^-) dcm^+ Tet^r gal λ(DE3) endA Hte [argU proL (Cam^r)]	protein expression

In the following text the *E.coli* strains have been abbreviated as BL-21 for BL-21(DE3) pLySE, Rossetta for Rossetta (DE3), RIL for CodonPlus RIL, and RP for CodonPlus RP.

Two vectors were used in encoding the bacterial channels and the mlCNBD. The details of which are listed below:

	Plasmid/vector (manufcturer)	Marker	Purpose (genes cloned)
1	pET-11a (Novagene)	Amp^r	All the bacterial CNG channels mlCNG, mmCNG, bjCNG, teCNG were cloned with C-terminal 6 x His sequence
2	pGEX-2T (Amersham Biosciences)	Amp^r	CNBD proteins (including the mutant R348A) were cloned with N-terminal GST gene and a thrombin cleavage site interspersed in between.

The bacterial CNG channels carry a two-letter prefix, which has been derived from the bacterial species the gene was cloned from. mlCNG stands for CNG channel cloned from *Mesorhizobium loti,* mmCNG stands for CNG channel cloned from *Magnetospirillum magnetotacticum,* teCNG stands for CNG channel cloned from *Trichodemium erythraeum,* bjCNG stands for CNG channel cloned from *Bradyrhizobium japonicum.*

2.1.2 Culture media used to grow *E.coli* cells

LB (Luria-Bertani)-Medium:

1 % (w/v) Bactotryptone

0.5 % (w/v) Yeast extract

1 % (w/v) NaCI

To prepare LB-agar-plates 1.5 % (w/v) agar was added to LB Medium.Both the medium and the medium-agar suspension were autoclaved for 20 min, 121^{o}C at 15 pounds per inch pressure. The autoclaved medium was maintained at room temperature and incubated 30 min at 37^{o}C prior to usage.

The liquified-agar-medium was cooled to roughly 50^{o}C. Ampicillin (final concentration: 100 μg/ml; LB-Amp medium) was added before plating it into sterile petri-dishes.

2x YT

1.6 % (w/v) Bactotryptone

1 % (w/v) Yeast extract

0.5 % (w/v) NaCl

2x YT was autoclaved with the specifications mentioned above and mixed with equal volume of autoclaved double distilled water.

2.1.3 Transformation of competent cells

A tube of frozen competent cells was thawed on ice. The DNA solution (1-10 ng) was added to the cells and incubated on ice for 30 min. Each transformation tube was heat-pulsed for 1 min in a 42°C heater and placed on ice for 2 min. LB medium was added to each tube to a final volume of 500 µl and incubated at 37°C for 30 min. 500 µl of each transformation were spread on LB-agar plates containing 100 µg/ml ampicillin to select pET-11a transformed cells. The plates were placed on the bench for several min to allow excess liquid to be absorbed and then inverted and incubated overnight at 37°C.

2.1.4 Purification of plasmid DNA from *E.coli* cells

Overnight grown transformants were inoculated into 5 ml LB medium containing ampicillin. This pre-culture medium was used to inoculate a 500 ml flask containing 100 ml LB-Amp medium and was grown overnight at 37^{o}C at 180 rpm

Plasmid-DNA was maintained in

TE: 10 mM Tris/HCl pH 8.0, 1 mM EDTA

TE_{RNase}: TE with 5 µl RNase-Cocktail (Ambion)/ml

2.1.5 Mini-preparation of plasmid DNA by alkaline lysis method (Birnboim and Doly 1979)

The overnight grown *E.coli* cell suspension was pelleted by centrifugation (Sigma 3K16; 11133-Rotor; 5,500 g, 10 min, RT). The supernatant was discarded and the pellet was resuspended in 3 ml solution I. To the suspension 6 ml solution II was added and mixed by slowly inverting the tube several times in order to lyse the cells. This process leads to denaturation of proteins and DNA (plasmid and genomic). The suspension is neutralized by addition of 4.5 ml of solution III.

This suspension is centrifuged (Sigma 3K16, 11133-Rotor, 5,500 g, 30 min, 4°C). The supernatant was carefully extracted and mixed with equal volume of 100% ethanol and incubated at 4°C for 30 min. The suspension was centrifuged to pellet the DNA (Sigma 3K16, 11133-Rotor, 5,500 g, 30 min, 4°C). The pellet was DNA at RT and solubilized in 600 µl TE. To remove RNA from the preparation, the TE suspension was treated with ice-cold 1 ml 4 M LiCl (final concentration of LiCl – 2.5 M). This results in precipitation of RNA, which is pelleted by centrifugation (Sigma 3K15, 11133-Rotor, 5,500 g, 2 min, 4°C). The supernatant was collected in a new microfuge tube and treated with RNAse in order to hydrolyze any residual RNA at 37°C for 30 min. The suspension was further treated with phenol-chloroform in order to remove any residual protein.

The supernatant was mixed with equal volume of 100% ethanol to precipitate the plasmid DNA and incubated at 4°C for 60 min. The DNA was collected by centrifugation (Sigma 2K15, 12148-Rotor, 21,000 g, 30 min, 4°C). The pelleted DNA was air-dried and suspended in 200 µl of TE. To determine the DNA concentration, the samples were run on an agarose gel and quantified to a DNA standard using the Gel-Doc system (Peq-lab).

Solution I:	**Solution II:**	**Solution III:**
50 mM Glucose	0.2 M NaOH	3 M KAc pH 4.8
10 mM Tris-HCl pH 7.5	1 % (w/v) SDS	
10 mM EDTA		

2.2. Over expression and purification of bacterial CNG channel

Over expression and purification strategy used for all the CNG channels is similar. As they all carry a C-terminal hexahistidine ($(His)_6$) tag, they were all purified on Co^{2+} affinity column (His-trap, Amersham Biosciences) followed by gel filtration. This section is broadly divided into two parts, one describes the experimental details of all the bacterial channels except mlCNG, wheras the other focusses exclusively on mlCNG.

2.2.1 Over expression of bacterial CNG channels in *E.coli* cells

The DNA encoding the respective CNG channel was cloned from genomic DNA. The gene was modified at the 3'-end to encode a $(His)_6$ tag. For optimization of expression in *E. coli*, four

different strains were tested: BL-21 pLysE, Rosesetta, Codon plus RIL, and Codon plus RP. Single colonies harbouring pET-11a/CNG constructs were used to inoculate 5 ml of LB-Amp medium. From this preculture, 500 µl was added to 100 ml of LB-Amp medium to over express the protein. For each construct, the expression and purification protocol had to be optimized separately. Conditions tested included growth temperature, concentration of isopropyl-thio-®-D-galactoside (IPTG), detergents to solubilize the protein, and to determine the optimal detergent concentration to extract the protein.

The cell pellets following over expression were flash frozen in liquid N_2 and stored at -80^oC.

2.2.2 Purification of bacterial CNG channels

The protein was purified with modifications, following a protocol of Riggs (1994). Briefly, the cells expressing CNG proteins were thawed and maintained at 4^oC. All the purification steps were performed at 4^oC unless otherwise mentioned. 50 ml of lysis buffer was added to cells obtained from 1.25*l* of pelleted culture medium. The resuspended *E. coli* cells were added to a French pressure cell (Hydraulic press, SLM Aminco). The samples were ruptured by three passages through the apparatus at approximately 10,000 pounds per square inch. The lysate was separated from cell wall debris and unbroken cells by centrifugation (Sorvall, SA-300, 50,000g, 30 min, 4^oC). DNase I (2-3 mg) was added and incubated on ice for 30 min. The DNase I treated sample was centrifuged (Sorvall, SA-300-rotor, 50,000g, 30 min, 4^oC). The supernatant was discarded and the pellet was homogenized in 100 ml solubilization buffer 1 by 1. stirring it and 2. by a short pulse of sonication. The homogenized sample was mixed with an equal volume of solubilization buffer 2. This mixture was stirred for two h using magnetic beads. The sample was centrifuged (Sorvall, SA-300-rotor, 50,000g, 30 min, 4^oC). The supernatant was collected and run on Co^{2+} loaded His-trap column in a fast protein liquid chromatography system (Aekta™ FPLC; Amersham Pharmacia Biotech) equilibrated with wash buffer. Bound protein was eluted with imidazole. In the first step, the imidazole concentration was raised to 125 mM to remove non-specifically bound proteins. In the second step the imidazole concentration was raised to 500 mM to elute His_6-tagged proteins. The eluate was collected in 2 ml fractions. Individual fractions were tested for protein content and the purity of the eluted protein. The protein containing fractions were pooled and further purified by gel filtration.

2.2.3 Gel filtration chromatography of bacterial CNG channels

The gel filtration column was equilibrated with two volumes of gel filtration buffer. The Superdex 200 analytical grade, 10/30 column was calibrated with the following proteins: Blue dextran, Thyroglobulin (669 kDa), BSA (67 kDa), Ovalbumin (43 kDa), and Ribonuclease (13.7 kDa) Up to 1 ml of the eluate from Co^{2+}-affinity column was loaded onto the column at a flow rate of 0.5 ml/min (Aekta™ FPLC system).

Gel filtration buffer

20 mM $NaHPO_4$, pH 8.0

295 mM NaCl

5 mM KCl

5 mM Decyl maltoside (DM)/5 mM Dodecyl Maltoside (DDM)

2.2.4 Over expression of mlCNG in *E.coli* cells

The gene encoding the *M. loti* CNG channel (mlCNG) was cloned from genomic DNA. The gene was modified at the 3'-end to encode a $(His)_6$ tag. For expression in *E. coli* (BL21 (DE3)-pLysE), the gene was subcloned into the pET-11a vector. Single colony of bacterial strain BL21-pLysE (DE3) cells transformed with pET-11a/mlCNG were used to inoculate 5 ml of LB-Amp medium. Large scale expression was done in 500 ml of LB-Amp medium in 2*l* Erlenmeyer flasks for aerobic growth at 37°C with vigorous agitation (180 rpm). mlCNG expression was induced at OD_{600} ~0.4-0.6 with 1000 μM IPTG (final concentration). Cells were grown for 4 h at 20°C before harvesting. The cell pellets were flash frozen in liquid N_2 and stored at -80°C.

2.2.5 Purification of mlCNG protein by affinity chromatography

The protein was purified according to modification of Riggs (1994) with modifications as mentioned above. The purification protocol was optimized by Novak (2006). *E.coli* cells expressing mlCNG were thawed and maintained at 4°C. All the purification steps were performed at 4°C unless otherwise mentioned. 50 ml of lysis buffer was added to cells obtained from 2.5 *l* of culture medium. The cells were lysed using short pulses of sonication (Branson Sonicator B-12, 6 x 15 s). The lysate was treated as mentioned in section 2.2.2 in order to purify mlCNG.

Lysis Buffer:

20 mM $NaHPO_4$, pH 8.0
295 mM NaCl
5 mM KCl
2 mM $MgCl_2$
Complete (Protease inhibitor (Roche); 1 Tablet/50 ml)
2-3 mg DNase I (Applichem)

Solubilization Buffer 1:

20 mM $NaHPO_4$, pH 8.0
295 mM NaCl
5 mM KCl
10 % Glycerol (v/v)
20 mM Imidazole

Solubilization Buffer 2:

20 mM $NaHPO_4$, pH 8.0
295 mM NaCl
5 mM KCl
20 % Glycerol (v/v)
20 mM Imidazole
60 mM Decylmaltopyranoside (DM)

Wash Buffer:

20 mM $NaHPO_4$, pH 8.0
295 mM NaCl
5 mM KCl
10 % Glycerol (v/v)
5 mM Imidazole
5 mM DM

Elution Buffer:

20 mM $NaHPO_4$, pH 8.0
295 mM NaCl
5 mM KCl
10 % Glycerol (v/v)
500 mM Imidazole
5 mM DM

2.2.6 Purification of mlCNG by gel-filtration chromatography

To further purify mlCNG, the pooled fractions of the mlCNG preparation were subjected to gel-filtration chromatography using Superdex 200 prep grade, Hi-Load 16/60 (Amersham Biosciences). The superdex 200 column allows to separate proteins with molecular weight between $1x\ 10^4$ und $6x\ 10^5$ Da. The mlCNG protein has a molecular weight of 1.6×10^5 Da.

The gel-filtration column was equilibrated with two volumes of gel-filtration buffer. Up to 5 ml of the Histrap eluate was loaded onto the column at a flow rate of 1 ml/min (Aekta™ FPLC system).

Gel filtration buffer for mlCNG:

20 mM $NaHPO_4$, pH 8.0
100 mM KCl
2.5 mM DM/ 3 mM LDAO
50 µM cAMP

2.2.7 Removal of cAMP from mlCNG protein

To remove residual cAMP from mlCNG, the protein was loaded on a Talon Co^{2+}-affinity column (Clontech) and was incubated "in-situ" three times with the low affinity ligand 8-CPT-cGMP (1.25 mM) in equilibritation buffer, followed by washing steps with 20 ml equilibritation buffer. Finally, the column was washed with 200 ml washing buffer; and the protein was eluted with elution buffer.

Equilibriation buffer	**Elution buffer**
20 mM $NaHPO_4$, pH 8.0	20 mM $NaHPO_4$, pH 8.0
100 mM KCl	100 mM KCl
5 mM DM	500 mM Imidazole
	5 mM DM

2.3. Purification of CNBD and its mutant R348A

2.3.1 Over expression of CNBD

The fragment encoding the CNBD of mlCNG was amplified by PCR and starts immediately at the 3' end of the S6 transmembrane region of the mlCNG protein. For expression in *E.coli* (BL21 (DE3)-pLysE), the fragment was subcloned into the pGEX-2T vector (Amersham Biosciences) When expressed, a fusion protein is generated consisting of glutathione S-transferase at the N-terminus followed by a thrombin cleavage site and the CNBD.

Single colonies of *E.coli* strain BL21-pLYSE (DE3) transformed with pGEX-2T/CNBD(s) were used to inoculate 5 ml of LB-Amp medium. From this preculture mixture, over expression of CNBD was performed as mentioned for mlCNG in section 2.2.4. For large scale expression the

LB medium was replaced by 2x YT medium for CNBD. The harvested cells were flash frozen in liquid N_2 and maintained at -80^{o}C.

The fragment encoding the R348A substitution was generated by PCR (Novak, 2006). The fragement was subcloned in the pGEX-2T vector and the over expression strategy followed was similar to that of native CNBD.

2.3.2 Purification of CNBD proteins and its mutant by affinity chromatography

The CNBD protein or the R348A were purified by lysing *E.coli* cells using short pulses of sonication (Branson Sonicator B-12 ; 6 x 15 s). To the sonicated sample(s) DNase I (2-3mgs) was added and incubated on ice for 30 min. The DNase treated sample was centrifuged (Sorvall; SA-300-rotor; 50,000g; 30 min). The pellet was discarded and the supernatant was loaded on to a glutathione affinity column (Glutathione Sepharose-4B). After washing with 10 ml (per 1 ml column) of washing buffer, the CNBD part of the fusion protein was cleaved off by thrombin. 40 units of thrombin were added to 1ml of Glutathione Sepharose-4B column to release ~10 mg of CNBD protein. Incubation was done overnight at 27^{o}C. The CNBD was eluted by a washing step whereas the GST part remained bound to the column.

2.3.3 Purification of CNBD protein and R348A by gel-filtration chromatography

To further purify CNBD or R348A, the pooled fractions of protein from the affinity column was subjected to gel-filtration chromatography. The CNBD protein was run on a Superdex 75 prep grade, Hi-Load 16/60 column (Amersham Biosciences). The superdex 75 column allows separating proteins with molecular weight between 3x 10^3 und 7x 10^4 Da. The CNBD protein has a molecular weight of 1.5 x 10^4 Da.

The gel-filration column was equilibriated with two times the column volume of gel-filtration buffer. Up to 5 ml of the CNBD was loaded on the column at a flow rate of 1 ml/min (Aekta™ FPLC system).

Gel-filtration buffer for CNBD:

PBS (pH 7.4):

7 mM Na_2HPO_4

3 mM NaH_2PO_4

130 mM NaCl

2.3.4 Removal of cAMP from mlCNBD protein

To remove residual cAMP bound to CNBD, the purified protein was denatured on a PD10 column equilibrated with 6 M guanidine hydrochloride (GuCl). The buffer was exchanged several times until cAMP was completely removed. The denatured cAMP-free CNBD (20 ml) was refolded by rapid dilution into renaturation buffer (final volume 120 ml). The final concentration of GuCl was 1 M. The protein was stirred at 4^{o}C for 48 h in renaturation buffer. The volume was concentrated to 10 ml using an Amicon stirred Ultra filtration cell (stirred cell model 8400; Amersham Biosciences; 10 kDa cutoff – Ultra filtration membrane). The solution was centrifuged (Sigma 3K16; 11333; 5,500g 20 min, 4^{o}C) before loading the samples on Superdex 75 prep grade, High load 16/60 column. The gel-filtration column was equilibrated with buffer (composition given below) without GuCl and 5ml of sample was loaded per run in order to remove the GuCl and refold the protein. The refolded cAMP free CNBD is henceforth referred to as rCNBD

PBS (pH 7.4) + 6M GuCl:

10 mM Na-Phosphate, pH 7.4
130 mM NaCl
6 M GuCl

Renaturation buffer

100 mM NaCl
10 mM Na-Phosphate pH 8.0
5 mM glutathione (reduced)
0.5 mM glutathione (oxidized)
0.5 mM L-arginine
10 mM Na_2-EDTA

Gel-filtration equilibriation buffer

10 mM Na-Phosphate, pH 7.4
100 mM KCl

2.4 Determination of protein concentration

2.4.1 Absorbance at 280 nm

Protein concentrations can be measured by absorbance spectroscopy. The absorbance *A* is a linear function of the molar concentration *c* according to the Beer-Lambert relation:

$A = \varepsilon * c * l$

where ε (in $M^{-1}*cm^{-1}$) is the molar absorption coefficient and *l* is the cell length.

Only tryptophan, tyrosine, and disulfide bonds contribute to the absorbance of a protein between 270 nm and 300 nm. The molar extinction coefficient of a protein at 280 nm, ε_{280}, is calculated by using following equation

$\varepsilon_{280} (M^{-1}*cm^{-1}) = 5690 * n (Trp) + 1280 * n (Tyr) + 125 *n (S-S)$

The molar absorption coefficient at 280 nm of CNBD is 5690 $M^{-1}*cm^{-1}$. CNBD contains one tryptophan and no other residues which could contribute to absorbance at 280 nm.

The molar absorption coefficient at 280 nm of mlCNG is 47510 $M^{-1}*cm^{-1}$, mlCNG contains seven tryptophan and six tyrosine residues.

2.4.2 Bradford's assay

Protein estimation was also performed by Bradford's assay (Bradford 1976) in which 200 µl of Bradford's reagent (Bio-rad) was mixed with 800 µl of water. To this reagent, 1-5 µl of purified protein solutions not exceeding 10 µg/µl protein was added and mixed. The absorbance was measured at 595 nm against a blank after 5 min and within 1 h. The protein concentration was estimated from a calibration curve using BSA as the standard protein.

2.5 Protein biochemistry techniques

2.5.1 SDS polyacrylamide gel electrophoresis (SDS-PAGE)

SDS-PAGE gels consisted of a 4% (w/v) acrylamide stacking gel and 10-15% (w/v) resolving gel and were in a Tris / glycine buffer system (Laemmli 1970). Approximately 1−10 µg of protein were mixed with SDS sample buffer and loaded onto the gel after boiling for 10 min at 95°C. The electrophoresis was carried out in an electrophoresis chamber (Whatman, Biometra) at 20 mA for 1−2 h. The proteins were stained with Coomassie staining solution for 1 h and then destained overnight with destaining solution. Electrophoretic molecular mass determination of

the proteins were performed following the methods of Weber and Osborn (1969) using the low molecular weight standards from Amersham Pharmacia AB: α-lactalbumin (14.4 kDa), soy bean trypsin inhibitor (20.1 kDa), carbonate anhydrase (30 kDa), ovalbumin (43 kDa), BSA (67 kDa), and phosphorylase b (94 kDa). Calibration proteins ('standards') are essential for determination of the molecular weight of unknown proteins. The calibration graph was obtained by plotting the logarithm of molecular weight (*log* M_w) versus the relative migration distance (R_f), required for comparing results obtained from the separating gels.

$$R_f = \frac{\text{distance of protein migration}}{\text{distance of tracking dye migration}}$$

2.5.2 Immunoblotting

All incubation and washing steps were performed at room temperature with agitation.

The proteins were transferred from SDS-PAGE gels to Immobilon-P membranes (Millipore) by electroblotting at 0.8 mA/cm^2 for 30 min in blotting buffer. After transfer, membranes were incubated in Ponceau S staining solution for 2 min and destained in distilled water until bands were visible. Ponceau S stain was washed with PBS-T (PBS with 0.5% (v/v) Tween-20). The non-reacted sites on the membrane were blocked by soaking the membrane in PBS/1% (w/v) milk solution for 1 h. The immunoblot was incubated with anti-His antibody (1:1000 dilution Amersham Biosciences) in PBS/0.05% (w/v) milk for 1 h and rinsed with PBS-T buffer. The incubation was continued with horseradish peroxidase (HRP)-labeled anti-rabbit secondary antibody (1:5,000 dilution, Sigma) in PBS/0.05% (w/v) milk for 1 h and washed in an excess of PBS-T buffer. Finally the blot was treated with ECL substrate (Amersham) for 1 min according to the manufacturer's protocol. The immunoreactive band was detected by exposing the blot to Kodak (Rochester) XAR-2 film for a few s. The membranes were stained by Amido black solution for documentation.

2.5.3 Cross-linking experiments

The purified protein was incubated with 0.25 μM of the cross-linker. at RT in a buffer containing (in mM): 10 Hepes at pH 7.4, 300 NaCl, 5 KCl, 2 $CaCl_2$, and 5 DM. The two cross-linkers used in my experiments were amino specific cross-linker - Bis(sulfosuccinimidyl)suberate (BS^3, Pierce) and carboxy specific cross-linker - 1,4-bismaleimidyl-2,3-dihydroxybutane (BMDB,

Pierce). The crosslink reaction was terminated after different incubation times by adding SDS sample buffer (50 mM Tris-HCl at pH 6.8, 2 % (w/v) SDS, 12.5 % (v/v) glycerol, 1 % (v/v) β-mercaptoethanol, 0.01 % (w/v) Bromphenol Blue). Crosslink products were analyzed by SDS-PAGE and Western blotting. The cross-linked products were separated on a 7.5 to 15 % gradient SDS gel.

2.5.4 Size-exclusion chromatography (SEC)

Size-exclusion chromatography was used to estimate the molecular weight of the CNBD protein. The Superdex 75 Hi-load 16/60 gel filtration column was prepared as mentioned before in section 2.3.3. The Superdex 75 Hi-load 16/60 column was calibrated with the following proteins; BSA (67 kDa), Ovalbumin (43 kDa), Chymotrypsinogen (25 kDa), and Ribonuclease (13.7 kDa) (Figure 2.1). Up to 5 ml of the purified CNBD was loaded onto the column at a flow rate of 1 ml/min. The volume of solvent between the point of injection and the peak maximum of a solute is known as the elution volume (V_e). The separation can be characterized in terms of the partition coefficient, K_{av}, defined by:

$$K_{av} = \frac{V_e - V_o}{V_t - V_o}$$

Where K_{av} describes the fraction of stationary column volume available for diffusion of a given protein. Whereas V_o and V_t are the 'void volume' and 'total volume' of the column respectively. The V_o of the column is 40 ml, determined by blue dextran and the V_t is 120 ml.

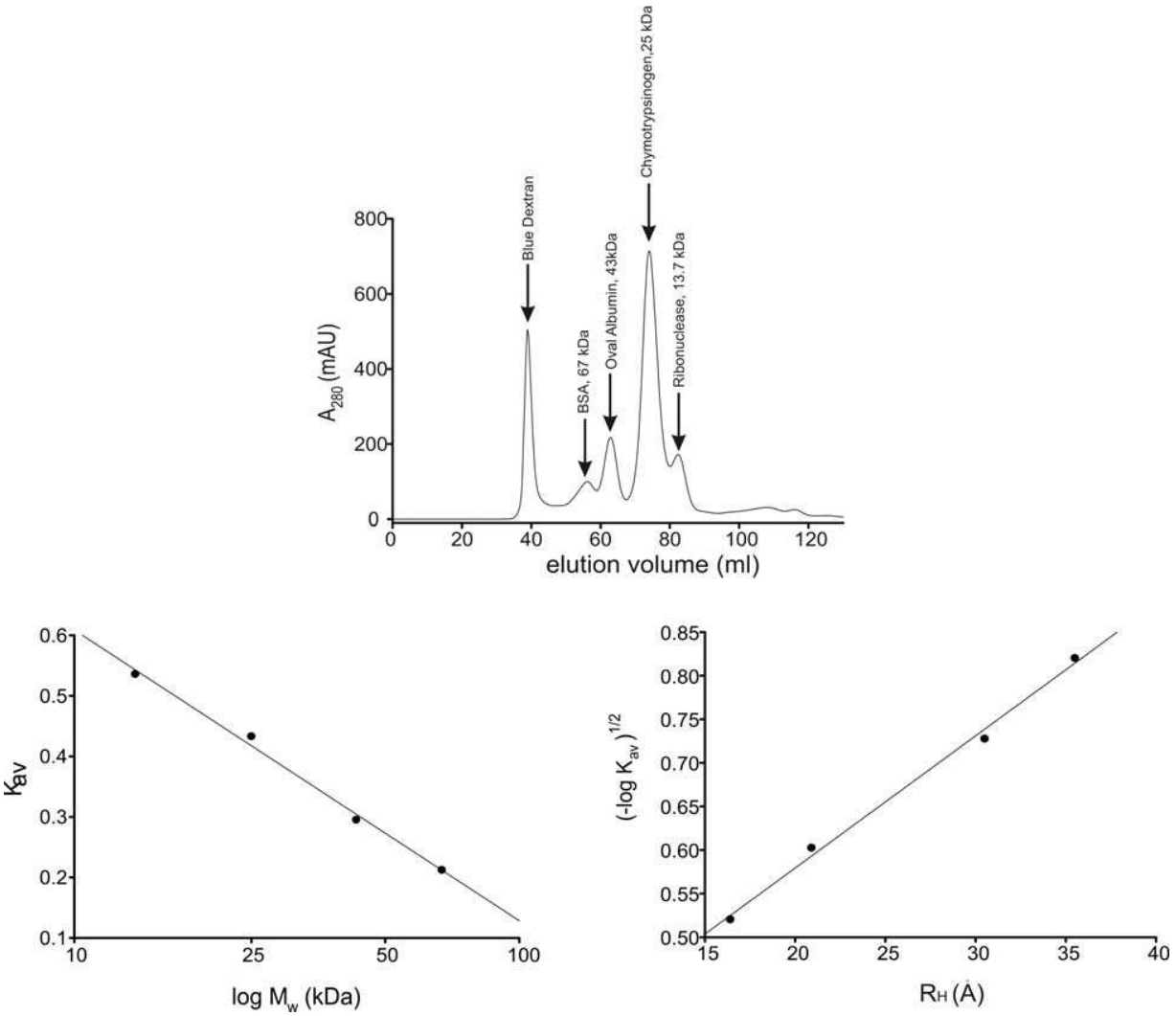

Figure 2.1: Chromatogram and calibration curve of Superdex 75 preparative grade column with standard markers. (A) Chromatogram showing the elution profile of the standard markers on the Superdex 75 preparative column. The markers used were Blue dextran, BSA, Ovalbumin, Chymotrypsinogen, Ribonuclease and the elution volumes are 38.9, 56.1, 62.9, 74.1 and 82.4 ml, respectively. (B) Calibration curve of K_{av} versus log M_w of standard proteins. (C) Calibration curve of the hydrodynamic radius (R_H) of the standard proteins against (-log K_av)^1/2

Size-exclusion chromatography was also used to determine mlCNG stability in various detergents. The experiments were performed on analytical grade Superdex 200 HR 10/30 gel filtration column (1.0 x 30 cm; from Pharmacia Biotech). The column was equilibrated with two column volumes of equilibration buffer with the detergent (section 2.2.6) at a flow rate of 0.5 ml/min using the Aekta™ FPLC system. The detergents tested were BIG CHAP, O-gluco pyranoside (OGP), CHAPS, O-thiogluco pyranoside (OTGP), Zwittergent 3-14, Deoxycholate, Dodecyl Maltoside (DDM), N-LaurylSarcosine. The Superdex 200 HR 10/30 column was

calibrated with the following markers: Blue dextran, Thyroglobulin (669 kDa), BSA (67 kDa), Ovalbumin (43 kDa), and Ribonuclease (13.7 kDa) (Figure 2.2).

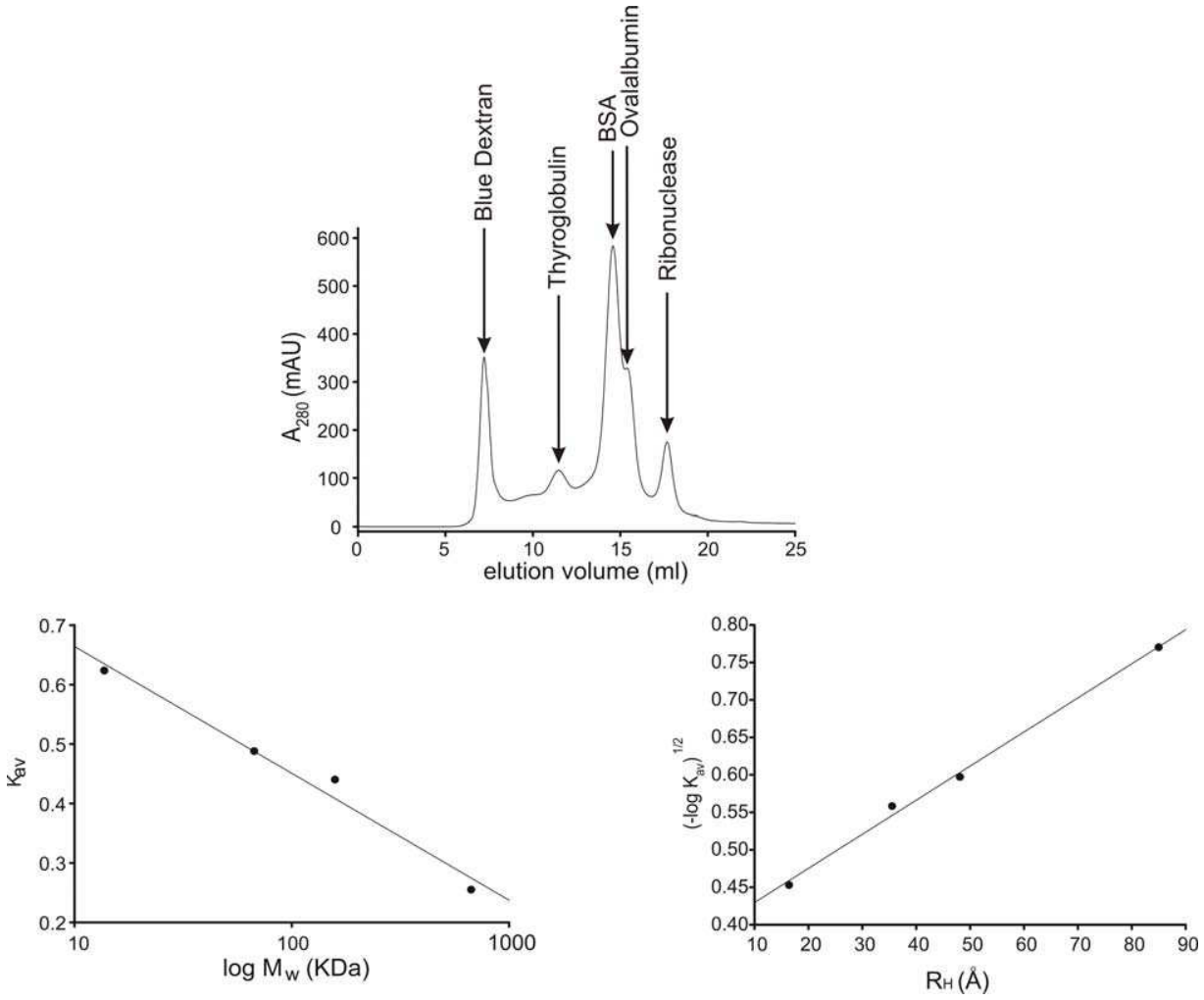

Figure 2.2: Chromatogram and calibration curve of Superdex 200 analytical grade column with standard markers. (A) Chromatogram showing the elution profile of the standard markers on the Superdex 200 analytical column. The markers used were Blue dextran, Thyroglobulin, BSA, Ovalbumin, Ribonuclease and the elution volumes are 7.2, 11.5, 14.6, 15.4 and 17.7 ml, respectively. (B) Calibration curve of K_{av} versus log M_w of standard proteins. (C) Calibration curve of the hydrodynamic Radius(R_H) of the standard proteins against (-log K_{av})^$^{1/2}$.

2.5.5 Ion-exchange chromatography

The mlCNG protein was subjected to ion-exchange chromatography in order to screen for conditions to improve protein homogeneity. After purification of the mlCNG protein from the affinity column, the solution in the eluate was replaced by a equilibration buffer on a PD-10

column (Amersham biosciences). The mlCNG protein was then loaded either on a Uno Q1R (Anion exchanger, Bio-rad) or a Uno S1R (Cation exchanger, Bio-rad) ion-exchange columns containing resins charged with quartenary ammonium salts or sulphonic groups respectively. The columns were equilibrated with the equilibration buffer. The bound protein was eluted with a linear gradient of elution buffer containing NaCl. The fractions collected were run on a SDS-gel for further analysis.

Equilibriation buffer	**Elution buffer**
20 mM Na-Phosphate, pH 8.0	20 mM Na-Phosphate, pH 8.0
5 mM KCl	5 mM KCl
	1M Nacl

2.6 High performance Liquid Chromatography (HPLC)

The presence of cAMP in the protein preparation was detected by reverse phase-HPLC. HPLC equipment was from Waters GmbH. I used a LiChrosphere® 100 RP-18 column (5µm) (Merck). The absorption was monitored at 258 nm. Protein samples were denatured with 5 % (v/v) perchloric acid at 4°C for 30 min and centrifuged (Sigma 2K15; 12148-Rotor; 21,000 g, 30 min, 4°C). The supernatant was neutralized und passed over the column. A linear methanol (HPLC grade) gradient was applied over 20 min. Then the column was washed with 5mM KH_2PO_4, pH 5.0.

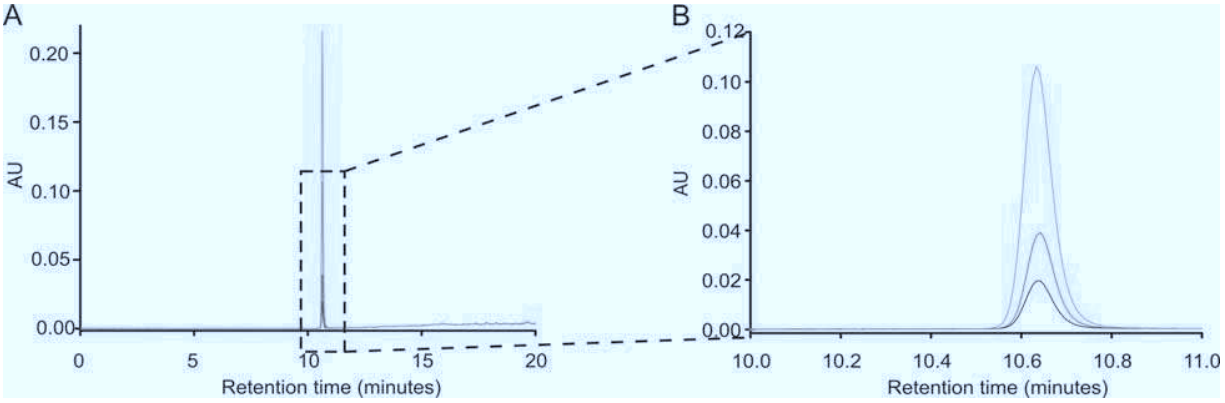

Figure 2.3: Reverse phase HPLC chromatogram of cAMP on RP C-18 column: Retention time of cAMP on the column is 10.65 min in a linear methanol gradient from 0 -100% in 20 min. (A) Chromatogram of four different amounts of cAMP: 10 nmoles (black), 20 nmoles (red), 50 nmoles (green) and 100 nmoles (orange). (B) Resized chromatogram from (A) cAMP at 100 nmoles is not shown for clarity.

2.7 Circular Dichroism (CD) Spectroscopy

2.7.1 Principle

The intensity of light passing through a medium is dependent on the concentration of the sample, its absorptivity and the path length (Beer and Lambert's law). The light velocity is dependent on the refractive index of the medium. When light consisting of left and right circularly polarized light passes through a medium containing an optically active compound, both light components are differentially absorbed. The property of selective absorption of light is known as dichroism. Selective absorption of circularly polarized light is referred to as CD (Figure 2.4).

CD spectroscopy takes into account the projection of amplitude arising due to differential absorption of circularly polarized light and can be written as:

$$\Delta A = A_L - A_R$$

The difference in the absorption is generally small in the order of 1/100 to 1/10th of a percent.

The ellipticity θ_d monitored during a measurement is given as:

$$\theta_d = \frac{2.303}{4} * \frac{180}{\pi} * \deg * \Delta A$$

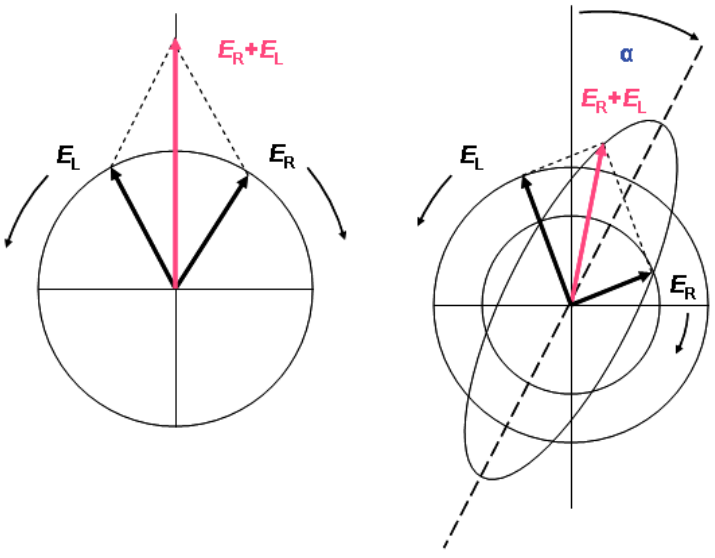

Figure 2.4: Principle of CD spectroscopy: (Left) Linear polarized light can be viewed as a superposition of opposite circular polarized light of equal amplitude and phase. (Right): Differential absorption of the left- and right hand circular polarized light leads to ellipticity ($\varepsilon = E_R/E_L$) and optical rotation (OR, shown as α).This figure is adapted from http://ruppweb.dyndns.org/level1/new_tutorials_page.htm

It is very common to find the ellipticity as molar ellipticity rather than expressed in degrees. Molar ellipticity θ_m is given as:

$$\theta_m = \theta_d * \frac{M_w}{c * l * N_r}$$

where M_w is the molecular weight, c is the concentration, l is the path length and N_r is the number of residues of the polypeptide.

CD has found wide scale application in protein biochemistry. It is used in deriving rough estimates of Secondary Structure Elements (SSE) of proteins whose structures at atomic resolution are unavailable (Greenfield *et al* 1967; Greenfield and Fasman 1967). A text book CD spectrum of peptide made only of α-helix has minima at 208 and 222 nm, and a maximum at 192 nm. β-sheets have a minimum at 217 nm and a maximum at 195 nm, and random coils have a maximum at 215 nm and a minimum at 200 nm (Figure 2.5). CD spectroscopy is also often used in studying structural changes in proteins, e.g. protein unfolding and refolding, as well as conformational changes of proteins on ligand binding or photoactivation. Although CD spectroscopy is a very sensitive technique and rather easy to perform, it suffers from a major drawback in quantifying the SSE. One should be very careful in interpreting the data, because the results obtained from CD Spectra may contain up to 10% error in elucidating SSE.

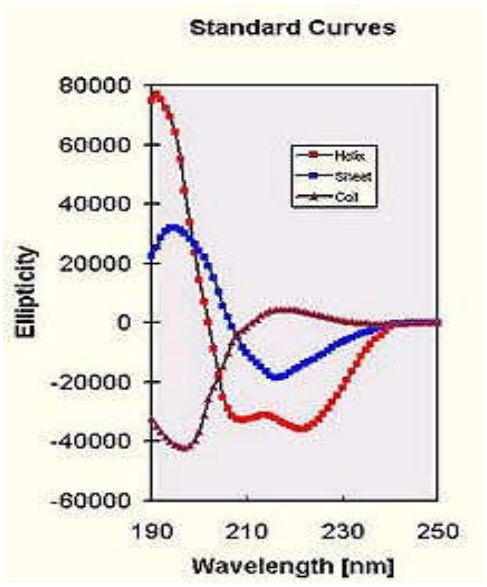

Figure 2.5: CD spectra of poly-Lysine in 100% a-helical structure (red circles), β-sheets (blue circles) and random coils (brown triangles). This figure is adapted from http://www.cryst.bbk.ac.uk/cdweb/html/home.html

2.7.2 CD spectra measurements

Far-UV spectra of CNBD proteins were recorded on a Jasco J-810 spectropolarimeter at RT (0.2 / 0.1 cm path-length cuvette) in 20 mM Na^+ phosphate buffer at pH 7.4 at scan rate of 50 nm/ min. The protein concentration was 8-11 μM cAMP (5-30 μM) was added to the solution of rCNBD at various concentrations to determine cAMP dependent comformational changes. The CD spectra were analysed for SSE on an online database provided on the server of Birkbeck College, London (Dichroweb, Whitmore and Wallace 2004). In short the raw CD spectrum was converted into a text file and loaded on the dichroweb server. The input and the output ellipiticity were read in mdeg. The wavelength step was 1 nm and the reference database used was CDSSTR-Set 7. This database consists of CD spectra of 48 different proteins including unfolded and refolded proteins.

Far-UV CD spectra of mlCNG solubilized in 5 mM DM / 3 mM LDAO in 20 mM Na^+ phosphate buffer at pH 7.4 were recorded in a 0.2 ml cuvette. No SSE estimations were performed from the spectra of mlCNG because detergents change the dielectric constant of the medium thereby interfering with the spectrum and hence may result in wrong estimations of SSE. Instead, CD spectra of mlCNG solubilized in the two detergents were visually compared against each other at the same protein concentration.

2.8 Macromolecular crystallography

2.8.1 Principle

Several techniques are used in determining the structure of a protein. Some of them are crystallography techniques which comprise x-ray, neutron and electron diffraction techniques. Another technique - not involving crystallizing a macromolecule - is NMR. Solution NMR suffers from a major drawback that it is limited to small proteins (~30 kDa, Wuethrich 2001), while ssNMR has made recent strides into elucidating the structure of large macromolecules. One of the greatest advantages of crystallography techniques is that size is not a limitation. I opted to crystallize mlCNG for x-ray and electron diffraction experiments. The principle of crystallization regardless of the diffraction method applied is the same.

Macromolecular crystallography is not very different from conventional crystallography. The major difference though between the two is that conventional crystallography in most cases results in highly ordered crystals, while macromolecular crystallography generally results in less

ordered crystals. This is due to the fact that macromolecules; e.g. proteins are large and generally globular or ellipsoidal. This property leads to several points of contact and large void spaces that are filled by water molecules and other solutes. The solvent content in the crystal can range from 30-90 %. Hence macromolecular crystallography results in small and fragile crystals. They also exhibit weak optical properties and the x-ray diffraction maps have much lower resolutions than the theoretical limits.

Unlike conventional crystallography, a supersaturated solution of sample is absolutely necessary for macromolecular crystallization (McPherson *et al* 1995; Blundell and Johnson 1976). Crystallization and aggregation both show a similar growth trend and both require the macromolecular solution to be supersaturated. Several factors influence macromolecular crystallization:

1. Precipitant concentration / Ionic strength: Ionic strength of the medium is a crucial parameter in protein solubility. Increasing the ionic strength of the medium results in increased solubility of the protein in the initial phases, which is referred to as 'salting-in' effect. First, the electrostatic interactions between the protein and the solutes results in increased solubility. Further increase in ionic strength may result in decreased solubility of the protein, as both salt and proteins compete for water (Figure 2.6).

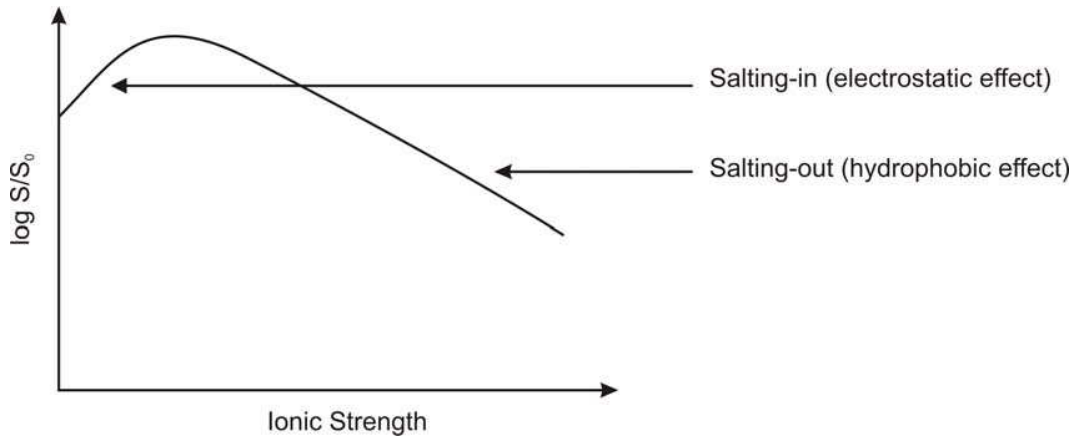

Figure 2.6.: Solubility curve - Salt dependence of protein solubility (S) shows two effects: In the initial phase when the ionic strength is low, solubility is enhanced by electrostatic interaction of protein and salt. Under high ionic strength salt and protein compete for water, resulting in decreased solubility of both the molecules.

2. pH: Another important parameter determining a protein's solubility is pH. The iso-electric point,'pI' is defined as the pH at which the protein carries a net charge of zero, i.e. the protein is least soluble at its pI.
3. Temperature: Increased temperature leads to an increased solubility of protein in pure water, and similarly it also results in increased solubility of ions in pure water. In a medium containing protein and ions, interplay between the two (or more) molecules determines protein solubility. Increasing the temperature can have detrimental effects and can result in protein denaturation.

As membrane proteins are highly hydrophobic and insoluble in aqueous solution, solubilization in detergent is a pre-requisite. Detergents again like the proteins are subject to the aforementioned factors.

One of the most widely used techniques in protein crystallography is vapour-diffusion. Three such prevalent methods are sitting drop, sandwich and hanging drop (Figure 2.7). I prepared crystal setups by using the hanging drop and the sitting drop technique. For both, hanging drop and sitting drop the supersaturated solution of protein is mixed with the precipitant in different ratios (in most of the cases it is mixed 1:1) on a siliconized cover slip and polypropylene micro bridge, respectively. They are in reservoirs partially filled with the precipitant the system and sealed off from air. The precipitant slowly concentrates in the droplet by vaporization facilitating crystallization (alternatively precipitation).

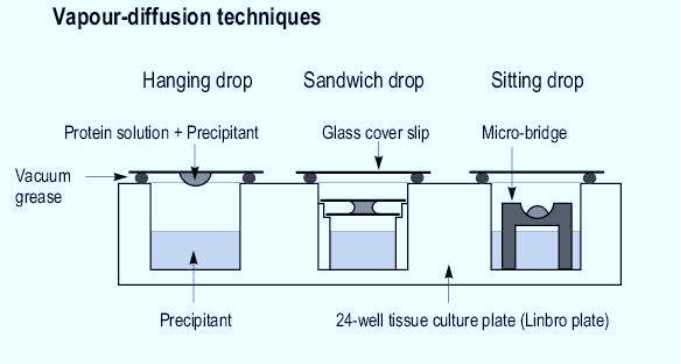

Figure 2.7: Diagrammatic representation of different vapour-diffusion techniques

Several other techniques are also used in protein crystallography which will not be discussed here (pleases refer to Blundell and Johnson 1976.), but one another method that will be introduced here is membrane dialysis, which was used in attempts to crystallize the protein in

bilayers. Ternary mixture of protein and detergent is mixed with varying concentrations of detergent and lipid in a dialysis button. The button is then capped off with a dialysis membrane (10 kDa cutoff). The detergents slowly diffuse out of the dialysis chamber resulting in reconstitution of the protein in the lipids. This process may lead to aggregation, reconstitution or crystallization in 2D.

2.8.2 Crystallization attempts for x-ray diffraction experiments

Crystal setups were prepared by either hanging drops or sitting drops at 17^{o}C and 4^{o}C. mlCNG solution containing 20 mM Na^{+} phosphate pH 8.0 /10 mM Tris pH 8.0, 2.5 mM DM/ 3 mM LDAO and 100 mM KCl were mixed (1:1) with reservoir solution containing solutions from crystallization kit or manually made.

The 24 welled linbro plates used were purchased either from Hampton or Greiner for the hanging drop method. Siliconized coverslips (Hampton) were placed inverted on the plate and sealed using silicone grease (Dow corning).

For sitting drop setups, Hampton plates were used with built-in micro-bridges that could hold up to 10 µl of solution. After preparing the drop, the linbro plate was covered with transparent tape (crystal clear), which does not hamper visualization under a microscope.

The different crystallization kits used were:

1. Crystal Screen 1 (Hampton Research)
2. Crystal Screen 2 (Hampton Research)
3. Memb Fac (Hampton Research)
4. Crystal Cryo Screen (Hampton Research)
5. Wizard I random Sparse matrix crystallization screen (Emerald Biosystems)
6. Wizard II random Sparse matrix crystallization screen (Emerald Biosystems)
7. Crystallization extension kit (Sigma)
8. Crystallization Basic kit for proteins (Sigma)
9. Crystallization Basic kit for membrane proteins (Sigma)
10. Crystallization Low Ionic kit (Sigma)
11. Crystallization PEG Grid screening kit (Sigma)
12. Crystallization Cryo kit (Sigma)

A list of buffers and precipitants used in constructing grid screens (Figure 2.8) is given below. The final concentration of buffer in the reservoir was 100 mM. The buffer constituents and their pH were:

1. Na-acetate buffer pH 3.6, 4.6, and 5.6
2. Na-citrate, pH 5.6
3. Na-MES, pH 6.2 and 6.7
4. K-MES, pH 6.2 and 6.7
5. Tris-HCl, pH 7.0 and 8.0
6. Glycine-HCl, pH 8.6 and 9.6

The precipitants used were:

$MgSO_4$, Li_2SO_4, $(NH_4)_2SO_4$, Zn $(CH_3COO)_2$, 2-methyl 2,4-Pentanediol (MPD) and a series of PEG's of different chain length them being 200, 400, 600, 1000, 2000, and 3000.

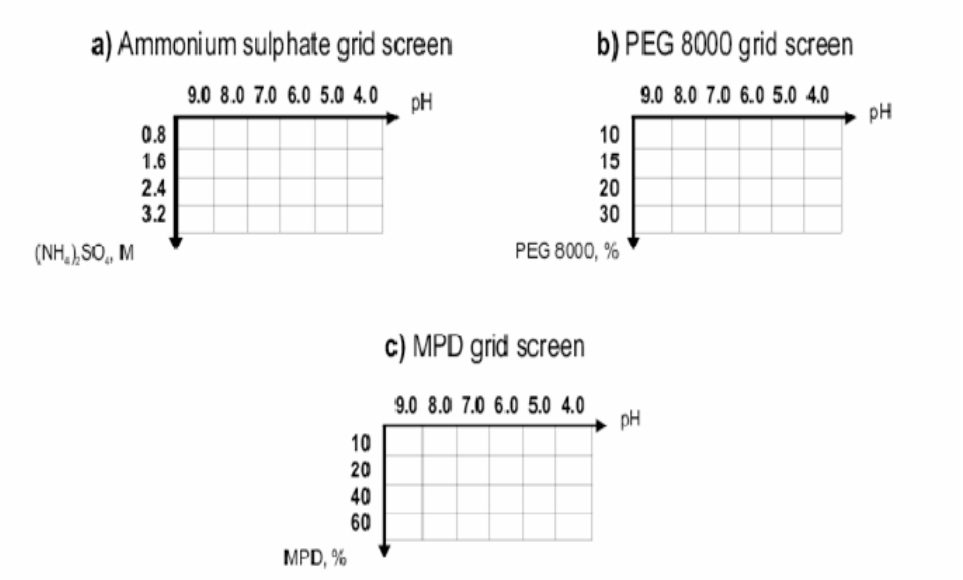

Figure 2.8: Schematic representation of grid screens

2.8.3 Crystallization attempts for electron diffraction

Electron microscopy and single particle analysis:

A 4 µl droplet of the mlCNG was applied to a glow discharged, carbon-coated electron microscope grid. After 40 s, excess solution was removed and the grid was washed thrice with double distilled de-ionized water and negatively stained with two washes of 2% uranyl acetate.

Grids were examined with a TEM (Hitachi H-7000). Images were recorded at 100 kV at a magnification of 50,000 and on Kodak SO-163 film, developed in concentrated D19 developer for 12 min. The negatives were digitized at 4 Å/pixel with a drum scanner (Primescan D 7100). Particles were selected manually picked and analyzed from the images with the EMAN boxer software.

Crystallization trials: The mlCNG protein (~1 mg/ml) was mixed with different varying concentrations of lipids ranging from 0.1-1.5 mg/ml. 60 µl of the ternary mixture was applied to dialysis buttons avoiding air bubbles. A 10 kDa dialysis membrane was capped onto the dialysis button containing the ternary mixture. 60 µl of ternary mixture was dialyzed against 200 ml of detergent free buffer for 5-6 days at 25^{o}C. The lipids which were used in reconstitution were either 1, 2-Dimyristoyl-sn-glycero-3-phosphocholine (DMPC) or *E.coli* polar lipids (Avanti lipids).

Note: - The crystallization attempts were performed at 25^{o}C because; below 23^{o}C DMPC shows lipid phase transitions, which may affect protein reconstitution.

The composition of the dialysis buffer was:

10 mM buffer (buffer constituent and respective pH mentioned below)

150 mM NaCl

5mM KCl

100 µM cAMP

0.01% Na-azide

The list of buffer systems tested was:

1. Na-citrate, pH 5.0
2. Na-MES, pH 6.0
3. Na-HEPES, pH 7.0
4. Tris-HCl, pH 8.0
5. Glycine-HCl, pH 9.0

2.9 Dynamic Light Scattering

2.9.1 Principle

Incident light impinging on a sample is absorbed, reflected or scattered. Light scattering is a weak phenomenon with low probabilities. One can enhance the signal by using a strong and coherent particle sources (LASER, X-rays, neutron) and a sensitive detection system. Light scattering is monitored either in the μs or ms time range. Fluctuations of scattering light intensity are directly related to the Brownian motion of the particle in a small volume. In static light scattering (SLS), the average is derived of the scattered intensity over time (ms) is recorded (Santos and Castanho 1996; Wen *et al* 1996). Dynamic light scattering (DLS) monitors fluctuations of scattered light in the μs time range (Figure 2.9). DLS is also referred to as Photon co-relation spectroscopy (PCS) and quasi-elastic light scattering (QELS).

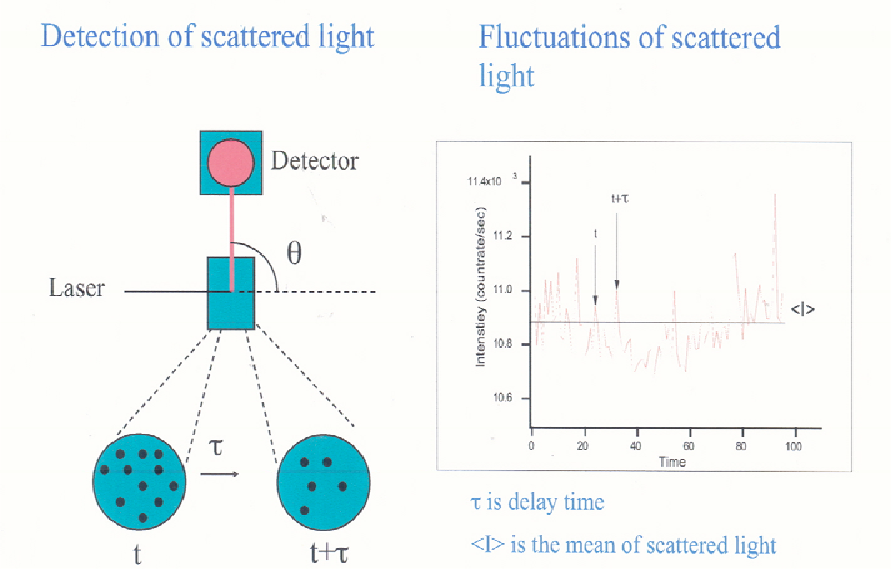

Figure 2.9: Instrumentation (left) of DLS and a display of detected signals (right).The signal detected arises due to fluctuation in scattered light arising from a movements of particles from time t to time t + τ.

The principle behind measuring DLS is, the "Doppler effect". Light waves emitted from a moving object moving relative to the detector experience a frequency shift. Light is scattered by interaction of electrons with the incident light. As the electrons are moving with the molecules they are bound to (due to Brownian motion), they would shift the frequency of radiation to higher or lower values depending on the velocity. A faster diffusing (small) molecule leads to a wider broadening effect of the incident light than a slowly moving (large) molecule. The

broadening effect is a direct measure of the diffusion coefficient of a molecule. Because the broadening effect of large molecules is small, and difficult to detect, a power spectrum is generated using the Fourier-transform domain to obtain the decay time of the function. This is compared to the auto-corelation function that describes the likelihood of finding photons scattered by one and the same particle as a function of time. The diffusion coefficient so derived is used to calculate the radius of the molecule according to the Stoke-Einstein equation:

$$R_H = \frac{kT}{6\pi\eta D}$$

where R_H is the hydrodynamic radius, k is the Boltzmann's constant, η is the viscosity of the medium, and D is the diffusion coefficient.

The Stokes-Einstein equation was derived for spheric particles. Proteins come in various shapes; one derives the effective hydrodynamic radius of a freely tumbling protein in the solution assuming a spherical shape.

2.9.2 DLS measurements

DLS measurements were performed on a temperature and humidity controlled instrument, Dynapro Titan (Protein solutions). It is important that the probes are dust and aggregate free. Therefore samples were centrifuged (Sigma 2K15; 12148-Rotor; 21,000 g, 30 min, 4°C,) and the supernatant was used for the measurements. The sample was placed in a 57 µl quartz cuvette (Hellma, z = 8.5 mm, path length= 3 mm) and measured for at least 20 acquisitions of ten s each. Data acquisition and analysis was performed using the Dynapro software, Dynamics version 6.0 (Protein solutions).

2.10 MALDI-TOF Mass Spectrometry

2.10.1 Introduction to mass spectrometry

Matrix Associated Laser Desorption Ionization-Time of Flight (MALDI-TOF) mass spectrometry is arguably one of the most sensitive analytical methods for molecular identification. A mass spectrometer is used to determine the molecular masses of ionized molecules by separating them according to their mass-to-charge ratio (*m/z*) in an electric or magnetic field. In many cases, the ions encountered in mass spectrometry have just one effective charge (z=1) so the m/z value is numerically equal to the molecular (ionic) mass in Da. MALDI-

TOF usually consists of three parts: the ion source, the mass analyzer, and the detection system. To ionize non-volatile, thermally labile organic compounds, particularly large bio-molecules, a soft ionization technique such as MALDI has to be applied.

In MALDI the macromolecular sample is embedded in a solid low-molecular organic matrix on a metallic substrate and then inserted into the high vacuum line of the ion source. By irradiating the sample with a pulsed UV laser, the matrix absorbs the laser pulse and transfers enough energy to the sample by a process similar to flash thermal evaporation. This results in generation of (predominantly) singly charged quasi-molecular ions. The charged ions are accelerated in an electric field of about 20 kV, where they pick up an amount of energy proportional to their net charge. Accordingly, ions of lower mass enter the mass analyzer with a higher speed than the heavier ones. The analyzer consists essentially of a field-free tube in high vacuum. Due to the different drift velocities the ions arrive at the detector at different times after having passed the drift distance of 1−2 m, namely the time-of-flight mass spectrometer (TOF). The molecular masses can be determined, using the fact that the mass or ratio mass / charge of a molecule is proportional to the square of the flight time. For exact mass determination, calibration with known standards is necessary.

2.10.2 Mass spectrometry measurements

For peptide mass fingerprinting, protein spots of interest were excised from destained poly-acrylamide gels and subjected to in-gel digestion with trypsin (Schaefer *et al* 2001). Briefly, gel pieces were washed twice for 10 min with 350 µl of 0.1 M ammonium bicarbonate in 30 % w/v acetonitrile. The destained and shrunken gel pieces were then vacuum-dried for 20 min in a conventional vacuum centrifuge and subsequently rehydrated with 1 µl of 3 mM Tris-HCl, pH 8.8, containing 10 ng / µl trypsin. After 20 min, 2 µl of 3 mM Tris-HCl, pH 8.8, without trypsin were added. Digestion was allowed to proceed overnight at room temperature. Peptides were extracted by sequential addition of 6 µl water and 5 ml of 0.1 % v/v trifluoroacetic acid in 30 % v/v acetonitrile. An aliquot of 0.5 µl of the resulting peptide solution was mixed on a stainless steel sample plate with 0.5 µl of a saturated α-cyano-4-hydroxy-*trans*-cinnamic acid solution in 50 % v/v acetonitrile, 0.25 % v/v trifluoroacetic acid. Samples were analyzed eithermanually or automatically in positive reflector mode with 20 kV accelerating voltage, 63 % grid voltage and

the delay time set at 125 ns. Data acquisition and analysis was performed using the Voyager Control Panel software, version 5.0 and the Voyager Data Explorer software, Version (Applied Biosystems).

2.11 Fluorescence Spectroscopy

2.11.1 Principle

Fluorescence is a phenomenon by which a molecule absorbs light of one wavelength and emits light of a longer wavelength. Typically fluorescence occurs in the ns time range. Fluorescence is best illustrated by Jablonski's diagram (Figure 2.10).

Characteristics of fluorescence emission:

1. Stoke's shift: Energy of emission is typically lower (longer wavelengths) than the absorption (shorter wavelengths).
2. Kasha's rule: Emission spectra are independent of excitation wavelength.
3. Mirror image rule: In most of the cases the emission spectrum is a mirror image of the excitation spectrum. Exceptions are also observed, e.g. the emission spectrum of Trp is structured and a mirror image of its absorption spectrum in an apolar solvent, while the emission spectrum is unstructured in polar solvent.

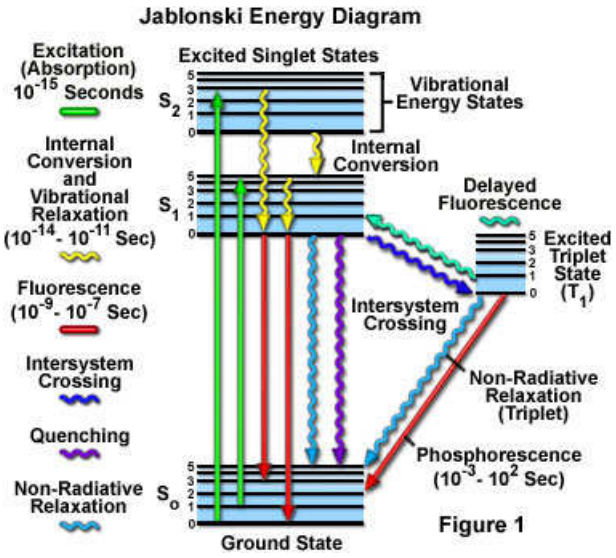

Figure 2.10: Pictorial representation of principle of fluorescence. The picture is adapted from http://www.olympusmicro.com/primer/techniques/fluorescence/fluorescenceintro.html

Two modes of fluorescent measurements are the steady-state and the time-resolved mode. In steady state measurements, the sample is continuously illuminated at one wavelength and the emission spectrum is recorded. Lifetime measurements, on the other hand, measure the fluorescence intensity decay as a function of time. The sample is illuminated by a pulse of light, where the width of the pulsed light is shorter than the decay time of the sample. Lifetime measurements require more complicated instrumentation than steady-state measurements.

The steady-state fluorescence signal is an average of several individual fluorescent events that are not corelated in time. Its intensity is proportional to the absorption and the emission efficiency of the fluorophore, the emission detection sensitivity, the fluorophore concentration, and the excitation light intensity. It is used for spectral investigations, i.e. the energetic of the emitting and the absorbing states of a molecule. With environment sensitive fluorophores (like Trp or NBD as used in this work) solution properties or protein conformational changes can be monitored.

Time-resolved fluorescence can be mathematically described as:

$$I_t = \sum_{i=1}^{n} I_o * e^{\frac{-t}{\tau}}$$

where τ is the lifetime of the fluorophore.

Fluorescence quenching: The processes by which fluorescence intensity are decreased is referred to as quenching. A variety of molecular interactions can result in quenching, which include excited-state reactions, molecular rearrangements, energy transfer(s), ground-state complex formation and collisional quenching.

Collisional quenching (physical quenching) refers to collisional encounters between fluorophores and a quenching molecule that reduces the probability of fluorescence. In most of the cases the quencher is a small molecule or an ion. Collisional quencing is best described by the Stern-Volmer plot:

$$\frac{F_o}{F} = 1 + K_{SV}[Q] = 1 + k_q \tau_o [Q]$$

where K_{SV} is the Stern-Volmer quenching constant, k_q is the bimolecular quenching constant, τ_o is the unquenched lifetime of the molecule, and *[Q]* is the quencher concentration.

Collisional quenching can provide information about the location of a fluorophore in a protein, e.g. quenchers like iodide (small quencher) and acrylamide (large quencher) have been used to determine the position of Trp or small fluorescing probe molecules in protein.
Molecular rearrangements in a protein lead to dynamic quenching of a fluorophore. Dynamic changes can also lead to varying accessibility of the fluorophore to the solvent resulting in fluorescence quenching.

2.11.2 Binding experiments using fluorescence techniques.

The binding of 8-NBD-cAMP to the CNG channels, the CNBD and the R348A was recorded with a fluorescence spectrophotometer (QM-4; PTI, New Jersey, USA) or in a fluorescence plate reader (FlexStation II 384, Molecular Devices, München, Germany) at RT. 8-NBD-cAMP was excited at 470 nm and the emission spectra were collected between 480-650 nm. The cAMP analogue and the mlCNG were suspended in standard buffer (in mM): 100 KCl, 20 Na^+ phosphate, pH 8.0 and 2.5 DM. Binding measurements with the CNBD were performed in a solution without detergent (in mM): 100 KCl, 10 Na^+ phosphate, pH 7.4. In competition experiments, binding of 8-NBD-cAMP to the mlCNG or CNBD was studied in the presence of various concentrations of cAMP or cGMP.
In the fluorescence plate reader, excitation and emission wavelengths were λ_{exc} = 471 nm and λ_{em} = 530 nm for 8-NBD-cAMP. 2 μM CNG channels solubilized in detergent were mixed with 0.5 μM 8-NBD-cAMP. The non-fluorescent analogues (cAMP and cGMP) were added to the mixture to monitor the decrease in fluorescence due to competitive binding.
Steady-state tryptophan fluorescence measurements on the CNBD were performed on the PTI spectrofluorometer. Since the CNBD has no Tyr and only one Trp was the experiments were performed by exciting Trp at 280 nm and the emission spectra were collected between 300-450 nm. CNBD concentration was maintained at 5 μM. 10 μM cAMP was added to the sample to measure Trp fluorescence change upon cAMP binding to CNBD.

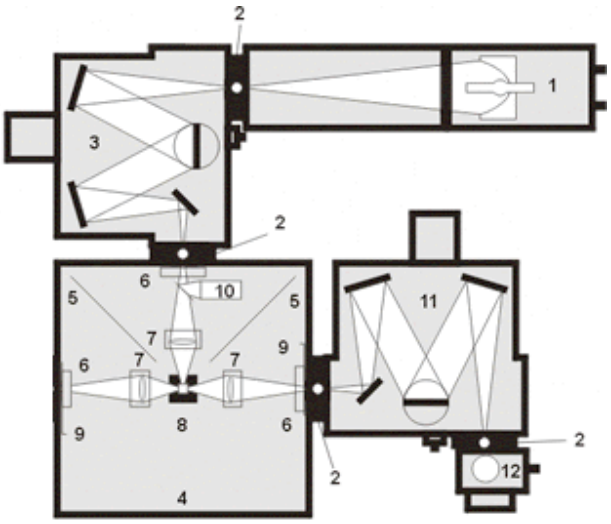

2.11: Instrumentation of Fluorescence spectrophotometer. Key: 1 - Xe Arc Lamp (excitation source), 2 - slits, 3 - Excitation Monochromator (selects ex wavelength), 4 - Port, 5 - Blender, 6 - Excitation Polarizer, 7 - Collecting lens, 8 - Sample Holder, 9 - Emission polarizer, 10- Beam splitter,
11 - Emission Monochromators (selects fluorescence wavelength) 12 - Detector Photomultiplier Tubes. This picture is adapted fro www.pti-nj.com

Data analysis: The fluorescence binding data was analyzed in terms of a simple binding scheme:

$$R + L \underset{k_{-1}}{\overset{k_1}{\rightleftharpoons}} RL$$

K_D is given by:

$$K_D = \frac{k_{-1}}{k_1} = \frac{R \cdot L}{RL} = \frac{(R_t - RL)(L_t - RL)}{RL} \qquad (1)$$

$$\rightarrow RL = \frac{1}{2}(R_t + L_t + K_D) - \sqrt{\frac{1}{4}(-R_t - L_t - K_D)^2 - R_t \cdot L_t} \qquad (2)$$

$$\Delta F = RL \cdot x \qquad (3)$$

wherein R, L, and RL refer to the concentrations of the receptor, ligand, and receptor-ligand complex, respectively. R_t and L_t refer to the total concentrations of receptor and ligand, respectively. The normalization factor *x* relates the concentration of bound 8-NBD-cAMP to the fluorescence change (ΔF).

In competition experiments, binding of 8-NBD-cAMP to the protein was studied in the presence of various amounts of cAMP or cGMP:

$$K_{Df} = \frac{(R_t - RL_f - RL_n)(L_{tf} - RL_f)}{RL_f} \quad (4)$$

$$K_{Dn} = \frac{(R_t - RL_f - RL_n)(L_{tn} - RL_n)}{RL_n} \quad (5)$$

wherein K_{Df} and K_{Dn} denote the K_D of the fluorescent and non-fluorescent ligand; RL_f, the concentration of the complex between receptor and the fluorescent ligand; RL_n, the concentration of the non-fluorescent ligand complex; L_{tf} and L_{tn}, denote the total concentration of fluorescent and non-fluorescent ligand. Combining equations (4) and (5) after some rearrangements one obtains:

$$\left(1 - \frac{K_{Dn}}{K_{Df}}\right) RL_f^{\,3} + \left(K_{Dn} - K_{Df} - R_t + R_t \frac{K_{Dn}}{K_{Df}} - L_{tf} + L_{tn} + 2L_{tf} \frac{K_{Dn}}{K_{Df}}\right) RL_f^{\,2} +$$

$$\left(R_t L_{tf} - \frac{R_t L_{tf} K_{Dn}}{K_{Df}} - L_{tf}^{\,2} \frac{K_{Dn}}{K_{Df}} - L_{tn} L_{tf} - K_{Dn} L_{tf} - \frac{R_t L_{tf} K_{Dn}}{K_{Df}}\right) RL_f + \quad (6)$$

$$\frac{R_t L_{tf}^{\,2} K_{Dn}}{K_{Df}} = 0$$

Equation 6 was solved for RL_f using Cardano's method. As,

$$\Delta F = RL_f \cdot x \quad (7)$$

the data were fitted with a least-squares routine to equation 7.

2.11.3 Fluorescence lifetime spectroscopy

Time-resolved measurements are widely used in fluorescence spectroscopy, especially for studies of biological macromolecules. This is because time-resolved fluorescence data often contain additional information than that available from steady-state fluorescence data. The main advantage of this technique is that it allows resolving two (or more) decay times displayed by a one molecule or mixtures of different molecules.

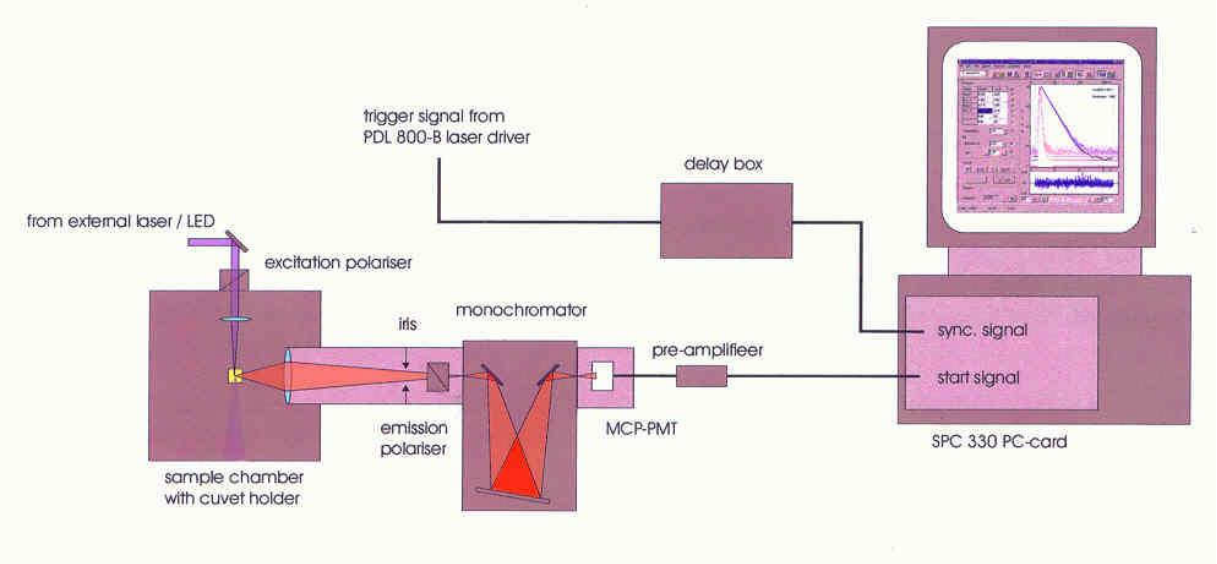

Figure 2.12: TCSPC instrumentation setup

The acquisition of fluorescence decay curves by means of Time corelated Single Photon Counting system (TCSPC) provides resolution and sensitivity of emission processes by histogramming arrival times of individual photons over many excitation and fluorescence cycles. TCSPC is a digital technique, counting photons, which are time-correlated to the excitation pulse. Central to this method is a time-to-amplitude converter (TAC), which is similar to a stopwatch. A pulsed light source is used to excite the sample with a high repetition rate (MHz). Each pulse starts the voltage ramp of the TAC either by an electronical trigger signal from the pulse unit of the excitation source or by optically monitoring the pulses with a fast-response photodetector. The voltage ramp is stopped, when the first fluorescence photon arrives. The TAC provides an output pulse, whose voltage is proportional to the time between the start and stop signals. A multi-channel analyser (MCA) converts this voltage to a time channel using an analog to digital converter (ADC). Recording photon arrival times for many pulses, the MCA builds up a probability histogram of counts versus time channels.

2.11.4 Fluorescence lifetime measurement

The time course of fluorescence intensity decays of CNBD was observed with a fluorescence spectrophotometer (Fluotime100, Picoquant, Berlin, Germany) using a pulsed LED (centre wavelength: 298 nm; pulse width: 550 ps) as excitation source. The fluorescence lifetime was reconstructed by repetitive measurements of the time between the excitation pulse and an emitted photon using time-correlated single-photon counting (TCSPC; Kaneko et al., 2002). The time resolution was below 500 ps.

Decay curves were analyzed with Fluofit4 (Picoquant, Berlin, Germany) using:

$$I_t = \sum_{i=1}^{2} A_i * e^{\frac{-t}{\tau_i}}$$

The average lifetime $\bar{\tau}$ is calculated as

$$\bar{\tau} = \frac{\sum_{i=1}^{2} A_i \tau_i}{\sum_{i=1}^{2} A_i}$$

3 Results

Recently, a number of cyclic nucleotide-activated ion channels have been identified in prokaryotic systems. Because prokaryotic proteins can be expressed with much higher yield compared to eukaryotic proteins, biochemical and biophysical studies of these ion channels have become possible. Such studies may further enhance our understanding of how cyclic-nucleotide binding leads to activation and opening of the ion channel pore.

3.1 The CNG channel from *Magnetospirillum magnetotacticum* (mmCNG)

The mmCNG protein is a K^+-selective channel cloned from the magnetotactic bacterium *Magnetospirillum magnetotacticum* (see Appendix section 6.1 for amino-acid sequence of the mmCMG protein). I first worked on establishing the heterologous expression of the mmCNG channel in *E.coli.* The experiments included the selection of a suitable bacterial strain, testing various temperatures and expression time and optimizing the induction protocol. Subsequently, I tested various detergents to solubilize the protein from the bacterial membrane.

3.1.1 Expression of mmCNG in various *E.coli* strains

The first set of experiments focused on identifying a suitable strain and temperature for the expression of the mmCNG protein. Four different *E.coli* strains were transformed with pET11a-mmCNG. The pET11a-mmCNG vector adds the coding sequence for a hexahistidine $(His)_6$ tag to the 3' region of the mmCNG gene to facilitate identification and purification of the expressed gene product. The bacterial strains used in experiments were RIL, RP, BL-21, and Rossetta (section 2.1.1). The cells were grown in 100 ml LB-Amp medium at 37^{o}C until it attained an OD_{600} of ~ 0.6. The cells were then induced by the addition of 1 mM IPTG and subsequently grown at 20^{o}C or 30^{o}C for four hours. Induced and uninduced cells were lysed by bath sonication. Proteins were separated on a 10% SDS-gel and transferred to a PVDF membrane for western blotting. The membrane was incubated with an anti-His antibody. Figure 3.1 A and B shows the results of this experiment. The mmCNG protein runs at 37 kDa (see lower arrow in Figure 3.1), while the expected M_w was 48 kDa. Additionally, a band at 67 kDa was very prominent (upper arrow). Possibly, this

band represents a mmCNG dimer. For both temperatures tested, RIL (lanes 3 and 4) was the strain that produced the mmCNG protein best.

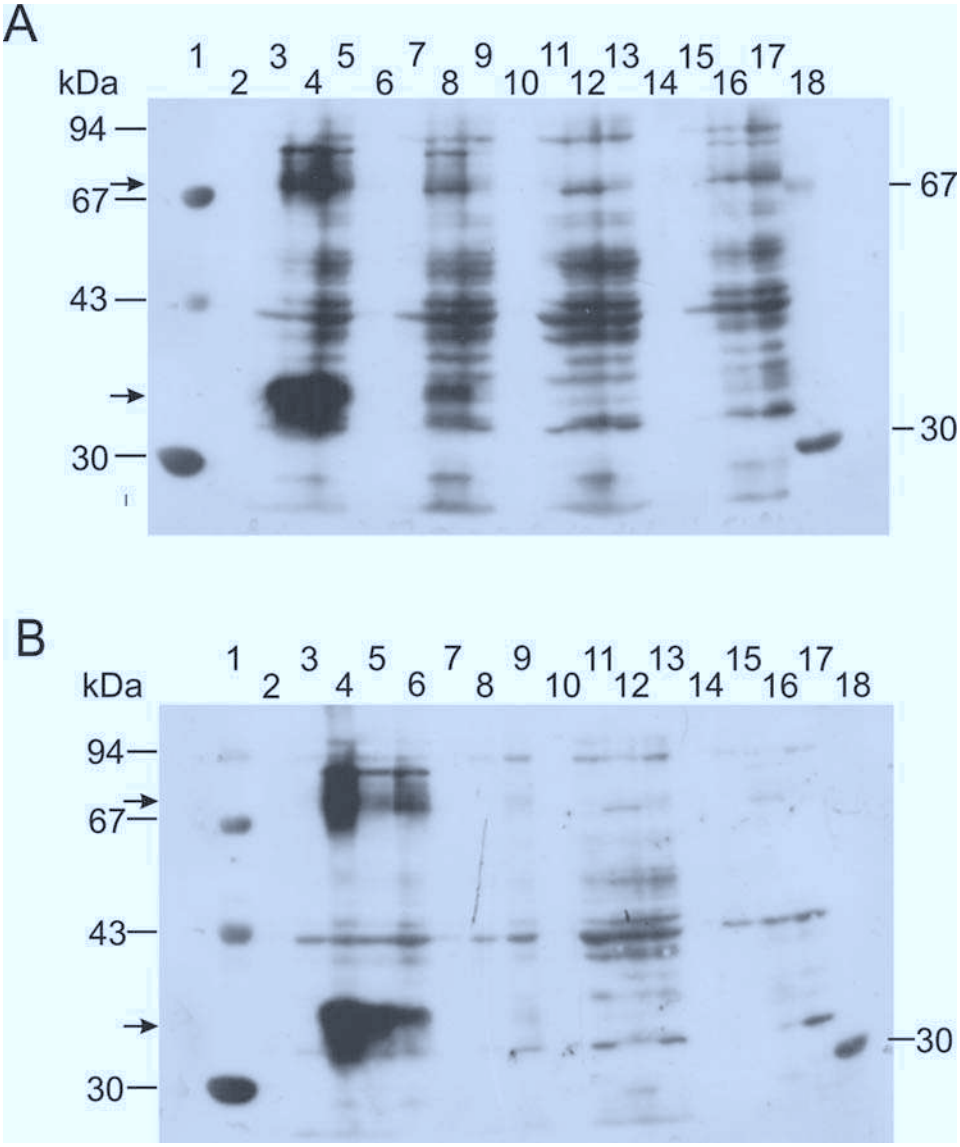

Figure 3.1: Heterologous expression of the mmCNG protein in several *E.coli* strains at two different temperatures.
(A) Western blot showing the expression of the mmCNG protein in several *E.coli* strains at 20°C.
(B) Western blot showing the expression of the mmCNG protein in several *E.coli* strains at 30°C.
Lane 1 - LMW, lanes 2 to 5 - RIL lysate, lane 2 - uninduced cell pellet, lane 3 - uninduced cell supernatant lane 4 - induced cell pellet in A (induced cell pellet in B), lane 5 - induced cell supernatant in A (induced cell pellet in B), lanes 6 to 9 - Strain Codon plus RP lysate, lane 6 - uninduced cell pellet, lane 7 - uninduced cell supernatant, lane 8 - induced cell pellet, lane 9- induced cell supernatant, lanes 10 to 13 - BL-21 pLysE, lane 10 - uninduced cell pellet, lane 11 - uninduced cell supernatant, lane 12 - induced cell pellet, lane 13 - induced cell supernatant, lanes 14 to 17- Rossetta, lane 14 - uninduced cell pellet, lane 15 -uninduced cell supernatant, lane 16 - induced cell pellet, lane 17 - induced cell supernatant, lane 18 - LMW. The arrows denote the mmCNG protein. The primary antibody used in the preparation of the western blot was an anti-His antibody.

3.1.2 Varying the IPTG concentration for induction

The next step was to systematically vary the IPTG concentration for the induction of RIL cells. Three different IPTG concentrations (0.6, 0.8, and 1 mM) were tested on cells grown to OD_{600} ~ 0.6 at 37°C. Following induction, cells were grown at 20°C for four hours. The expression was tested by western blotting of proteins from the cell lysate and probing the blot with an anti-His antibody (Figure 3.2). The two arrows in Figure 3.2 indicate the monomeric and the putative dimeric form of the protein on an SDS gel. Induction at 0.6 and 0.8 mM IPTG shows only a small difference of protein expression. Induction by1 mM shows somewhat higher expression of the mmCNG protein.

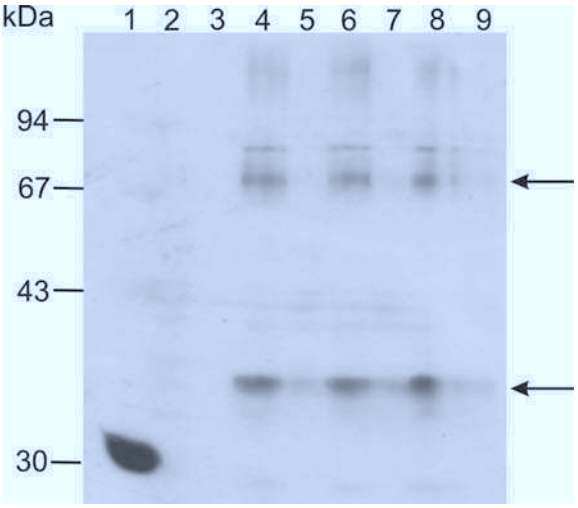

Figure 3.2: Expression of mmCNG in *E.coli* RIL codon plus by varying the concentration of IPTG. Lane 1 - LMW, lane 2 - uninduced pellet, lane 3 - uninduced supernatant, Lane 4 and 5 - pellet and supernatant of 0.6 mM IPTG induced culture, lane 6 and 7 - pellet and supernatant of 0.8 mM IPTG - induced culture, lane 8 and 9 - pellet and supernatant of 1 mM IPTG - induced culture. The arrows denote the mmCNG protein.

3.1.3 Varying the expression time

I next studied the expression of the mmCNG protein by varying the time following induction by IPTG. The cells were grown at 20°C after induction. The expression time was varied from 1 h up to 10 h. Figure 3.3 shows the western blot of this experiment. The two arrows again mark the position of the monomer and of the putative dimer band of mmCNG. With time, an increase in the expression of the mmCNG protein was observed. The highest expression level was observed 7 h after IPTG induction (lanes 11, 12. Figure 3.3). For longer expression times (t > 7 h), the level of mmCNG protein decreased. In addition, other bands appeared for long expression times. These

bands may represent degraded products of mmCNG. Alternatively, other endogenous proteins of the host strain may be expressed at higher levels that show cross-reactivity with the anti-His antibody. In either case, such large expression times may render the sample more heterogeneous. Therefore, the expression was stopped after seven hours of induction.

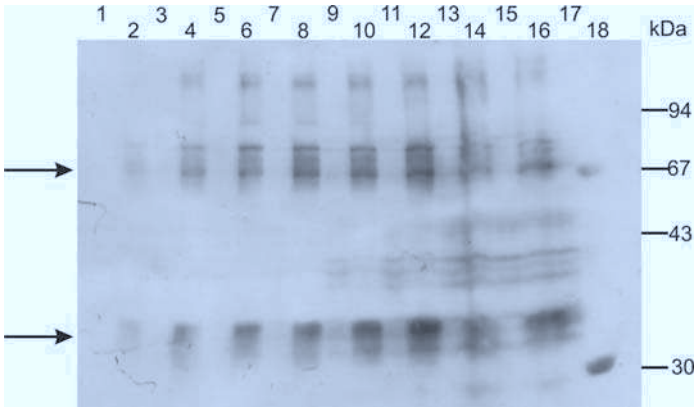

Figure 3.3: Expression of the mmCNG protein in *E.coli* RIL with time: Odd-numbered lanes are that of cell supernatant, while the even numbered were loaded with cell pellet. Lanes 1 and 2 - 1st h, lanes 3 and 4 - 2nd h, lanes 5 and 6 - 4th h, lanes 7 and 8 - 5th h, lanes 9 and 10 - 6th h, lanes 11 and 12 - 7th h, lanes 13 and 14 - 8th h, lanes 15 and 16 - 10th h after induction, lane 17 - empty lane, lane 18 - LMW. The arrows denote the mmCNG protein.

3.1.4 Testing various detergents and fine tuning the detergent concentration for maximal extraction of mmCNG

A battery of detergents was tested in order to solubilize the channel from the bacterial cell membrane. The different detergents that were tested were CHAPS, OGP, DM, DDM, and Tx-100 (Figure 3.4). After three hours of solubilization short-chain detergents like CHAPS and OGP (lanes 3 and 4, and 11 and 12, respectively) solubilize less protein in comparison to the longer chained detergents like DM (lanes 7 and 8) and DDM (lanes 9 and 10). Tx-100 also solubilized the mmCNG protein quite well (lanes 13 and 14).

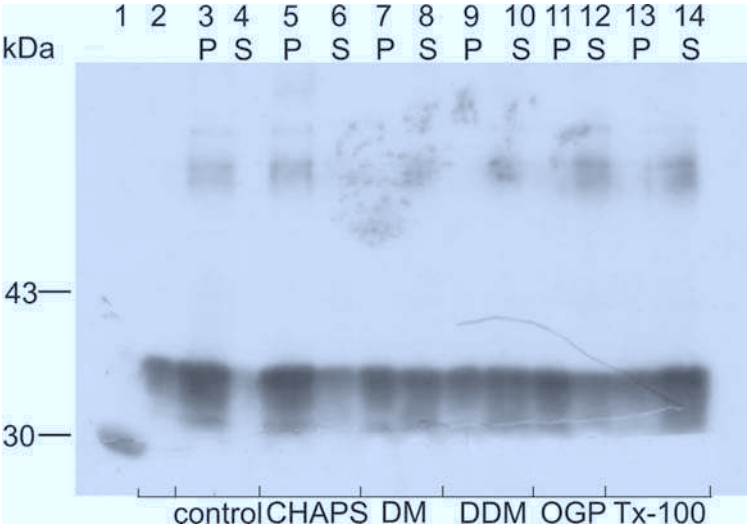

Figure 3.4: Solubilization of the mmCNG protein by testing several detergents. Lanes are marked according to the detergents used for solubilizing mmCNG.
Lane 1- LMW, lane 2 - cell lysate, lanes 3 and 4 - control (no detergent), lanes 5 and 6 - 40 mM CHAPS-treated sample, lanes 7 and 8 - 40 mM DM-treated sample, lanes 9 and 10 - 40 mM DDM treated sample, lanes 11 and 12 - 40 mM OGP-treated sample, lanes 13 and 14 - 2% Tx-100-treated sample. Lanes that contain pellet following detergent solubilization are marked P; while the lanes contain supernatant following the detergent treatment are marked S.

I continued to test different concentrations of the long-chain detergents to solubilize the mmCNG protein. Figure 3.5 A shows a western blot after solubilization of the mmCNG protein with varying concentrations of DM and DDM. Figure 3.5 B shows the respective experiment with different concentrations of Tx-100. The detergent of choice for mmCNG solubilization appears to be DDM. In most of the conditions using DDM, the relative percentage of the mmCNG protein was higher in the supernatant than in the pellet, indicating good solubilization.

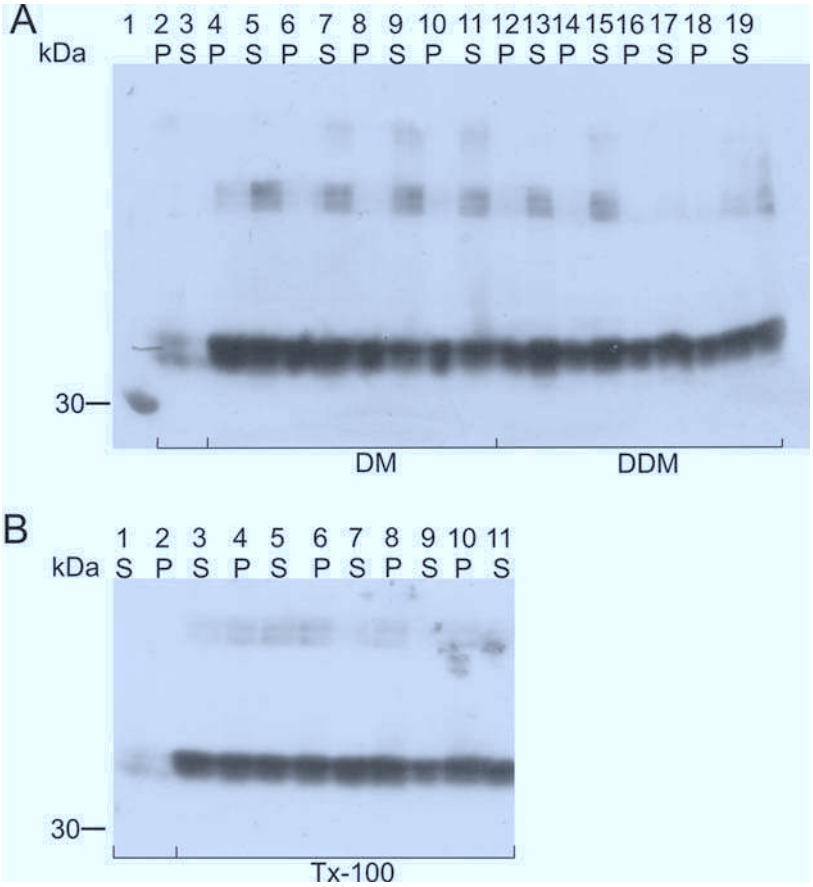

Figure 3.5: Solubilization of the mmCNG.protein by testing several detergents. Lanes are marked according to the detergents used for solubilizing mmCNG.
(A) Lane 1 - LMW, lane 2 - cell pellet, lane 3 - cell supernatant. Lanes marked under DM were samples in which mmCNG solubilized in varying concentrations of DM, lanes 4 and 5 - 10 mM DM , lanes 6 and 7 - 20 mM DM, lanes 8 and 9 - 40 mM DM, lanes 10 and 11 - 70 mM DM. Lanes marked under DDM were samples in which mmCNG was solubilized in varying concentrations of DDM, lanes 12 and 13 - 10 mM DDM, lanes 14 and 15 - 20 mM DDM, lanes 16 and 17 - 40 mM DDM, lanes 18 and 19 - 70 mM DDM. Lanes that contain pellet following detergent solubilization is marked P; while the lanes that contain supernatant following the detergent treatment are marked S.
(B) Lanes 1 and 2 - controls (prior to detergent treatment). Lanes marked under Tx-100 were samples in which mmCNG solubilized in varying concentrations of Tx-100. Lanes 3 and 4 - 0.5 %Tx-100, lanes 5 and 6 – 1 %Tx-100, lanes 7 and 8 - 2% Tx-100, lanes 9 and 10 - 3 % Tx-100. Lanes that contain cell pellet after detergent solubilization are marked P, while the lanes that contain supernatant following the detergent treatment are marked S.

The detergent concentration was fine tuned by using a wider range of detergent concentrations (Figure 3.6). There was hardly any difference between the different DDM concentrations tested to solubilize mmCNG. Concentrations of 10 and 20 mM DDM were sufficient. For further experiments, I decided to use 20 mM DDM to extract the mmCNG protein from the cell pellet.

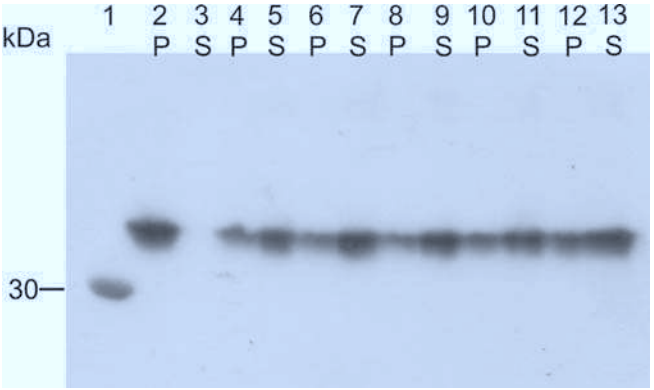

Figure 3.6: Optimization of DDM solubilization of mmCNG. Lane 1 - LMW, lanes 2 and 3 - control (prior to detergent treatment), lanes 4 and 5 - 5 mM DDM, lanes 6 and 7 – 10 mM DDM, lanes 8 and 9 - 20 mM DDM, lanes 10 and 11 - 40 mM DDM, lanes 12 and 13 - 70 mM DDM. Lanes that contain pellet following detergent solubilization are marked P. The lanes, which contain supernatant following the detergent treatment, are marked S.

3.1.5 Purification of the mmCNG protein

The mmCNG protein carries a C-terminal hexahistidine $(His)_6$ tag. It was purified on a Co^{2+}-affinity column on an Aekta FPLC system. Figure 3.7 A shows the entire sequence of the purification procedure including loading, washing off non-specifically bound proteins, and elution of bound protein with imidazole. Figure 3.7 B shows the elution profile of the mmCNG protein on an expanded scale. A two-step elution protocol was used. In the first step, the concentration of imidazole was raised from 20 to 125 mM to remove non-specifically bound protein. Next, the concentration of imidazole was increased to 500 mM in order to elute the bound protein. Figure 3.7 C shows the western blot of this experiment. Most of the mmCNG protein was found in the fractions in the second peak between 153 ml to 159 ml of the elution profile (Figure 3.7, lanes 13-18).

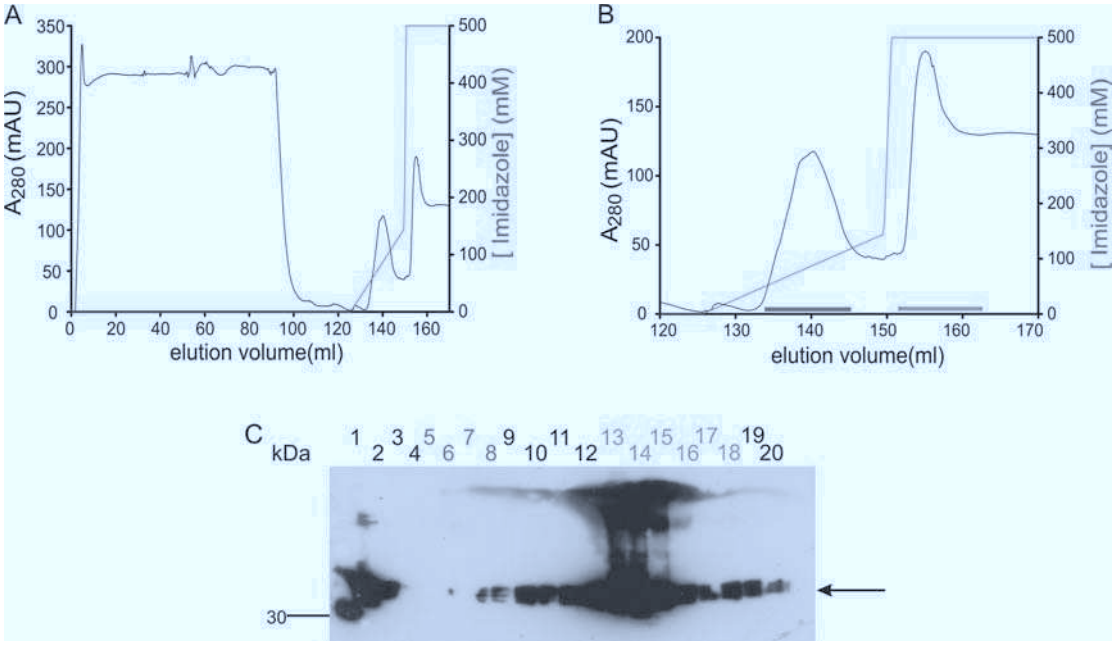

Figure 3.7: Purification of the mmCNG protein on Co^{2+}-His-trap affinity column. (A) Chromatogram of mmCNG purification on the affinity column. The black trace depicts the absorbance at 280 nm, while the red trace depicts imidazole concentration.
(B) Resized image of part A showing the elution profile of mmCNG on the Co^{2+}-His-trap affinity column by increasing the imidazole concentration.
(C) Western blot of several fractions from the mmCNG purification; Lane 1 - LMW, 2 - load; lanes 5 to 8 - non-specefically bound proteins eluted by raising imidazole concentration from 20 to 125 mM, lanes 13 to 18 - mmCNG eluted at ~ 500 mM imidazole. The arrow denotes mmCNG protein. The primary antibody used in the preparation of the western blot was anti-His mouse antibody. The gel lanes are colour coded according to the fractions collected after elution (see part B)

For further characterization, the eluted protein was concentrated using centricon 100 (Amicon) and loaded on a gel-filtration column. The profile of gel filtration showed three major peaks (Figure 3.8 A). The mmCNG protein eluted between 10 - 14 ml (as seen on the western blot, Figure 3.8 B) and had a rather broad distribution. The gel-filtration profile is indicative of a heterogeneous sample.

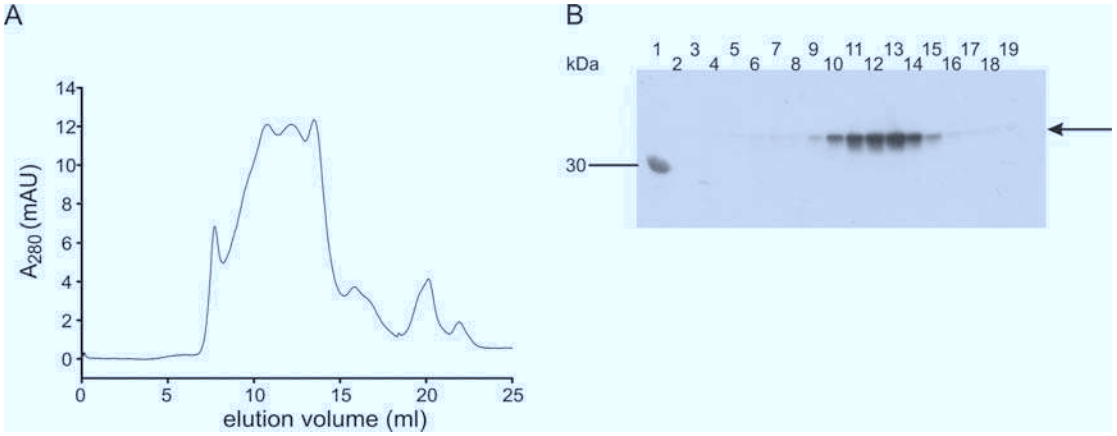

Figure 3.8: Chromatogram of the mmCNG protein on gel filtration Superdex 200 analytical grade column.
(A)The mmCNG protein elutes between 10 - 14 ml (as inferred form the SDS-Gel in(B)) and can be observed to elute in all fractions collected from the column. The arrow denotes mmCNG protein. The primary antibody used in the preparation of the western blot was anti-His antibody.

3.1.6 Tetrameric state of the mmCNG protein

In the western blots of the mmCNG protein, usually a second band appeared that may be a dimeric population of the mmCNG protein. I performed cross-linking experiments with the purified mmCNG protein to determine its oligomeric structure. Figure 3.9 A and B shows the appearance of cross-linked species at various times after addition of the cross-link reagents BS^3 (0.25 μM) or BMDB (0.25 μM). Figure 3.9 A and B reveal that in addition to the apparent monomer and dimer band, two bands of higher molecular weight (M_w) are observed. The M_w of these bands are 95.3 kDa, and 129.5 kDa. While cross-linking with the BMDB did not change the band pattern appreciably (Figure 3.9 A), treatment with BS^3 resulted in an increase in the intensity of the apparent dimer, trimer, and tetramer bands. Higher bands were not observed.

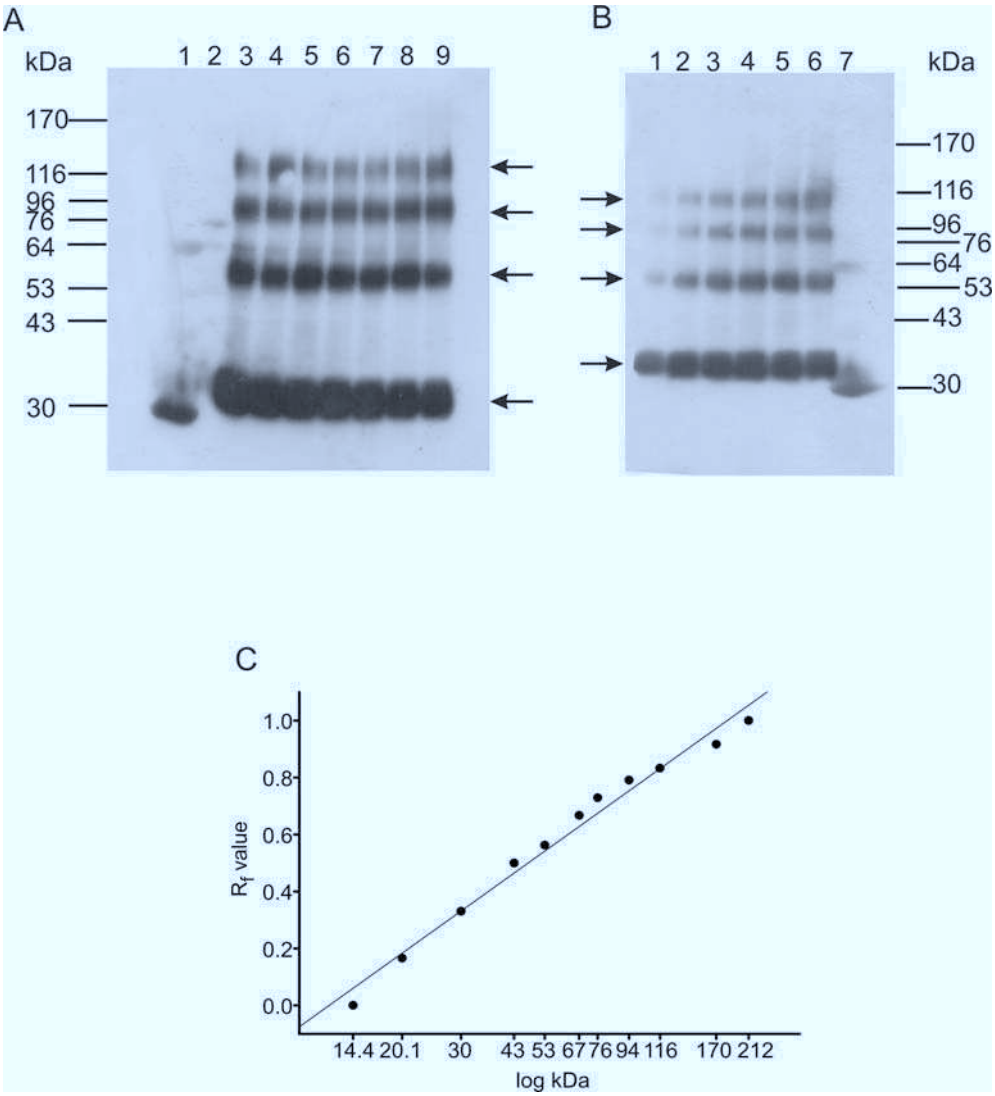

Figure 3.9: Cross-linking experiments to study oligomerization reveals that mmCNG exists as a tetramer.
(A) Carboxy-specific cross-linking of the mmCNG protein. Lane 1 - LMW, lane 2 - HMW (High M_w marker) Purified protein (lane 3 - control) prior to 0.25 μM BMDB treatment. Lanes 4 - 9 contain the mmCNG protein treated with BMDB. Lane 4 - mmCNG treated with BMDB; the reaction was immediately stopped, therefore it is considered as time 0, unlike sample in lane 3 where no cross-linker was added. The cross-link reaction was stopped after different incubation times (5, 10, 15, 30, and 60 min). The subsequent lanes contain samples in an increasing order of incubation time of the mmCNG protein with BMDB. The arrows indicate the position of the mmCNG protein.
(B) Amino-specific cross-linking of mmCNG, Purified protein (lane 1, control - mmCNG with no added cross-linker) was incubated with 0.25 μM BS^3 (lanes 2-6). The crosslink reaction was stopped after different incubation times (1, 5, 10, 30, and 60 min). Lane 7 - LMW. The arrows indicate the position of the mmCNG protein.
(C) The calibration curve was generated by plotting the relative mobility (R_f) of the molecular weight standards versus the logarithmic functions of their molecular mass (log kDa) of the standard. The molecular weight of mmCNG was computed by analyzing the calibration curve.

This result suggests that the mmCNG protein adopts a tetrameric structure. The expected M_w of a dimer, trimer, and tetramer are 95.6 kDa, 143.4 kDa, and 191.2 kDa, respectively. Differences between apparent and predicted M_w may result

from the moderate anomalous electrophoretic mobility of the protein and intra-subunit cross-links (Raab-Graham and Vandberg, 1998, Weitz *et al* 2002).

3.2 The CNG channel from *Trichodesmium erythraeum* (teCNG)

I followed a similar approach tuning teCNG expression testing host strains, temperature, induction protocol, and various detergents to solubilize the protein from the host cell membrane.

3.2.1 Expression of teCNG in various *E.coli* strains

I started with selecting the *E.coli* strain best suited to express teCNG protein. I worked with four different strains - RIL, RP, Rosetta, and BL-21. With the exception of BL-21, all strains showed robust expression of teCNG. The teCNG protein runs at a molecular weight (M_w) of ~ 43 kDa which is lower than the calculated M_w of 52 kDa. A large cleaved product was observed at 30 kDa. The cleavage appears to be prominent at 30^{o}C. Expression of the protein was slightly better at 20^{o}C (Figure 3.10 A) than at 30^{o}C (Figure 3.10 B). Therefore, for subsequent experiments, cells were grown at 37^{o}C until they reached an OD_{600} of ~ 0.6, and were then induced with 1 mM IPTG and grown at 20^{o}C for four hours. The strain chosen for most of the experiments was Rossetta. For some experiments mentioned below, teCNG was purified from RIL as well.

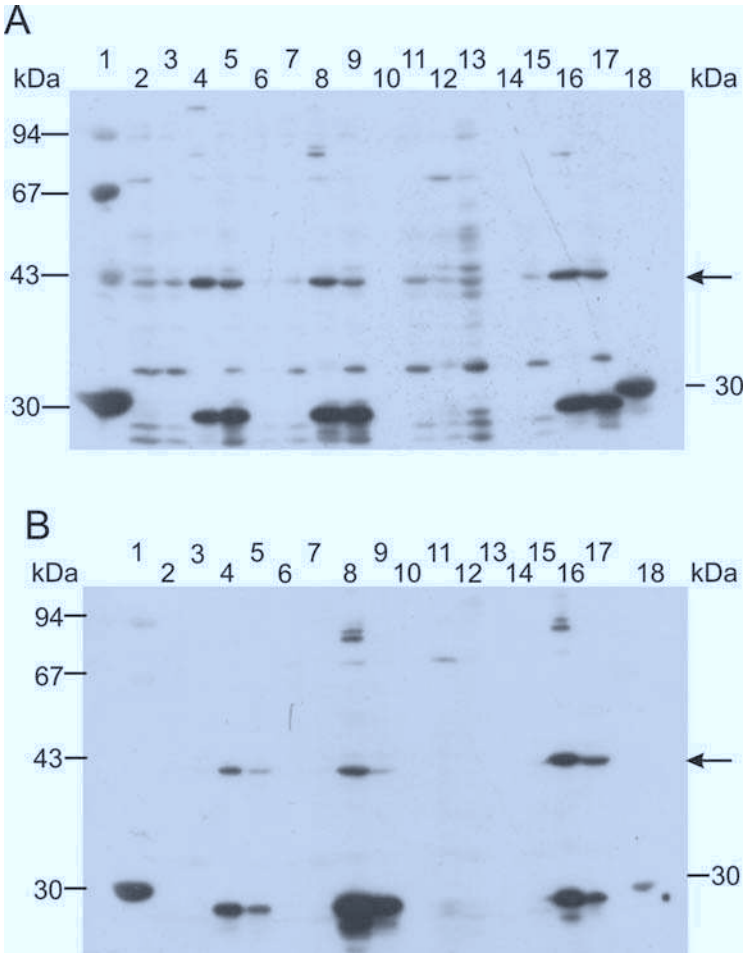

Figure 3.10: Heterologous expression of teCNG in several *E.coli* strains at two different temperatures
(A) Blot showing the expression of teCNG in several *E.coli* strains at 20°C.
(B) Blot showing the expression of teCNG in several *E.coli* strains at 30°C.
Lane 1 - LMW, lanes 2 to 5 - RIL lysate, lane 2 - uninduced cell pellet, lane 3 - uninduced cell supernatant, lane 4 - induced cell pellet, lane 5 - induced cell supernatant, lanes 6 to 9- RP lysate, lane 6 - uninduced cell pellet, lane 7 - uninduced cell supernatant, lane 8 - induced cell pellet, lane 9 - induced cell supernatant, lanes 10 to 13 - BL-21 pLySE, lane 10 - uninduced cell pellet, lane 11 - uninduced cell supernatant, lane 12 - induced cell pellet, lane 13 - induced cell supernatant, lanes 14 to 17- Rossetta, lane 14 - uninduced cell pellet, lane 15 - uninduced cell supernatant, lane 16 - induced cell pellet, lane 17 - induced cell supernatant, lane 18 - LMW. The arrow denotes teCNG. In all the conditions tested, the final IPTG concentration was 1 mM. The primary antibody used in the preparation of the western blot was anti-His antibody.

3.2.2 Varying the IPTG concentration for induction

Three different IPTG concentrations were tested: 0.6, 0.8, and 1 mM. The western blot revealed that 1 mM IPTG was best for the expression of teCNG in the *E.coli* Rossetta strain (Figure 3.11).

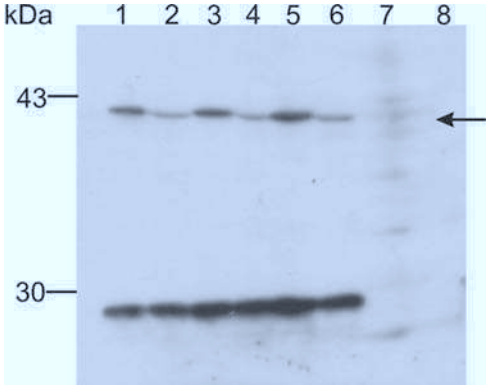

Figure 3.11: Expression of teCNG in *E.coli* Rosetta by varying the concentration of IPTG. Lanes 1 and 2- supernatant and pellet of 0.6 mM IPTG induced culture, lanes 3 and 4- supernatant and pellet of 0.8 mM IPTG induced culture, lanes 5 and 6- supernatant and pellet of 1mM IPTG induced culture, lanes 7 and 8 - uninduced supernatant and pellet.

3.2.3 Solubilization of teCNG

Several long-chain and short-chain detergents were tested to solubilize the teCNG protein expressed in Rosetta. The detergents used were CHAPS, DM, DDM, OGP, and Tx-100 (Figure 3.12 A and B). The teCNG protein is difficult to solubilize from the membrane: For all detergents tested, I found more teCNG protein in the pellet than in the supernatant. Possibly, part of the protein may be present in inclusion bodies. The protein showed a slightly better extraction in DM in comparison to other detergents used.

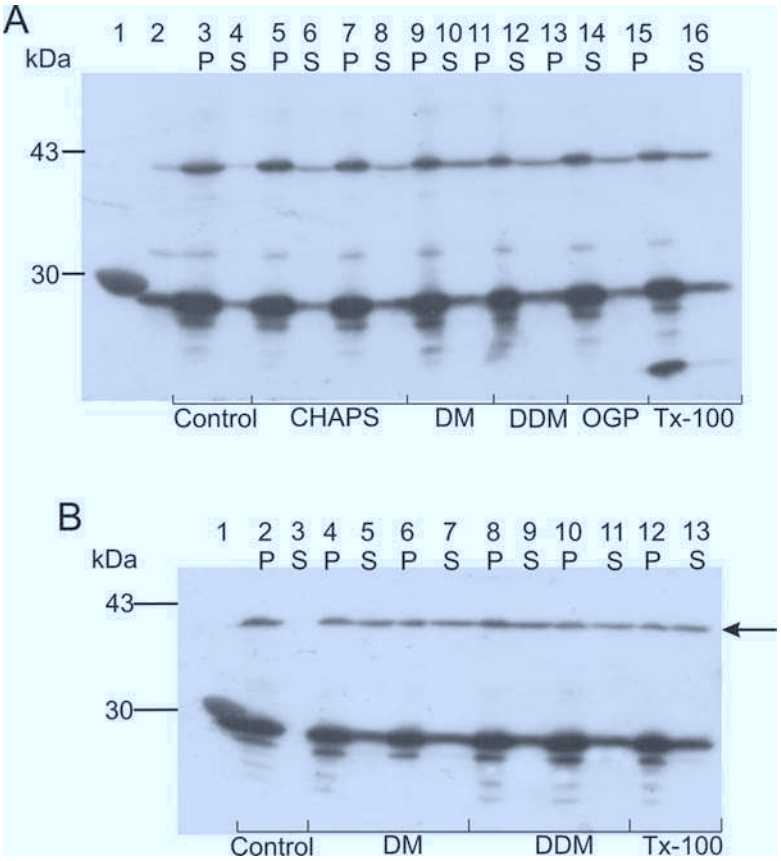

Figure 3.12: Optimization of protein purification by trying several detergents to solubilize teCNG. Lanes is marked according to the detergents used for solubilizing teCNG.
(A) Lane 1 - LMW, lane 2 - Cell lysate, lanes 3 and 4 - Control (no detergent), lanes 5, 6, 7 and 8 - 40 mM and 80 mM CHAPS treated sample, C - 40 mM DM treated sample, D - 40 mM DDM treated sample, lanes 9 and 10 - 40 mM OGP treated sample, lanes 11 and 12 - 2%. Tx-100 treated sample. Lanes that contain pellet following detergent solubilization is marked P; while the lanes that contain supernatant following the detergent treatment is marked S.
(B) Lane 1 - LMW, lanes 2 and 3- control, lanes 4, 5 , 6 and 7 - 10 and 40 mM DM, lanes 8, 9, 10, and 11 - 10 and 40 mM DDM, lanes 12 and 13 - 2% Tx-100. Lanes that contain pellet following detergent solubilization is marked P; while the lanes that contain supernatant following the detergent treatment is marked S.

Figure 3.13 shows solubilization of the mmCNG protein, expressed in either Rossetta or RIL, with various concentrations of DM. While Rossetta expressed more mmCNG protein, it seems that it is easier to solubilize the protein from RIL; i.e. more mmCNG protein was present in the supernatant (see lanes 10 - 19).

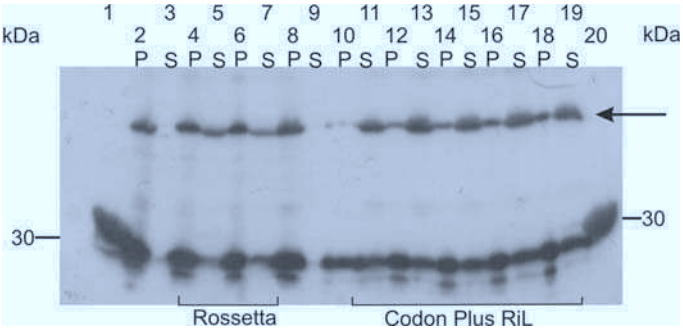

Figure 3.13: Optimization of protein purification by trying varying DM concentration to solubilize teCNG from two different bacterial strains. Lane 1-LMW, lanes under Rossetta are samples of teCNG protein solubilized from *E.coli* Rossetta cells. Lanes 2 and 3 - Controls, lanes 4 and 5 - 10 mM DM, lanes 6 and 7 - 40 mM DM.
The teCNG protein solubilized from *E.coli* codon plus RIL cells are marked under Codon plus RiL. Lanes 8 and 9- control, lanes 10 and 11 5mM DM, lanes 12 and 13- 10 mM DM, lanes 14 and 15- 20 mM DM, lanes 16 and 17- 40 mM DM, lanes 18 and 19- 70 mM DM, lanes 20-LMW. The lanes that contain pellet following detergent solubilization are marked P, while the lanes that contain supernatant following the detergent treatment are marked S.

3.2.4 Purification of the teCNG protein

The teCNG protein carried a C-terminal $(His)_6$ tag. The protein was purified on a Co^{2+}-affinity column. The chromatograms are shown in Figure 3.14 A and B. A two-step gradient was used. The first step was a continuous gradient of imidazole from 20 to 125 mM to remove non-specifically bound proteins from the column. Subsequently, a step gradient of 500 mM imidazole was used in order to elute the teCNG protein. It largely eluted at high imidazole concentrations, as one can visualize from the western blot (lanes 12-15, Figure 3.14 C). Lanes 13-18 correspond to the fractions eluted at 500 mM imidazole. The teCNG protein runs at an apparent M_w of 47 kDa (expected M_w is 54.5 kDa).

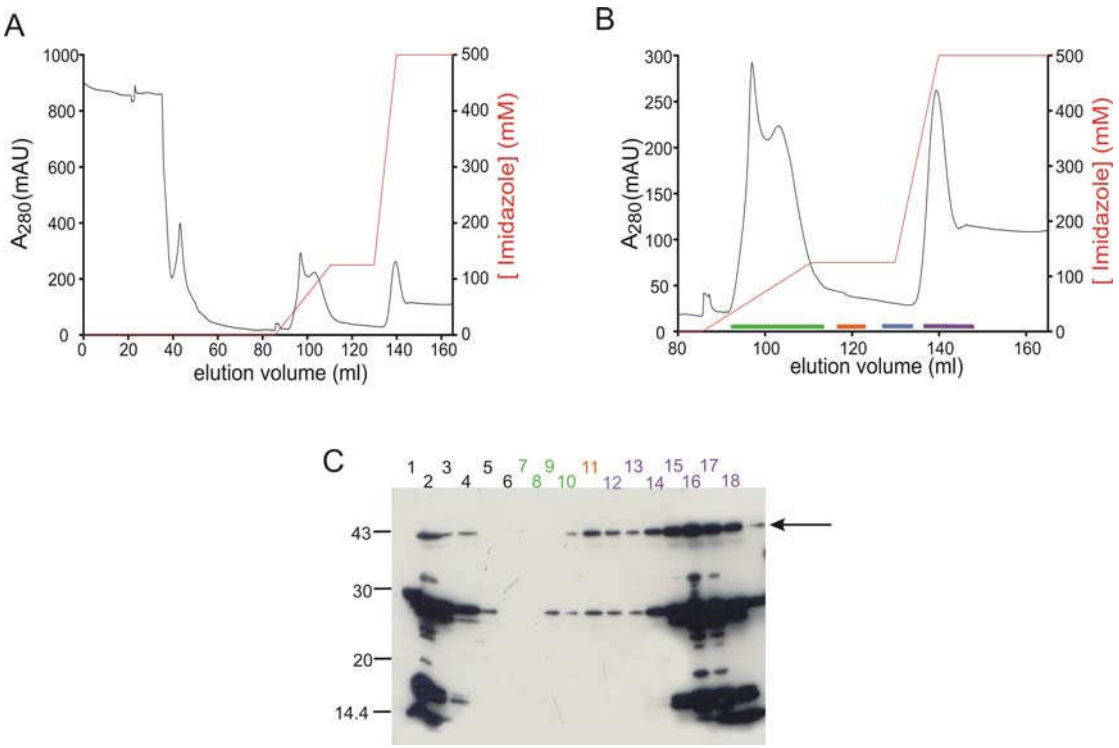

Figure 3.14: Purification of teCNG on Co^{2+}-His-trap affinity column. (A) Chromatogram of teCNG purification through the affinity column. The black trace depicts the absorbance at 280 nm, while the red trace depicts the imidazole concentration.
(B) Elution profile of teCNG through the Co^{2+}-His-trap affinity column by increasing the imidazole concentration.
(C) Western blot of several fractions from the teCNG purification; Lane 1 - LMW ; lane 2 - cell lysate supernatant; lane 3 - load; lane 4 - cell lysate pellet; lane 5 - wash; lanes 7 – 11 – non-specefically bound proteins eluted by raising the concentration of imidazole form 20 to 125 mM, lanes 13 to 18 - teCNG eluted at ~ 500 mM imidazole. Arrow denotes the teCNG protein. The primary antibody used in the preparation of the western blot was anti-His antibody. The gel lanes are colour coded according to the fractions collected after elution (see part B)

The eluted protein was passed over a gel-filtration column (Figure 3.15). One major peak and at least three minor peaks (shown in arrows) were observed.

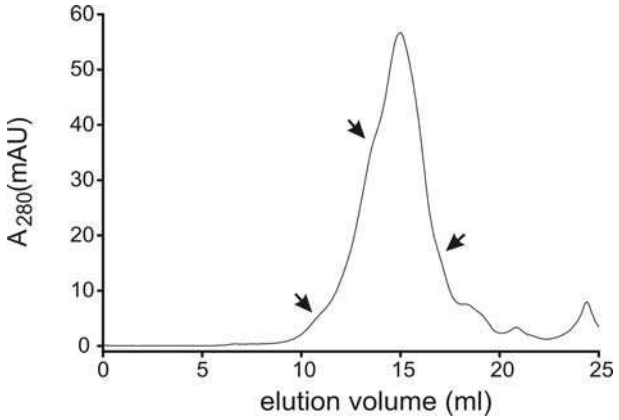

Figure 3.15: Chromatogram of the teCNG protein on gel-filtration Superdex 200 (analytical grade) column. The teCNG elutes between 14 and16 ml. The arrows indicate three minor peaks along with the major peak of teCNG protein.

3.3 The CNG channel from *Bradyrhizobium japonicum* (bjCNG)

The bjCNG protein is one of two CNG channels from the bacterium *Bradyrhizobium japonicum.* The parameters of expression and purification of the bjCNG protein were optimized by my colleagues W. Boenigk and K. Novak. The protein was best expressed in three *E.coli* strains (Figure 3.17). In this study, I expressed the bjCNG protein in the *E.coli* Rossetta strain. Cells were grown for four hours at 20°C following induction. The bjCNG protein was maximally extracted from Rosetta cells using 60 mM DM.

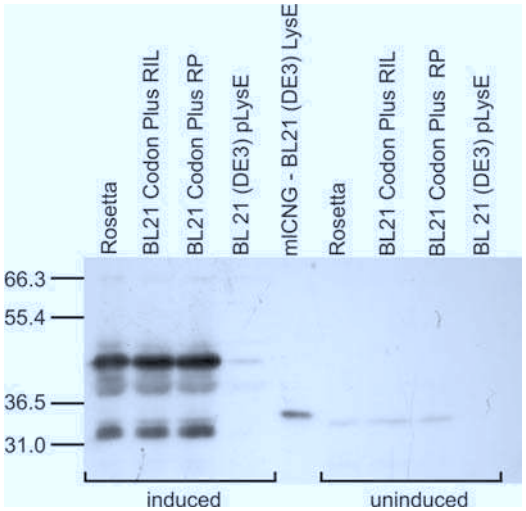

Figure 3.16: Expression of the bjCNG protein in different *E.coli* strains. **Left**: induction of cells with 1 mM IPTG. **Right**: uninduced cells. As a positive control, the mlCNG protein (Novak 2006) was expressed in *E.coli* BL-21 pLysE.

3.3.1 Purification of bjCNG protein

The bjCNG protein was purified on a Co^{2+}-affinity column as it carries a C-terminal $(His)_6$ tag. A two-step elution protocol was used to purify the protein from the Co^{2+}-affinity column. In the first step, the imidazole concentration was raised from 20 to 125 mM to elute non-specifically bound proteins from the column. Increasing the imidazole concentration to 500 mM resulted in elution of the protein (Figure 3.17 A and B). Figure 3.17 C shows the western blot of protein fractions collected during the purification procedure. The majority of protein in lanes 9 to 15 represents the bjCNG protein. It runs at 42 kDa, the expected M_w is 50.4 kDa.

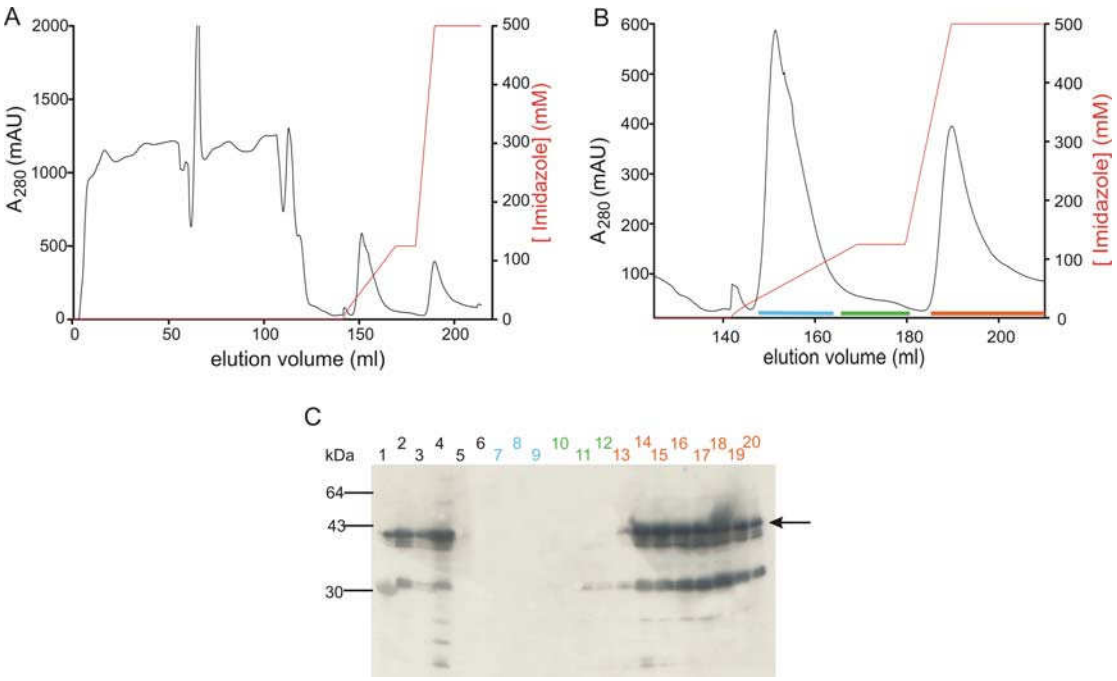

Figure 3.17: Purification of bjCNG on Co^{2+}-His-trap affinity column.
(A) Chromatogram of bjCNG purification through the affinity column. The black trace depicts the absorbance at 280 nm, while the red trace depicts the imidazole concentation
(B) Resized image of part A showing the elution profile of the bjCNG protein.
(C) Western blot of l fractions from bjCNG purifcation; Lane 1- LMW, lane 2 - cell lysate pellet, lane 3 - cell lysate supernatant, lane 4 - load, lane 5 - wash, lanes 7 to 12 – non-specefically bound proteins eluted by raising the imidazole concentration from 20 to 125 mM, lanes 13 to 15 - bjCNG eluted at ~ 500 mM imidazole. Arrow denotes the bjCNG protein. The primary antibody used in the preparation of the western blot was anti-His antibody. The gel lanes are colour coded according to the fractions collected after elution (see part B)

3.4 The CNG channel from *Mesorhizobium loti* (mlCNG)

The mlCNG protein was the first bacterial CNG channel to be cloned. Expression of the protein in *E.coli* was established by Novak (2006) and Grueter (2006). The mlCNG protein was expressed in the *E.coli* BL-21 strain. Cells were grown for four hours at 20^{o}C after induction. The mlCNG protein was solubilized from the bacterial membrane by 60 mM DM for two hours.

3.4.1 Purification of mlCNG protein protein

The solubilized protein was loaded on to a Co^{2+}-affinity column. It was eluted from the column by a two-step elution profile, similar to the one employed for the other prokaryotic CNG channels. In the first step, the imidazole concentration was raised from 20 to 125 mM to remove non-specifically bound proteins. In the next step, the

imidazole concentration was increased to 500 mM in order to elute the mlCNG protein (Figure 3.17 A, B, and C).

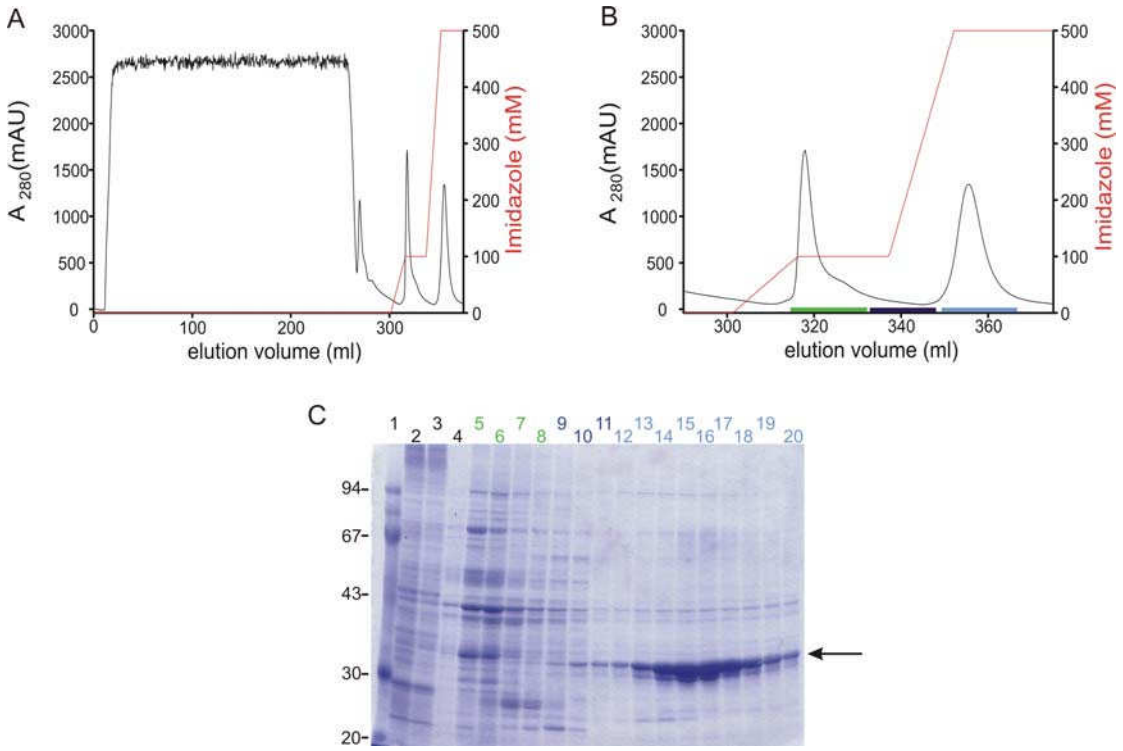

Figure 3.18: Purification of mlCNG on Co^{2+}-His-trap affinity column.
(A) Chromatogram of mlCNG purification through the affinity column. The black trace depicts the absorbance at 280 nm, while the red trace depicts imidazole concentation
(B) Resized image of figure A showing the elution profile of mlCNG through the Co^{2+}-His-trap affinity column by increasing the imidazole concentration.
(C) SDS-gel of fractions from mlCNG purifcation; Lane 1 - LMW, lane 2 - load, lane 3 - unbound fraction, lane 4 - wash, lanes 5 to 8- non-specifically bound proteins to Co^{2+}-His-trap affinity column eluted at ~ 100 mM imidazole, lanes 12 to 20 - mlCNG eluted at ~ 500mM imidazole. The arrow marks mlCNG. The gel lanes are colour coded according to the fractions collected after elution (see part B)

The mlCNG protein runs at a position corresponding to 32 kDa. The expected M_w of the protein is 39 kDa. The purified protein was subjected to gel-filtration chromatography to remove contaminant proteins (5%) and aggregated material. Figure 3.18 A and B shows a chromatogram of the mlCNG protein.

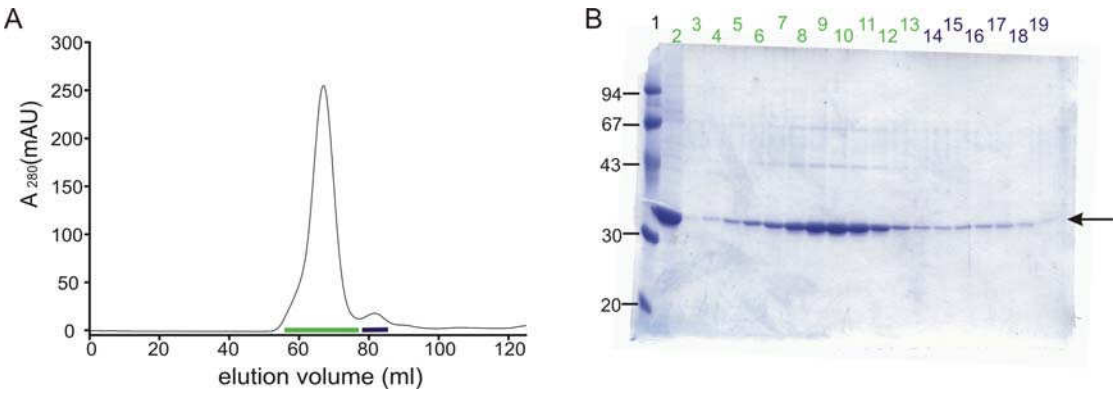

Figure 3.19: (A) Chromatogram of mlCNG on a gel filtration column (Superdex 200 analytical grade). The mlCNG protein elutes at 65 ml.
(B) SDS-gel of peak fractions of eluate from the gel-filtration column. The arrow indicates the mlCNG protein. The gel lanes are colour coded according to the fractions collected after elution (see part A)

3.5 Ligand binding assay

3.5.1 Ligand binding assay on prokaryotic CNG channels

I used the fluorescent 8-NBD-analogue of cAMP to study ligand binding to the purified prokaryotic CNG proteins.

The NBD ((2-((7-Nitro-4-benzofurazanyl)amino)ethyl)thio) group is a polarity sensitive molecule. It is largely non-fluorescent in aqueous solution and becomes fluorescent in a hydrophobic environment (Fery-Forgues *et al* 1993, 1996). This property of NBD group has been widely utilized in biophysical studies on lipids. 8-NBD-cAMP has been successfully used to study ligand binding of EPAC, which is an epithelial exchange factor that is activated by the binding of cAMP. The fluorescence of 8-NBD-cAMP was shown to increase ~ 6 fold upon binding to the CNBD of EPAC (Kraemer *et al* 2001).

I followed a similar approach to study ligand to the prokaryotic channel proteins. An increase in fluorescence after mixing the solubilized CNG channel protein (2 μM) with 8-NBD-cAMP (0.5 μM) may indicate binding of the ligand to the protein. To ascertain that an increase in fluorescence actually reflects the binding of 8-NBD-cAMP (0.5 μM) to the channel protein, 100 μM of cAMP was added. A decrease in signal would demonstrate competition of cAMP and 8-NBD-cAMP for the same binding site. Figure 3.20 A shows the relative fluorescence of 8-NBD-cAMP in the presence of the different channel proteins and in the absence or presence of non-fluorescent cAMP. Figures 3.20 B displays the men values of the data shown in part (A).

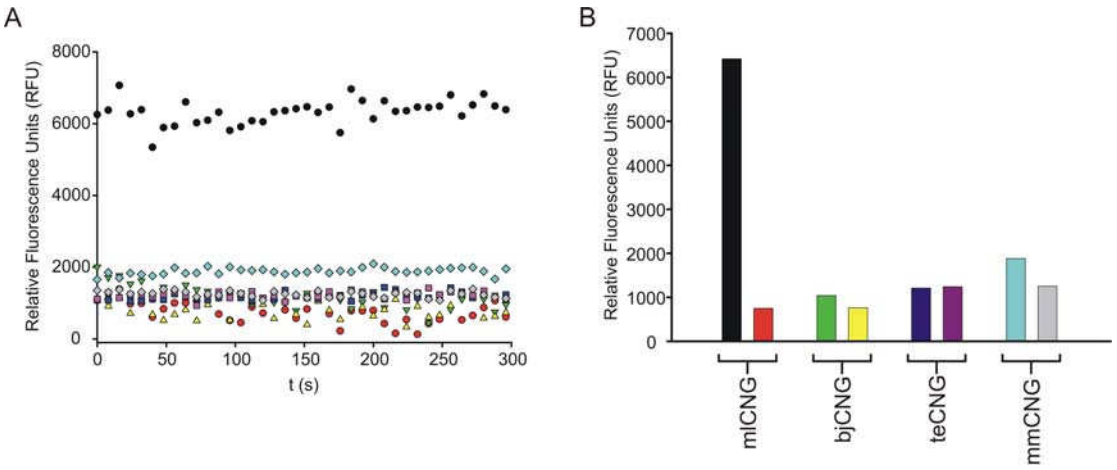

Figure 3.20: (A) Ligand binding experiments on the prokaryotic CNG channels using fluorescent analogue of cAMP. 8-NBD-cAMP binding of 0.5 µM 8-NBD-cAMP to 2 µM prokaryotic CNG channels, mlCNG (black circles), bjCNG (green triangle), teCNG (purple square), and mmCNG (cyan diamond).
100 µM cAMP was added to compete against the 8-NBD-cAMP binding to the prokaryotic channels. The traces from the competition experiments are shown for mlCNG (red circles), bjCNG (yellow triangle), teCNG (pink squares), mmCNG (grey diamond).
(B) The results of part A shown in a bar plot. The bars are colour coded in similar manner to part A.

The fluorescence intensity ratio I_{-cAMP}/I_{+cAMP} is 8.54 for the mlCNG protein, 1.36 for bjCNG channel, 0.98 for the teCNG channel and 1.51 for mmCNG protein. This may indicate that mlCNG is the only functional prokaryotic CNG protein capable of binding cAMP. However, one cannot rule out that cAMP co-purifies with the channel protein and prevents binding of 8-NBD-cAMP. It was shown that the mlCNG protein contains cAMP when purified and even the crystal structure of the isolated CNBD from mlCNG contained cAMP (Clayton *et al*, 2004). I performed reverse phase HPLC (RP-HPLC) to investigate, if cAMP was bound to the channel protein after purification. The proteins were denatured by using 5 % perchloric acid for 30 min. The samples were centrifuged and the supernatant was neutralized. It was then injected onto a RP-HPLC column. Only the mlCNG protein contained a significant amount of cAMP.

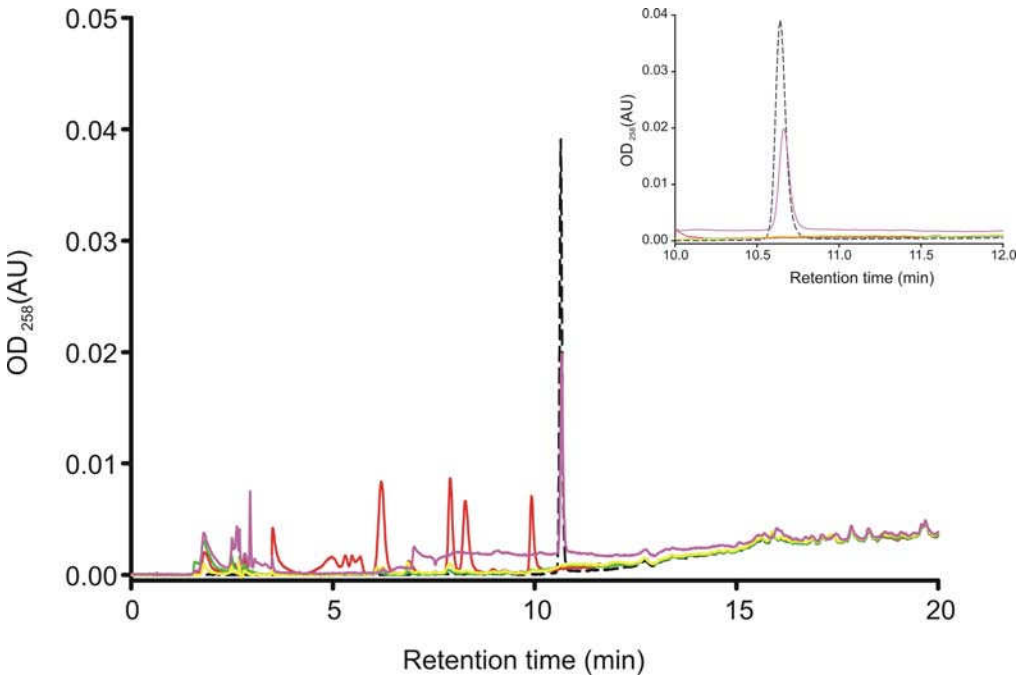

Figure 3.21: Reverse phase HPLC chromatogram on an RP C-18 column: Retention time of cAMP on the column is 10.65 min (black dotted trace) when a continuous methanol gradient from 0 -100 % in 20 min is applied. The concentration of cAMP was 20 nmoles. The supernatant after precipitation of 50 nmoles (mlCNG) or 200 nmoles (bjCNG, teCNG, and mmCNG) channel protein was loaded on the column. Shown are the chromatograms of samples from mmCNG (red), teCNG (yellow), bjCNG (green) and mlCNG (pink). Approximately 10 nmoles of cAMP was detected form the extract of mlCNG. The *inset* shows the cAMP peak detected from the mlCNG sample in comparison to the control run of cAMP.

3.5.2 Ligand-binding studies on mlCNG

The mlCNG channel displays robust fluorescence signal on binding of 8-NBD-cAMP and is, therefore, the most suited candidate for further biophysical and biochemical characterization. First, I determined the binding affinity of the channel for the fluorescent ligand 8-NBD-cAMP in quantitative terms. The mlCNG protein was rendered devoid of cAMP by competing binding with a high concentration of weak competitor (8-pCPT-cGMP) and subsequent extensive washing steps (Grueter 2006).

To a given protein solution (0.5 μM), I added increasing amounts of 8-NBD-cAMP and recorded fluorescence emission spectra from 490 nm to 650 nm. To account for the background fluorescence of 8-NBD-cAMP, I performed the same experiments in the absence of protein. These spectra were subtracted from the respective ones in the presence of protein. Figure 3.22 A shows the result of the titration. The binding of 8-NBD-cAMP to mlCNG resulted in a 7 fold increase of fluorescence intensity. Shown are mean normalized fluorescence values from 5 experiments. At low concentrations of 8-NBD-cAMP, the fluorescence increases linearly. The

fluorescence signal saturated at concentrations > 0.9 µM, indicating that all of the protein bound a ligand molecule. The data was analyzed using a simple binding model (Equation 2, section 2.11.2). The mean K_D value was 15.9 ± 2.7 nM.

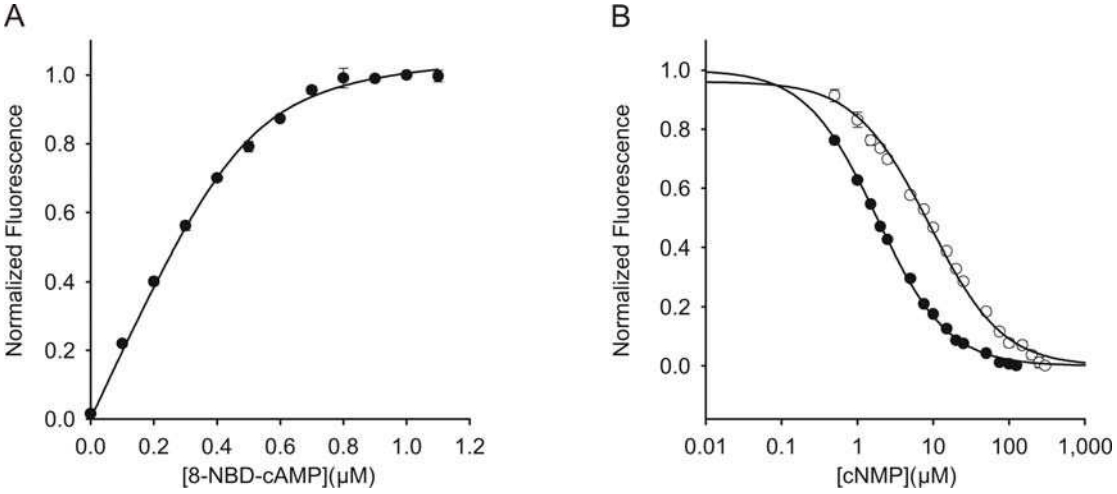

Figure 3.22: Ligand binding of the full-length mlCNG protein.
(A) Normalized increase of fluorescence of 8-NBD-cAMP on binding to mlCNG protein (0.5 µM). 8-NBD-cAMP fluorescence in the absence of the mlCNG protein was subtracted. The solid line represents non-linear least-squares fit to equation. 2. The K_D value was 17.3 nM.
(B) Competition between 8-NBD-cAMP (0.5 µM) and cAMP (closed circles) or cGMP (open circles) for binding to the mlCNG protein (0.3 µM). The solid lines represent non-linear least-squares fit to equation. 6. The K_D values were 71.3 nM (cAMP) and 363.9 nM (cGMP).

The binding of 8-NBD-cAMP to the mlCNG protein can be antagonized by incubation with non-fluorescent cyclic nucleotides. First, the mlCNG protein (0.3 µM) was saturated with 8-NBD-cAMP (0.5 µM) and the emission spectrum was recorded. Subsequently, increasing concentrations of non-fluorescent cNMP were added. At high cNMP concentrations (≥ 100 µM), decrease in fluorescence of 8-NBD-cAMP returned to baseline levels, demonstrating complete competition of cNMP and 8-NBD-cAMP for the same binding site. Figure 3.22 B shows the normalized dose-dependent inhibition of 8-NBD-cAMP binding by either cAMP or cGMP. We derived the binding affinity of cAMP and cGMP using equation 6, section 2.11.2. The K_D value was 81.6 ± 17.5 nM (n = 6) for cAMP and 320.7 ± 25.5 nM (n = 6) for cGMP.

3.5.3. Ligand binding to the isolated cyclic nucleotide-binding domain

Knowing the K_D value for ligand binding of the mlCNG channel is an important step towards understanding the complex interplay between binding and gating in CNG channels. The next step I took was to determine the binding affinity of the isolated cyclic nucleotide-binding domain, CNBD. The CNBD was originally constructed as a GST- fusion protein by Clayton *et al* (2004). The crystal structures of this construct in the presence of ligand as well as that of a mutant (R348A) with no ligand bound has been reported (Clayton *et al* 2004).

The CNBD was prepared as mentioned in Clayton *et al* (2004, see section 2.3.2.). The protein was expressed as a GST fusion protein with a thrombin cleavage site. It was purified on a glutathione affinity column. Following overnight treatment with thrombin, the protein was washed off the column, leaving the N-terminal GST bound to the column (Figure 3.23 A and B). The CNBD R348A mutant (referred to as R348A) was purified in a similar manner (Figure 3.24 A and D). Cyclic AMP co-purifies with the CNBD and HPLC analysis revealed that 80 – 90 % of the protein has cAMP bound after purification (Grueter, 2006). In contrast, R348A has no cAMP bound after purification.

To perform ligand binding experiments, it is necessary to obtain cAMP-free protein. This was accomplished by unfolding and refolding the CNBD protein (Figure 3.23 A and C; Novak 2006). HPLC analysis on the refolded CNBD (referred to as rCNBD) demonstrated that cAMP has been quantitatively removed.

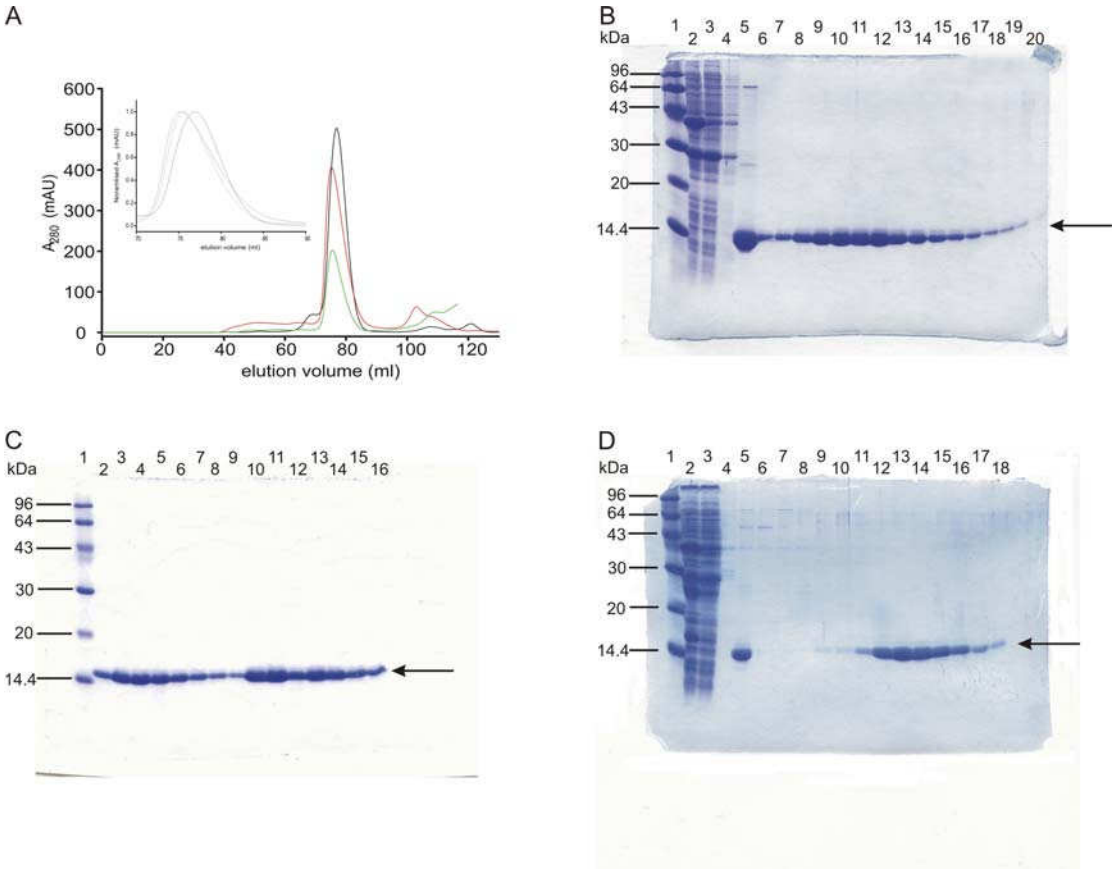

Figure 3.23: Purification of CNBD proteins:
(A) Gel filtration chromatogram of the CNBD proteins: purified cAMP containing CNBD (black) prior to refolding, cAMP free refolded CNBD (red) and R348A mutant (green) which when purified does not contain cAMP. (*Inset*) Normalized peaks of the individual chromatograms of the CNBD proteins depicting a shift in the elution volume of the cAMP bound CNBD in comparison to the cAMP free CNBD proteins. Samples from each purification step were analyzed on a 15% SDS-gel for all CNBD proteins.
(B) CNBD was purified by passing the *E.coli* cell lysate through a GST-affinity column. Lane 1-LMW; lane 2 - GST Load; lane 3 - flow-through; lane 4 - wash; lane 5 - eluate containing the CNBD; lanes 6 to 20 - Peak fraction (V_e ~ 80 ml).
(C)The purified cAMP containing was denatured using 6M GuCl and refolded by rapid dilution in the refolding buffer. Maximum 5ml of sample was loaded on Gel-filtration column per run. Lane 1-LMW; lanes 2 to 9 and lanes 10 to 17 - Peak fraction of the refolded cAMP free CNBD protein (V_e~75ml).
(D) Purification of R348A mutant, in a manner similar to the cAMP containing CNBD. Lane 1 - LMW; lane 2 - GST Load; lane 3 - flow-through; lane 4 - wash; lane 5 - eluate containing the CNBD; lanes 11 to 18 - Peak fraction (V_e ~ 75ml).

As for the full-length channel, I used the fluorescent analogue of cAMP, 8-NBD-cAMP, to study ligand binding to the CNBD and the R348A mutant.

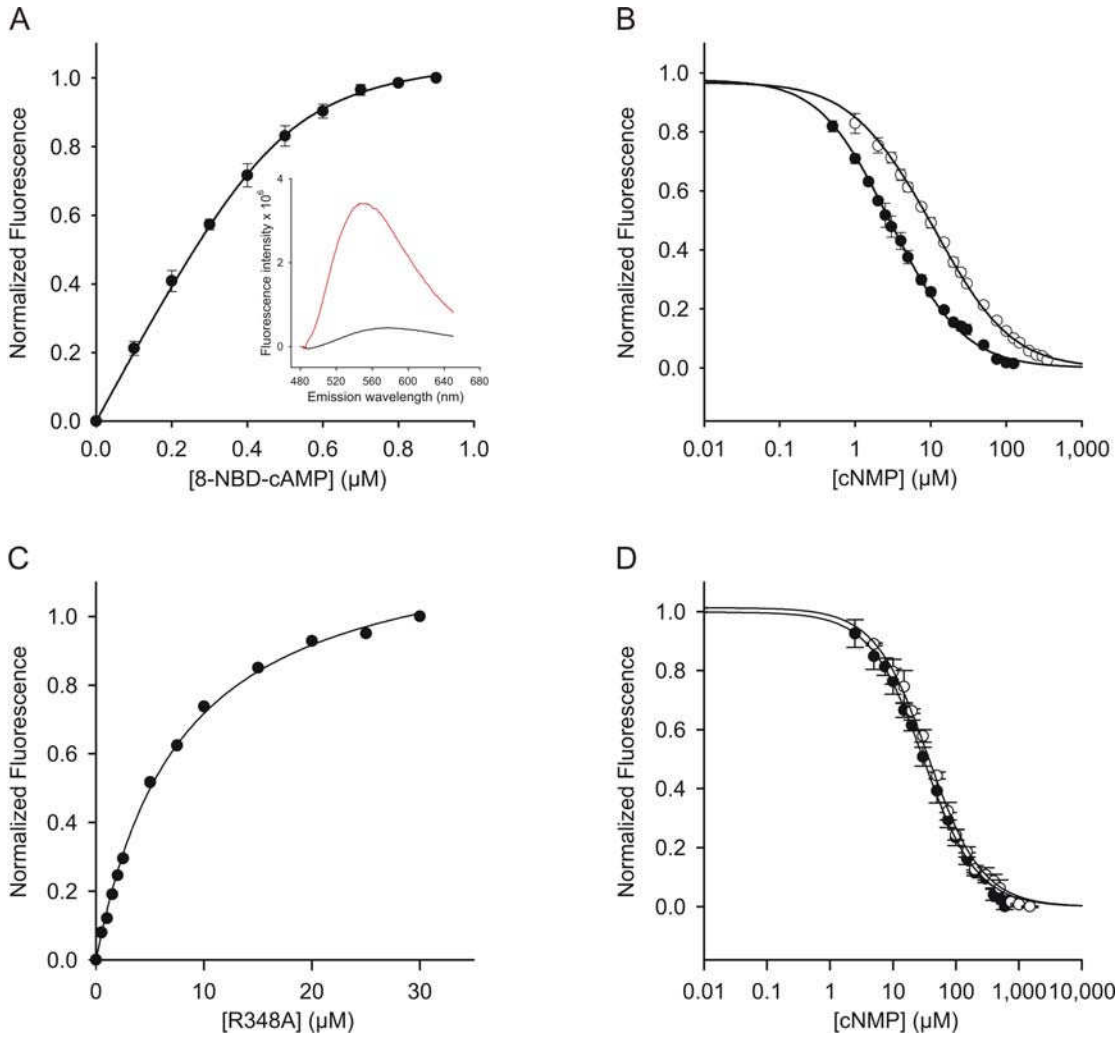

Figure 3.24: Ligand binding to the CNBD protein by fluorescence spectroscopy.
(A) Increase of 8-NBD-cAMP fluorescence (emission at 550 nm) on binding to the CNBD protein (0.5 µM). 8-NBD-cAMP fluorescence in the absence of the CNBD protein was subtracted. The solid line represents nonlinear least-squares The K_D value was 17.6 nM. Inset: emission spectrum of 8-NBD-cAMP (1 µM) in the absence (black) and presence of CNBD protein (1 µM) (red).
(B) Competition between cAMP (closed circles) or cGMP (open circles) and 8-NBD-cAMP (1 µM) for binding to the CNBD (1 µM). The K_D values were 73.5 nM (cAMP) and 296.9 nM (cGMP).
(C) Increase of fluorescence of 8-NBD-cAMP (0.5 µM) on binding to increasing concentrations of the mutant CNBD (R348A). The K_D value was 7.3 µM.
(D) Competition between cAMP and cGMP with 8-NBD-cAMP for binding to mutant CNBD (R348A) (3 µM). The K_D values were 22.9 µM (cAMP) and 27.7 µM (cGMP).

Figure 3.24 A shows the normalized change of fluorescence of 8-NBD-cAMP, background corrected for when binding to the CNBD protein. The dose-dependent increase of 8-NBD-cAMP fluorescence was fit by a simple binding model (Equation 2, section 2.11.2, Figure 3.24 A). The K_D value was 22.0 ± 10.9 nM

(n = 11), which is in close agreement to the value observed for the full-length channel. The K_D values for binding of cAMP and cGMP were derived from competition experiments. The data was well described by a single competition model (Equation 6, section 2.11.2, Figure 3.24 B). The K_D values were 67.8 ± 8.7 nM (n = 7) for cAMP and 300.4 ± 15.4 nM (n = 7) for cGMP. Again the data corresponds well to the K_D values obtained for the full length channel.

Next, I measured the binding affinity of cNMPs for the mutant CNBD R348A (Figure 3.24, C and D). In this case I reversed the order of events. First, I added 0.5 μM of 8-NBD-cAMP to the recording buffer. Subsequently, I titrated the compound with increasing concentrations of the R348A protein. This step was necessary because the affinity for cyclic nucleotides dropped significantly for R348A. A much higher concentration of 8-NBD-cAMP would be required to perform experiments similar to the ones performed for rCNBD. At high concentrations of 8-NBD-cAMP optical problems arise due to inner filter effects that prevent a proper analysis. Figure 3.24 C shows the fluorescence increase upon protein binding to the 8-NBD-cAMP. The K_D value in this case was 7.3 μM (8-NBD-cAMP). Figure 3.24 D shows the competition of unlabelled cAMP and cGMP with the binding of 8-NBD-cAMP. The K_D values that I obtained were 18.5 ± 4.3 μM (n = 7) for cAMP, and 22.3 ± 5.7 μM (n = 6) for cGMP.

3.6 Characterization by CD spectroscopy

The structures of the CNBD and the R348A mutant have been determined by X-ray crystallography (Clayton *et al* 2004). It was proposed that the R348A mutant represents the cAMP-free state of the protein and the structural differences between the CNBD and the R348A mutant suggest conformational changes on ligand binding. I used CD spectroscopy to study the conformation of the CNBD with and without ligand bound and compared it with that of the R348A mutant. This served two major purposes. First, the spectra of the CNBD before and after refolding can be compared. This allows evaluating the quality of the refolded protein. Second, it is possible to directly compare the spectra of the ligand-free CNBD and of the R348A mutant. Therefore, I can investigate whether R348A mutant is indeed a suitable model for the ligand-free state.

Figure 3.25 A shows the CD spectrum of native CNBD (nCNBD, cyan) and that of the refolded CNBD with cAMP (red). Both samples display a similar spectra with

minima at 210 nm and 223 nm. In addition, the spectra of rCNBD in the absence of cAMP (black) and of the R348a mutant (green) are shown.These two groups of spectra differ significantly. Because the former two samples (nCNBD and rCNBD plus cAMP) have cAMP bound, whereas the latter two (rCNBD free cAMP and R348A) are devoid of cAMP, I reasoned that the difference could reflect a cAMP-induced conformational change of the protein. This presumption is born out by experiment. Figure 3.25 B shows CD spectra of the refolded protein (rCNBD) at various cAMP concentrations. The spectra reflect the transition from the cAMP-free to the cAMP-bound conformation. At saturating concentrations of cAMP, the refolded protein exhibited a CD spectrum almost identical to that of the protein prior to unfolding. In conclusion, the refolded CNBD protein adopts a native structure and is suitable for quantitative binding studies. A similar change in CD spectra was reported for protein kinase A and G on binding of ligand (Johnson & Wong, 1989; Landgraf *et al*., 1990).

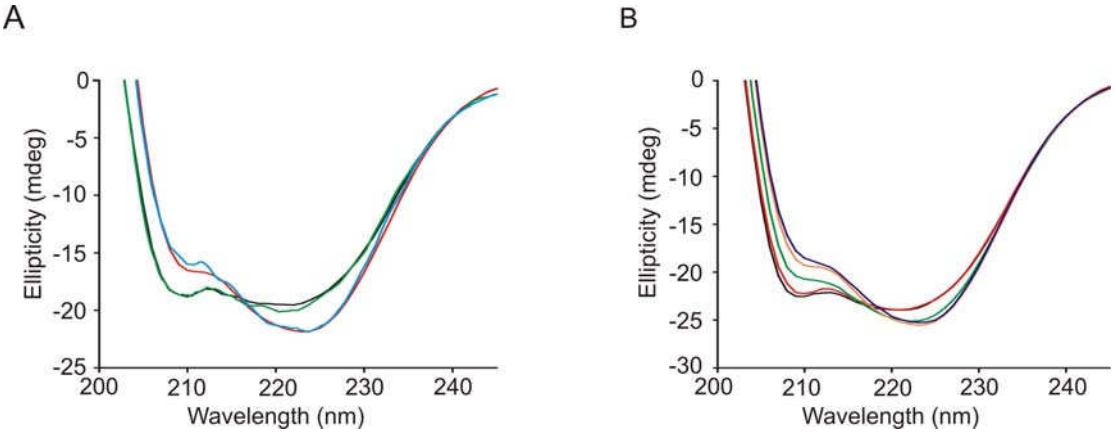

Figure 3.25: CD Spectra of CNBD proteins.
(A) CD spectra of the purified CNBD protein (8.2 µM) prior to unfolding (cyan), after refolding in the absence of cAMP (black), after refolding in the presence of cAMP (15 µM, red), and of the R348A mutant in the absence of cAMP (green).
(B) CD spectra of the refolded CNBD protein (11.4 µM) titrated with various cAMP concentrations (black, 0 µM; red, 5 µM; green, 10 µM; orange, 15 µM; blue, 20 µM).

We analyzed the CD spectra to estimate the changes in secondary structure that occur on ligand binding (Table 1). The helical content adopts slightly higher values in the ligand-bound form compared to the ligand-free form. The differences were most pronounced when we compared the helical content of the refolded CNBD in the presence of saturating cAMP (46%) with that of the R348A mutant (41%). The helicity was derived by adding α_R and α_D from Table 1. The overall helical content derived from the crystal structures of the wild-type CNBD and the R348A CNBD is

lower (36% and 30 %, Table 2) than predicted from the CD spectra; however, the difference in the helical content of the two proteins is in a similar range.

Table 1: Average secondary structure elements (SSE) in % derived from the CD spectra of the CNBD proteins. Sum of all SSE is equal to 100 ± 2.

	α_R	α_D	β1	β2	T	UO
Refolded CNBD	25.8	17.5	11.0	6.5	16.5	22.8
Refolded CNBD+cAMP	26.8	18.8	10.5	6.3	16.5	20.8
R348A	23.5	16.5	11.5	6.5	15	26.5
purified CNBD	26	17.3	9.8	6.3	16.8	23.8

Table 2: The residues contributing to the SSE of the purified liganded CNBD and the R348A unliganded CNBD, as determined by analyzing the crystal structures.
The percentage composition of SSE for the R348A is 30% α-helices and 26% β-sheets. The percentage composition of SSE for the purified CNBD is 36% α-helices and 24% β-sheets.
The PDB entries for the liganded and the unliganded (R348A) are 1VP6 and 1U12 respectively. The total number of residues in the CNBD protein is 142 amino acids.Legend: H- Helix, S- Sheets

R348A			**cAMP bound CNBD**		
residue number	**SSE**	**residues**	**residue number**	**SSE**	**residues**
221-231	H	11	**220-230**	H	11
241-248	H	8	**241-250**	H	9
252-256	S	5	**252-256**	S	5
261-265	S	5	**261-263**	S	3
271-277	S	7	**271-276**	S	6
280-283	S	4	**279-284**	S	6
288-291	S	4	**288-291**	S	4
294-297	S	4	**294-297**	S	4
310-313	S	4	**298-303**	H	6
317-323	S	7	**311-313**	S	3
324-333	H	10	**317-323**	S	7
336-348	H	13	**324-333**	H	10
			335-348	H	14

3.7. Studies of Trp fluorescence

CD spectroscopy provides a global picture of the secondary structure of the protein. However, it is possible that important conformational changes in a protein structure occur that are not reflected in the overall CD spectra. One very important region of cyclic nucleotide-activated channels is the "C-linker" region. This is the region that is believed to constitute at least part of the gating machinery of the channels. I exploited the fact that the CNBD protein contains a single Trp residue (W227) in the C-linker

region. Therefore, fluorescence of Trp may reveal information about the gating process.

3.7.1 Steady-state and life-time measurements on CNBD

Trp fluorescence emission in a hydrophobic solvent has a maximum at 320 nm, while in a polar solvent the maximum is red shifted to 350 nm. The single Trp of rCNBD shows an emission maximum of 340 nm indicating a partially buried Trp residue. The fluorescence measurements indicated a decrease of Trp fluorescence of rCNBD on binding cAMP. The spectrum is similar to the Trp spectrum of nCNBD (Figure 3.26 A). This indicates that binding of cAMP results in repositioning of Trp and nearby amino acids in such a manner that its fluorescence is decreased. The Trp on the C-linker region is exposed to the solvent and flanked by hydrophobic amino acids. The sequence of CNBD shows Trp interspersed between several hydrophobic residues, ^{223}FVRNWQLVA^{231}. Because the spectrum does not change, it indicates the environment of Trp remains unchanged.

Steady-state fluorescence is an average of several individual fluorescent events. In comparison to steady-state measurements, lifetime measurement can provide more information as they dissect individual components contributing to the fluorescence emission (see 2.11.3). Time-dependent fluorescence decay measurements provide the average lifetime of a fluorophore, which is often environmentally sensitive. Trp fluorescence is generally composed of at least two kinetic components (Lackowicz, 2nd Edn, pp 487-515).

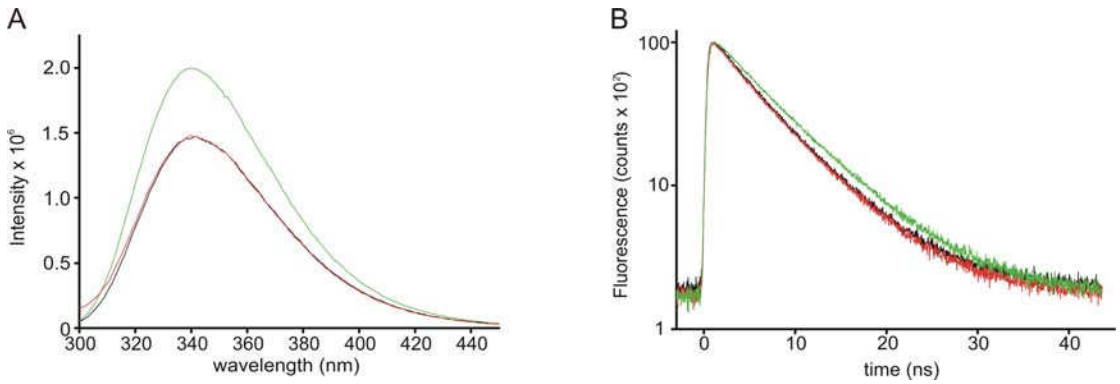

Figure 3.26: (A) Comparison of tryptophan emission spectra for rCNBD and CNBD with cAMP. Tryptophan fluorescence of rCNBD (green) and in presence of cAMP (red). Tryptophan fluorescence of nCNBD (black).
(B) Comparison of the fluorescence decay of tryptophan for rCNBD and CNBD with cAMP. Tryptophan fluorescence of the rCNBD (green) and in presence of cAMP (red). Lifetime of tryptophan fluorescence of nCNBD (black).
Under all conditions protein concentration was 5 μM and 10 μM cAMP was added to rCNBD.
Absolute values of lifetime were: rCNBD (A1 = 10886.3,τ1 = 6.792; A2 =1735.6, τ2 = 2.665, τ_{av}=6.55); rCNBD + 10 μM cAMP (A1 = 10437.4, τ1 =6.123; A2 =2455.4, τ2 = 1.905, = 5.836);nCNBD (A1 = 9845.9, τ1 = 6.206; A2 =2196.7, τ2 = 2.078, τ_{av} =5.911).

Lifetime measurements on Trp of rCNBD shows two components and reveal an average decay of 6.5 ns. A decrease of average lifetime of Trp fluorescence is observed in rCNBD on binding of cAMP. The average lifetime of Trp fluorescence of rCNBD bound to cAMP was similar to that of nCNBD (Figure 3.26 B). The decrease of lifetime is suggestive of slight changes in the local environment of W227. The simplest explanation is that on binding cAMP, the Trp residue repositions itself into the vicinity of a fluorescence quenching amino acid. While analyzing the crystal structure it comes to light that Trp may reposition itself to a nearby Phe, which is the only amino acid in its vicinity capable of significantly quenching fluorescence (for a list of amino acids which are shown to quench Trp fluorescence please refer to Chen *et al* 1996 and Lackowicz, 2nd Edn, pp 446-485). In the ligand-bound state, the distance between the two residues is 3.5 Å and in the ligand-free state it is separated by 8 Å. Quenching due to cAMP can be ruled out because the shortest distance between cAMP and Trp is 23 Å. FRET can also be ruled out, because there is no overlap between the spectrum of cAMP (maximum at 258 nm) and the red-shifted emission spectrum (maximum 340 nm) of W227 of the CNBD.

3.7.2 Kinetics of ligand binding - Fluorescence lifetime spectroscopy

The decrease of the lifetime of Trp fluorescence was used as a marker to study the effect of ligand binding. I challenged the CNBD with various concentrations of cAMP to a solution of rCNBD and determined for each condition the lifetime of Trp fluorescence (Figure 3.27). Fitting of equation 2, section 2.11.2 to the dose-response relation yielded a K_D value of 80 nM for cAMP, in agreement with the K_D from 8-NBD-cAMP steady-state fluorescence measurements.

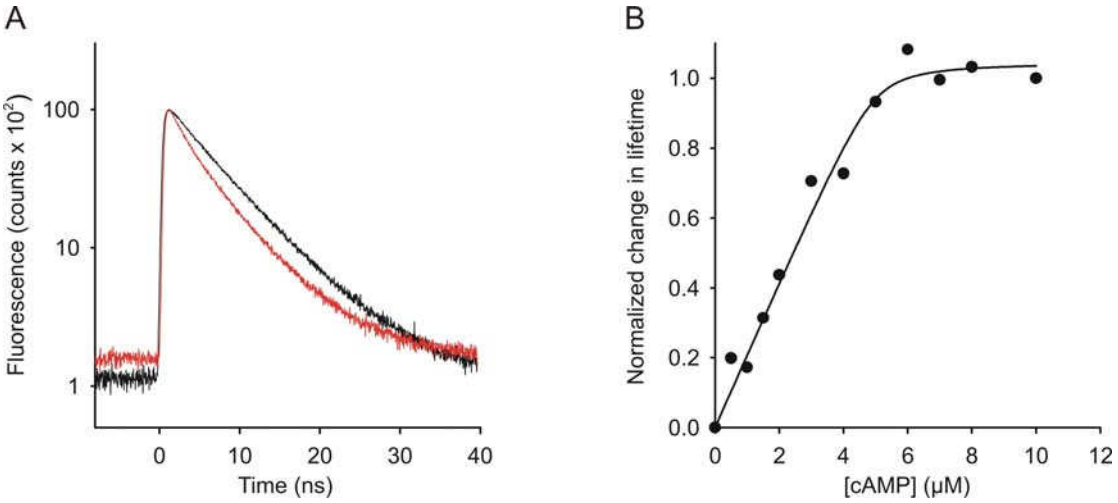

Figure 3.27: Ligand binding to the CNBD protein by fluorescence lifetime spectroscopy.
(A) Decay of fluorescence of the Trp residue of CNBD (5 µM) in the absence (black) and presence (red) of cAMP. Absolute values of lifetime were: 0 cAMP (A1 = 12252, $\tau 1$ = 6.778; A2 = 3133, $\tau 2$ = 2.035, τ_{av}= 6.357); 10 µM cAMP (A1 = 10999, $\tau 1$ = 6.258; A2 = 3889, $\tau 2$ = 2.185, τ_{av}= 5.674). CNBD concentration was 5 µM.
(B) Normalized changes in fluorescence lifetime of Trp as function of the cAMP concentration. The solid line represents nonlinear least-squares fit to eqn. 3. The K_D value is 80 nM.

It should be kept in mind that the change in Trp fluorescence is only an indirect measure of ligand binding because the Trp residue is not located within the binding pocket of the protein. The location of Trp makes this study very interesting because Trp is located in the C-linker region, which constitutes the gate, i.e. it relays ligand binding to gating.

3.8. Screening tests for mlCNG homogeneity

The chances for successfully crystallizing protein strongly depend on the homogeneity of the sample. Although a single band on the SDS-gel is a good starting material indicating the purity of the sample, it does not reflect the homogeneity of the sample in the solution. Combining some of the screening techniques like dynamic light scattering (DLS), CD, mass spectrometry (MS), chromatographic techniques

etc.provides information on the stability and the folding pattern of the protein. These techniques were used in studying the homogeneity of the the mlCNG sample.

3.8.1. Ion-exchange chromatography

On the SDS-gel the majority of the mlCNG protein runs as a 32 kDa band. Another band runs just below the 32 kDa band. It is approximately 1 kDa smaller. Both bands are labeled on the western blot using the anti-His antibody. This indicates that the lower band may represent a portion of the channel lacking some part of the N-terminal region of the protein.

In order to remove heterogeneity, the sample was subjected to ion-exchange chromatography. The mlCNG protein has a pI of 9.46 and in a buffer of pH 8.0, it should carry positive charge. Therefore, a cation exchanger would serve the best for the adsorption of the channel. Nevertheless both types of ion-exchanger were tested. The mlCNG protein was purified as mentioned above. After purification it is suspended in the elution buffer containing 300 mM NaCl and 500 mM imidazole. This buffer was replaced by exchanging it on a PD-10 column with a solution containing 20 mM Na^+ phosphate, pH 8.0 and 5 mM KCl. The protein after buffer exchange was immediately loaded onto the ion-exchange column.

Figure 3.28 A and B shows that considerable amounts of mlCNG bind to both column types. The mlCNG protein eluted as a distinct peak from the cation exchanger when the salt concentration was raised. On the anion exchanger, at least two different subpopulations of mlCNG were observed from the elution profile. The two bands of mlCNG are still visible on the gel (Figure 3.28 C, *inset*). Mass spectrometric analysis (peptide mass fingerprinting) of the two bands indicates that the lower band is an N-terminally cleaved protein that lacks the first eight amino acids (962 Da).

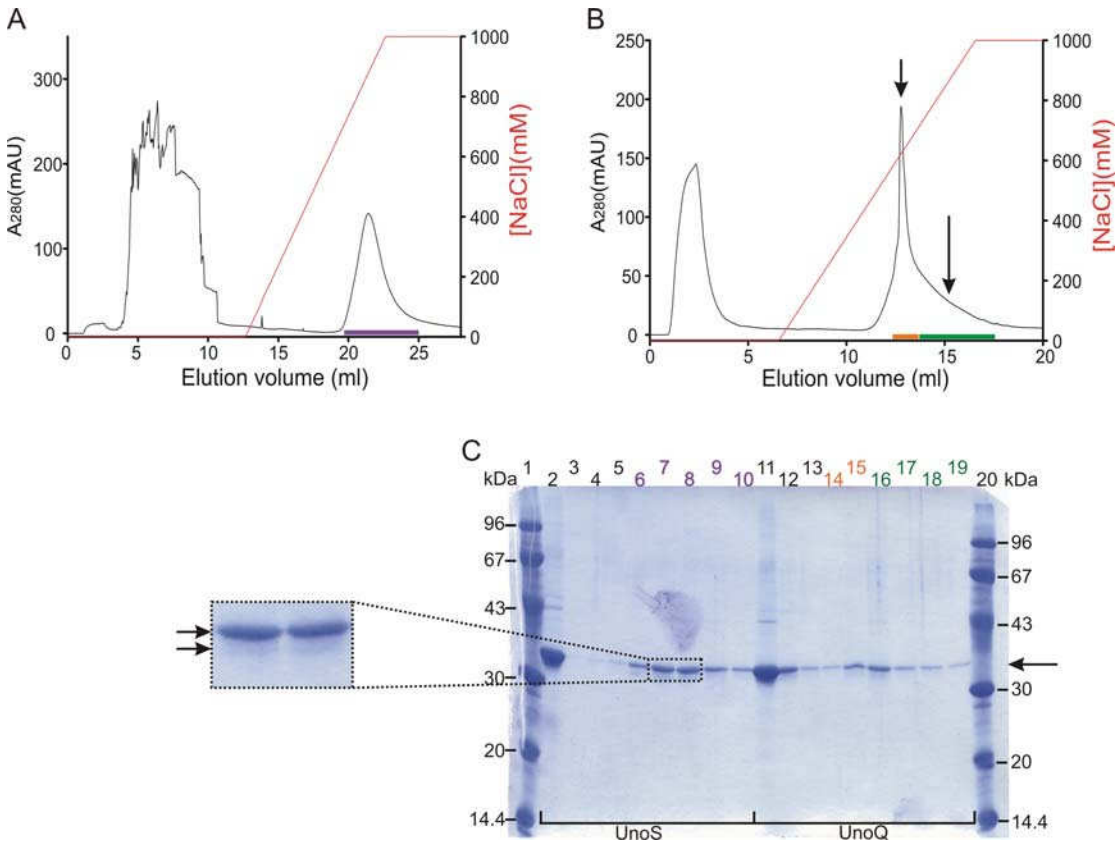

Figure 3.28: Ion-exchange chromatography to purify mlCNG protein.
(A) Cation exchange chromatography: chromatogram of mlCNG run on UnoS column.
(B) Anion exchange chromatography: chromatogram of mlCNG run on UnoQ column. The two subpopulations of mlCNG are marked by arrows.
(C) SDS-gel of fractions from the ion-exchange columns. Lane 1 - LMW, lane 2 - load, lane 3 - unbound fraction; lane 4- wash, lanes 5 to 10 - eluate, lane 11 - load, lane 12 - unbound, lane 13- wash, lanes 14 to 19 - eluate, lane 20 - LMW. The gel lanes are colour coded according to the fractions collected after elution (see part A and B). The *inset* shows the prominent mlCNG band at 32 kDa. Below it is the shorter version of mlCNG. Both the bands are denoted by arrows.

One speculation is that the cleaved protein could be arranged in the tetramer channel, thereby making it difficult to separate.

3.8.2 Mass spectrometry

MALDI-TOF analysis on the entire mlCNG channel was also applied. The idea behind performing this experiment was to see if any cleaved or degraded product could be identified. A very weak Gaussian peak was observed at 39 kDa (Figure 3.29), which is the expected molecular weight of the mlCNG channel plus $(His)_6$ tag. The reason for the weakness of the signal observed in MALDI-TOF was because mlCNG is highly hydrophobic; it does not fly well and probably adheres to the stainless steel plate of the mass spectrometer.

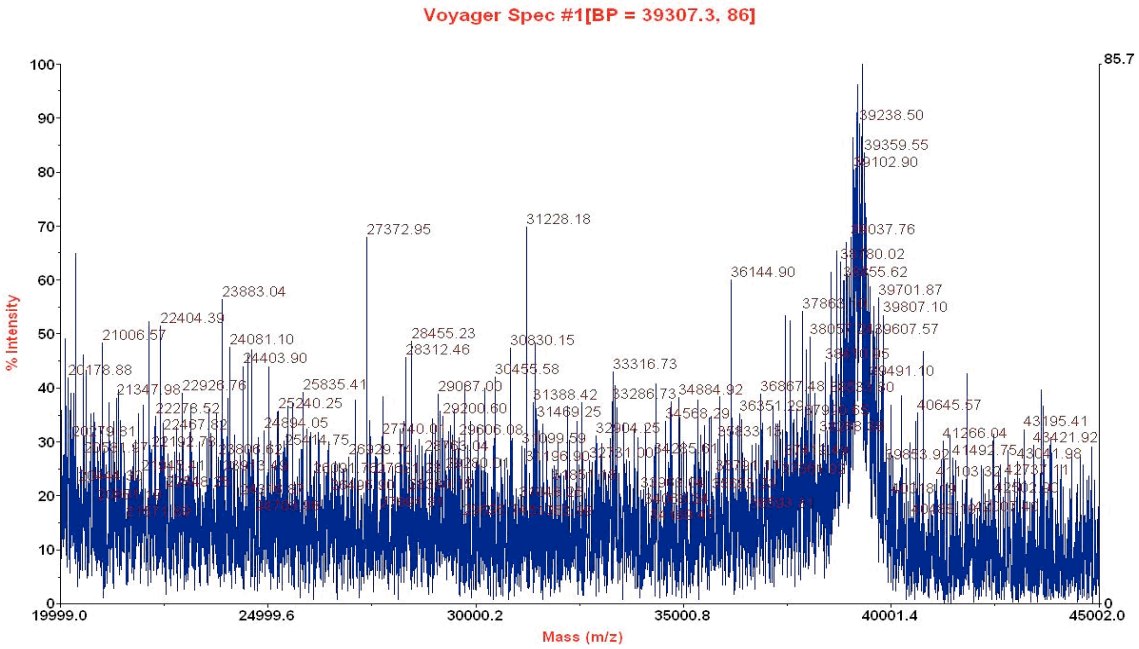

Figure 3.29: Spectrum of full length mlCNG detected on MALDI-TOF. The spectrum shows a weak gaussian signal at 39 kDa. The protein concentration was 7 mg / ml.

To check for the purity of the sample, different amounts of purified protein were loaded on the gel and every prominent band was subjected to MS analysis. MS analysis on the prominent band of mlCNG reveals four major peptides following in-gel tryptic digestion, although theoretical digestion predicts several other peptides in the range of ~ 600 to 3000 Da (Please refer to the table in the Appendix table 5). As expected, around 67 and 96 kDa dimeric and trimeric population of mlCNG was detected. The tetrameric population of mlCNG does not enter the 12.5 % polyacrylamide gel. Unexpectedly, some bands below 32 kDa were detected, which correspond to mlCNG protein.

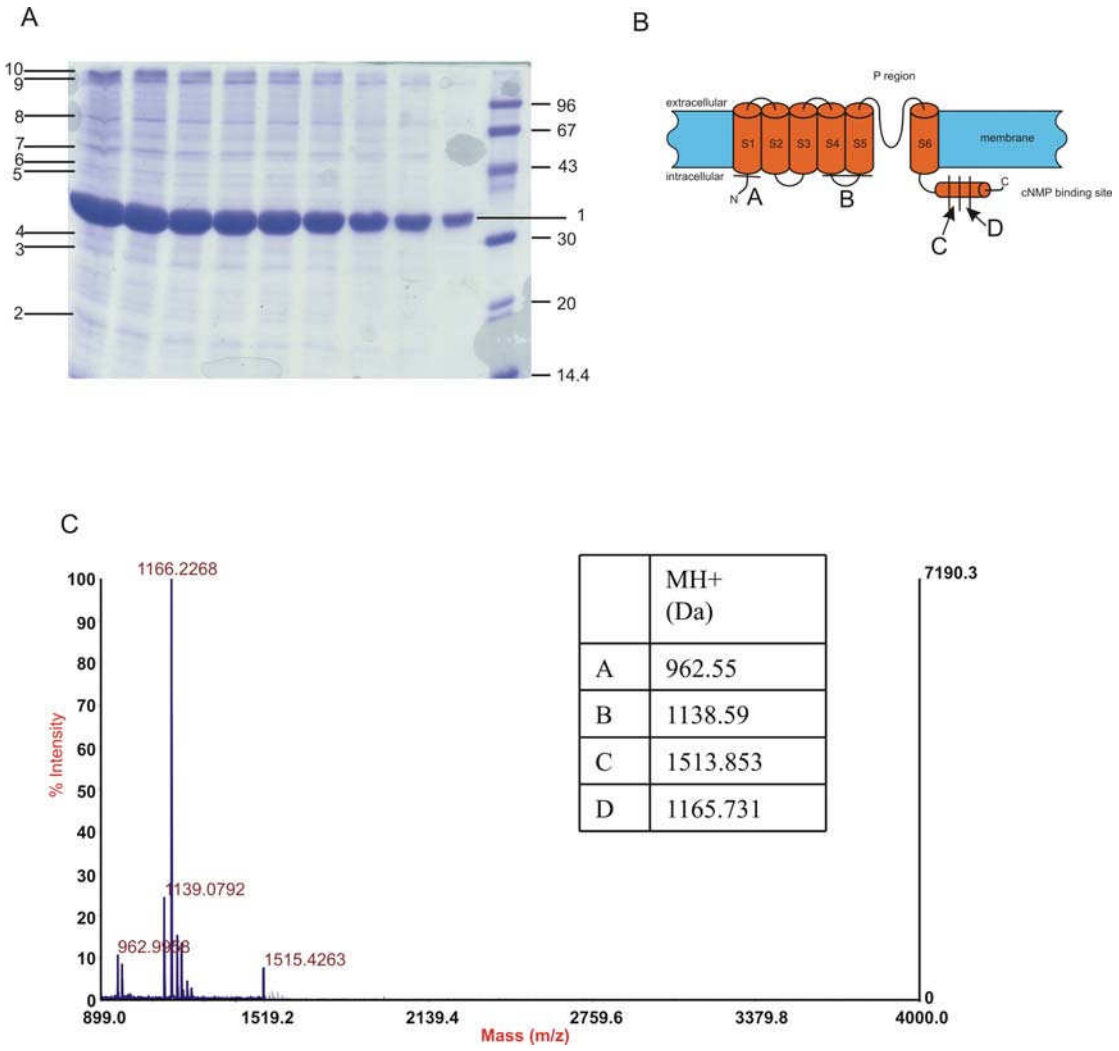

	MH+ (Da)
A	962.55
B	1138.59
C	1513.853
D	1165.731

Figure 3.30: Peptide mass fingerprinting: The mlCNG preparation was loaded onto a 12.5 % SDS gels at various mounts. Bands which were well isolated and stained by coomassie gel were sliced and tryptic digested for peptide mass fingerprinting.
(A) The numbered bands were sliced from the gel for tryptic digestion for MS analysis. Band numbered 1 corresponds to mlCNG; the spectrum of which is shown in (C) and a pictorial representation of the identified peptides from the channel is shown in (B). The other bands that could be assigned to proteins were: 2, 3, and 4 correspond to shorter versions of mlCNG that lacked the N-terminal end. 5 corresponds to a metalloprotease FtsZ, 6 to an accridine efflux pump, 7 to mlCNG which runs at an unexpected M_w of 45 kDa, 8 represents the dimeric population of mlCNG n the gel and Dna K, 9 and 10 represents trimeric populations of mlCNG and an ABC transporter respectively.

These bands carry the C-terminal $(His)_6$ tag as they are also recognized by the anti-His antibody. Not surprisingly, the peptides that fly on MS following the tryptic digestion are soluble regions of the protein (Figure 3.30 B and C).

3.8.3 Stability of the mlCNG protein in various other detergents

The initial phase of a crystallization setup is largely empirical trying out various conditions including the protein solubilized in various detergents and buffers. The mlCNG protein was normally extracted in DM (Section 2.2.5). Several other

detergents were tried. A list of detergents tried is mentioned in table 3. The chromatogram in Figure 3.31 A shows the elution profile of mlCNG solubilized in different detergents. The protein aggregated on the column when using some of the detergents e.g. in the presence of short chained detergents like CHAPS (green trace) and OGP (orange trace). The channel shows a broad distribution over the column when solubilized in a long chain detergent like DDM (black trace) and it could neither be concentrated above 4 mg/ml nor was it stable for longer than two days. The mlCNG protein shows a rather homogeneous and narrow distribution on a GF column when solubilized in detergents of intermediate chain length like DM, N-Lauryl sarcosine (Figure 3.31 A) and LDAO (Figure 3.31 B). N-Lauryl sarcosine is an ionic detergent and is typically used in solubilizing proteins from inclusion bodies. The detergent is a strong denaturant. Hence, it was not used in further experiments. The mlCNG protein solubilized in DM and LDAO showed similar SSE when studied by CD spectroscopy (Figure 3.31 C). These two detergents are of similar chain length and have a similar CMC (2.0 mM for LDAO and 1.7 mM for DM).

Table 3: Properties of different detergents used to solubilize mlCNG

Detergents	**Type**	**CMC (mM)**
BIG CHAP	Z	3.4
O-gluco pyranoside (OGP)	NI	20-25
CHAPS	NI	6-10
LDAO	NI	2.0
O-thiogluco pyranoside (OTGP)	NI	9
Zwittergent 3-14	Z	0.1-0.4
Deoxycholate	I	2-6
Dodecyl Maltoside (DDM)	NI	0.17
Decyl Maltoside (DM)	NI	1.7
N-LaurylSarcosine	I	14.6

Where Z-zwitterionic, NI-Non Ionic, I-Ionic

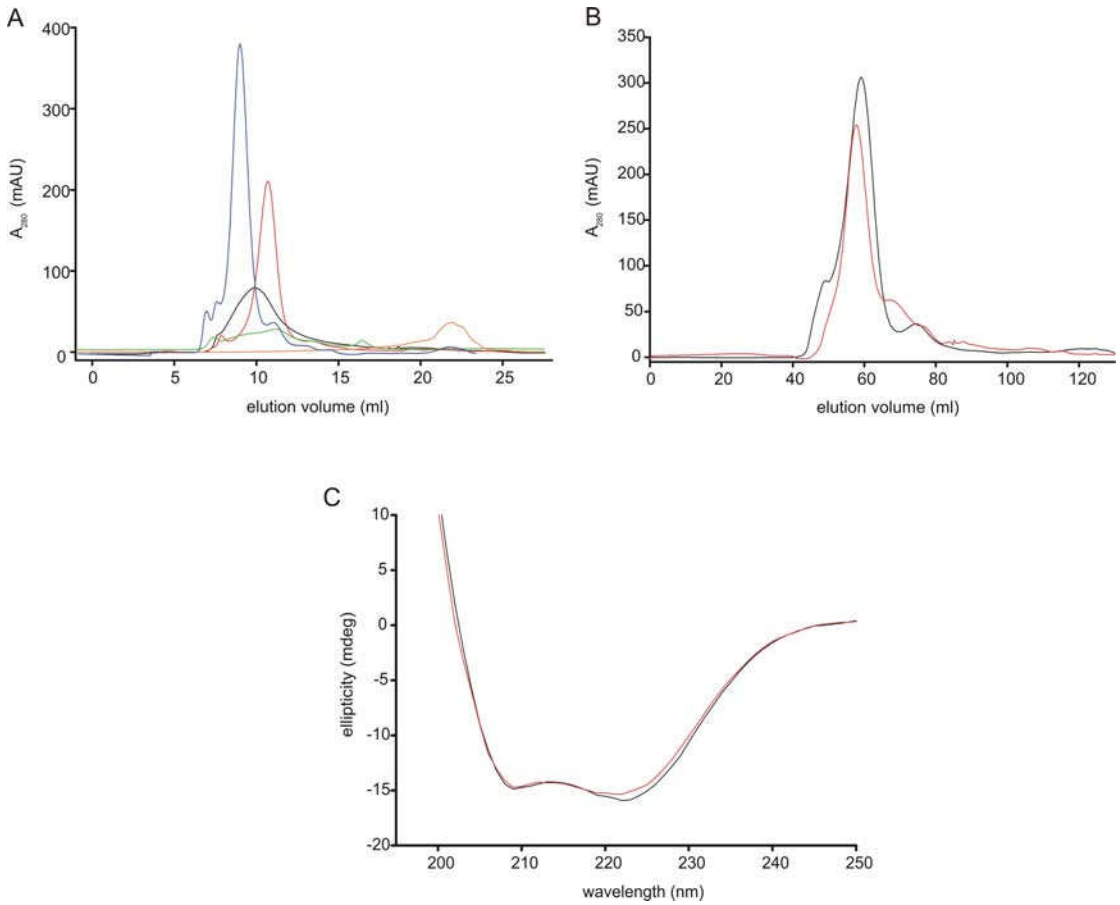

Figure 3.31: (A) Elution profile of mlCNG on a Superdex 200 analytical gel filtration column solubilized with the following detergents: n-Lauryl Sarcosine (violet); Decyl-maltoside (red); Dodecyl-maltoside (black), CHAPS (green);O-Gluco-pyranoside (orange).
(B) Elution profile of mlCNG on a Superdex 200 Preparative grade column solubilized with the following detergents: 5 mM DM (black) and 3 mM LDAO (red)
(C) CD spectra of mlCNG solubilized in the following detergents (same as in fig B): 5mM DM (black) and 3 mM LDAO (red). The protein concentration under both the conditions was 0.07 mg/ml.

3.8.4 Monitoring mlCNG stability in DM and LDAO

Stability of mlCNG solubilized in DM and LDAO was monitored over time using DLS spectroscopy. Two parameters were studied simultaneously, the protein concentration in the supernatant and the average scatter intensity of the sample. The samples were maintained at 17^{o}C in microfuge tubes. Each day before performing DLS measurements, the microfuge tubes were centrifuged at 21,000 g for 30 min in order to remove large aggregates. The sample was then subjected to DLS and protein estimation. Estimating protein concentration was possible for mlCNG solubilized in DM by Bradford's method. Protein estimation of mlCNG solubilized in LDAO was not possible as LDAO interferes with Bradford's reagent. Alternatively, I estimated the protein concentration from absorption spectra between 220 nm and 350 nm. What I observed was that, with time the absorption spectrum changed. The reason for this

may be: Light scattering is pronounced in shorter wavelengths and formation of aggregates may scatter light. Another explanation is that formation of aggregates may result in change in the environment of the chromophore and hence change in the absorption spectrum (see Figure 3.33 B). The stability of mlCNG was tested under four different DM concentrations. One concentration was chosen below the CMC (1.25 mM), the remaining three (2.5 mM, 4 mM and 5 mM) were above the CMC (1.7 mM). Regardless of the DM concentration used, mlCNG showed a decrease in protein concentration with time (Figure 3.32 A). The average scatter intensity first increases, possibly due to formation of aggregates, and then decreases parallel to the decrease in protein concentration (Figure 3.32 A and B).

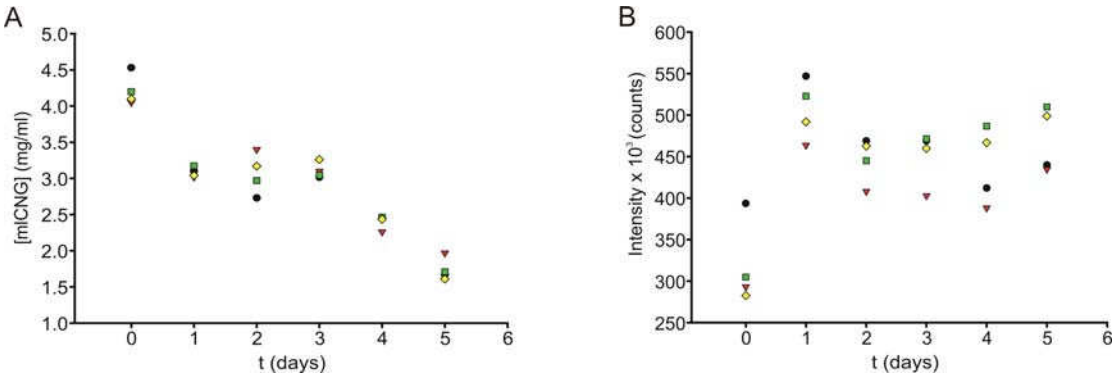

Figure 3.32: Stability of mlCNG under various concentrations of DM as studied using dynamic light scattering (DLS). In both the cases the filled circles indicate mlCNG solubilized in 1.25 mM DM, the red triangles indicate the protein solubilized in 2.5 mM DM, the green squares indicate mlCNG solublized in 4 mM DM, and the yellow diamonds indicate the protein solubilized in 5 mM DM. Under all conditions the protein samples were maintained at 17°C.
(A) Plot of protein concentration under the several detergent concentrations mentioned above as a function of time.
(B) Plot of average scatter intensity for the several detergent concentrations mentioned above as a function of time.

A similar experiment with LDAO showed rather stable average scatter intensity (Figure 3.34 A); although a pellet was clearly observed following centrifugation, again pointing towards growing aggregates in the supernatant. Figure 3.33 B shows the UV absorption spectra of mlCNG. The spectrum changes from day 0 (black trace) to day 4 (red trace). This makes the protein estimation unreliable although a pellet was observed on centrifugation, and a drop in protein concentration was expected. The difference (green trace) between the two spectra is not linear and thus indicates noise (aggregation) arising form the sample. In both detergents tested to maintain mlCNG protein, aggregation is noticed over time.

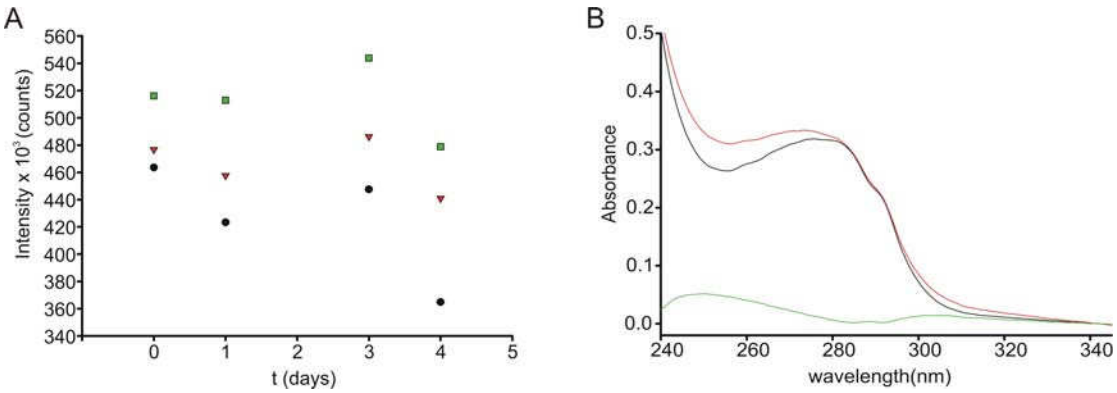

Figure 3.33: Stability of mlCNG under various concentrations of LDAO as studied using dynamic light scattering (DLS). Under all conditions the protein samples were maintained at 17°C.
(A) Plot of average scatter intensity under the several detergent concentrations mentioned above as a function of time. The filled circles indicate mlCNG solubilized in 1.25 mM LDAO, the red triangles indicate the protein solubilized in 2.5 mM LDAO, and the green squares indicate mlCNG solublized in 5 mM LDAO.
(B) Absorbance spectra of mlCNG in the near UV region on day 1 (black trace), and day 4 (red trace).The green trace indicates the difference between the two spectra.

3.8.5. Monitoring mlCNG stability in different buffers/pH

The stability of mlCNG protein was tested under various pH conditions and buffer constituents. The channel was solubilized in 5 mM DM and tested against 20 mM phosphate buffer pH 8.0, 20 mM HEPES pH 6.8, 20 mM MES pH 6.2 and 6.7. At around pH 6.8 I tested two different buffer constituents, HEPES and MES. This was chosen to discriminate whether pH alone had an effect on protein stability or buffer constitutents could also have an influence. Similar to the experiments shown in chapter 3.8.4, the protein concentration and the average scatter intensity was monitored. In all cases, a decrease in protein concentration was observed with time (Figure 3.34 A). At low pH the relative decrease of protein was lower than at high pH. Buffer constituents also seem to affect protein stability. MES seemed better than HEPES in maintaining mlCNG stability. The trend observed for average scattering intensity (Figure 3.34 B) in all buffers was alike, indicating formation of aggregates until day 1 and following the decrease in protein concentration on subsequent days.

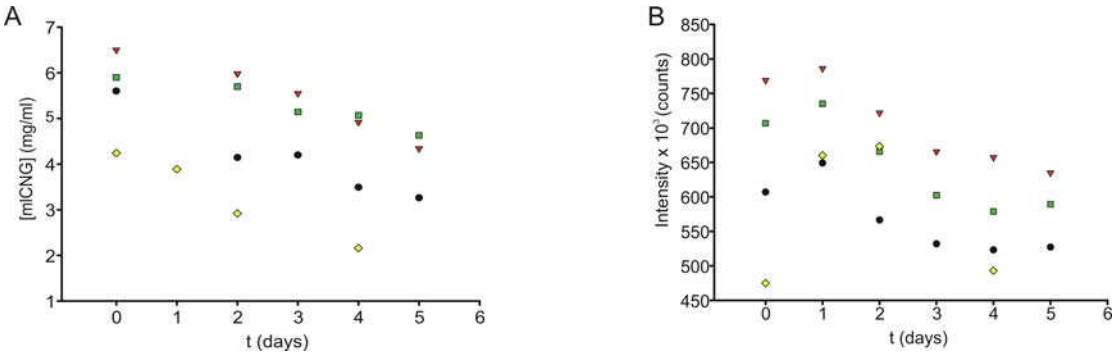

Figure 3.34 Stability of mlCNG under various buffer conditions as checked by dynamic light scattering (DLS). In both the cases the filled circles indicates mlCNG maintained in 20mM HEPES (pH 6.8), the red triangles indicate mlCNG maintained in 20mM MES (pH 6.7), the green squares indicate mlCNG maintained in 20mM MES (pH 6.2), and the yellow diamonds indicate mlCNG maintained in 20mM phosphate (pH 8.0). The protein samples were maintained at 17^{o}C under most of the conditions except under phosphate buffer of pH 8.0 (4^{o}C). Under all conditions the protein was solubilzed in 5 mM DM.
(A) Plot of protein concentration under the several detergent concentrations mentioned above as a function of time.
(B) Plot of average scatter intensity under the several detergent concentrations mentioned above as a function of time.

3.9. Crystallization attempts of the mlCNG protein

Crystallization of membrane proteins requires the detergent concentration to be as low as possible without hampering protein stability. It is advisable to keep the detergent concentration slightly below its CMC because otherwise the formation of micelles may interfere with the formation of proper crystal contacts. Attempts were made to crystallize the mlCNG in detergents for X-ray diffraction and by partially reconstituting the protein in lipids for 2D electron diffraction.

3.9.1 Crystallization of the mlCNG protein in detergents

Several crystallization attempts were performed on the channels solubilized in either DM or LDAO. The purification of the protein was also modified by replacing phosphate buffer by Tris. All permutations and combinations of the two detergents and buffers were tried against a battery of conditions mentioned in section 2.8.2.

Crystal drops were prepared separately in both sitting drop and hanging drop method, in which 1 µl of supersaturated protein was mixed with 1 µl of crystallization buffer. The drop was then sealed off in a reservoir either by tape for sitting drops or sealed with silicone grease for hanging drop. The drops were observed twice in a week for a period of one month.

Protein solubilized in DM was more prone to aggregation than the one solublilized in LDAO. In addition to using the crystallization buffer kits, I performed experiments

with grid screens (see Figure 2.8) in both the hanging and sitting drop technique. Basically, crystal drops were setup by varying pH and precipitant at the same time (see methods 2.11.2.). The mlCNG protein was certainly more stable in salts than in organic precipitants like MPD and polyols. Polyols of long chain length (PEG 1000 and higher) resulted in strong precipitation of the protein. Clear drops were observed at low pH and when salts were used as precipitants. This is in line with the results observed from DLS measurements, which also showed a reduced tendency to form aggregates at low pH. Similarly, short chained PEGs resulted in medium aggregates at high pH and tended towards clear drop at low pH. Under no condition tested, were trends for crystallization observable. From the DLS experiments and observations made from the crystal drops, one can reason that scanning around pH 6.0 and using salts as precipitants maybe fruitful. Some of the observations of crystallization trails are shown below (Figure 3.35).

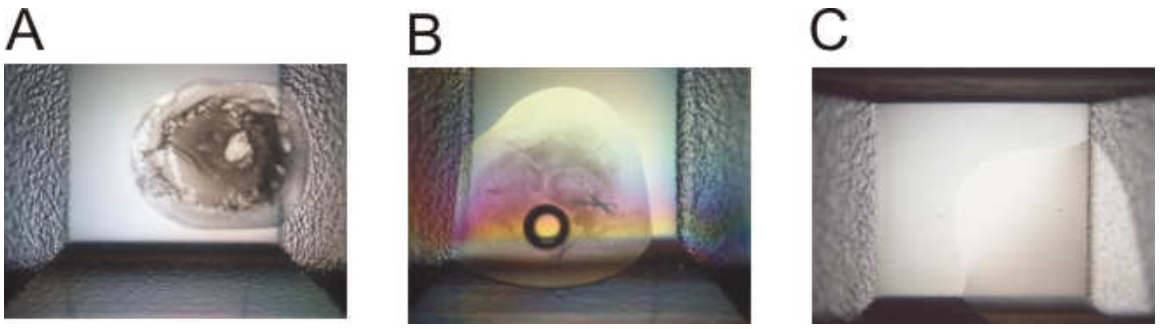

Figure 3.35: Observations from crystallization trial.
(A) Precipitate was observed when mlCNG was mixed with 0.1 M HEPES, pH 7.0, 30 % PEG 6000.
(B) Salt crystal was observed when mlCNG was mixed with 0.1 M $MgCl_2$, 0.1 M HEPES-Na, pH 7.5, 18 % PEG 400. Under both the conditions mlCNG was solubilized in 2.5 mM DM and 20 mM phosphate buffer, pH8.0.
(C) Clear drop was observed when mlCNG solubilized in 2.5 mM DM and 10 mM Tris, pH 8.0 was mixed with 1.26 M Na-Citrate, 0.09M Na-HEPES, pH 7.5, 10 % glycerol.

3.9.2 Crystallization of mlCNG by partial reconstitution in lipids

The mlCNG protein was purified as mentioned above. Following elution of the protein from the Co^{2+}-affinity, the protein sample is observed under the electron microscope for homogeneity. The sample is mixed with lipids to form a ternary complex. The detergent is dialyzed in the crystallization buffer (2.11.3), which results in protein reconstituting in the lipids. This may lead to crystallization. Unlike crystallization in detergent where the protein sample is concentrated following

purification, the affinity column eluate (~ 0.75 to 1 mg/ml) can directly be used for the crystallization trials. Concentration of the sample was avoided.

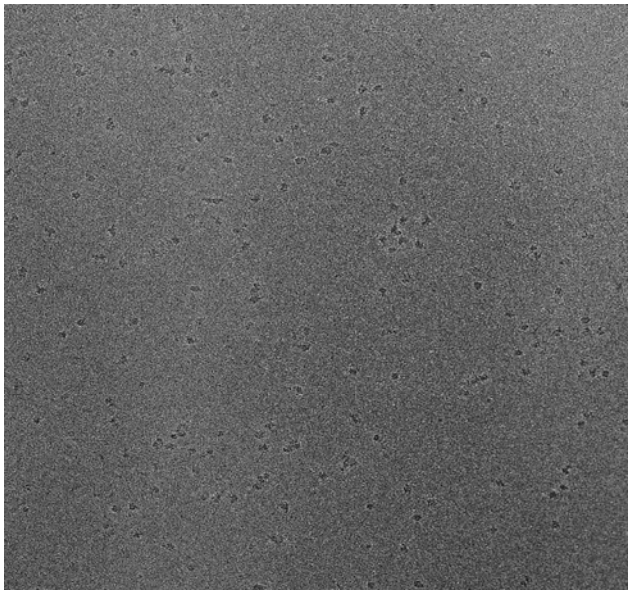

Figure 3.36: Electron micrograph of negatively stained mlCNG particles. The particles are shown in dark on the grey background

Figure 3.36 shows a negatively stained mlCNG preparation following purification from the affinity column. Single particle analysis was performed on the preparation. Well dispersed particles were manually picked using the program EMAN. 3D reconstruction was attempted from approximately 5000 single particles. On average the particle size was 10 ± 2 nm (standard deviation). The particle size fits well with the expected dimensions of a 6 TM domain channel. From the crystal structure of eukaryotic Shaker channel, the top view was shown to be 10 nm in length (Long *et al* 2005). Although the sample was well dispersed, the observed shapes were heterogeneous. For this reason 3D reconstruction was not possible.

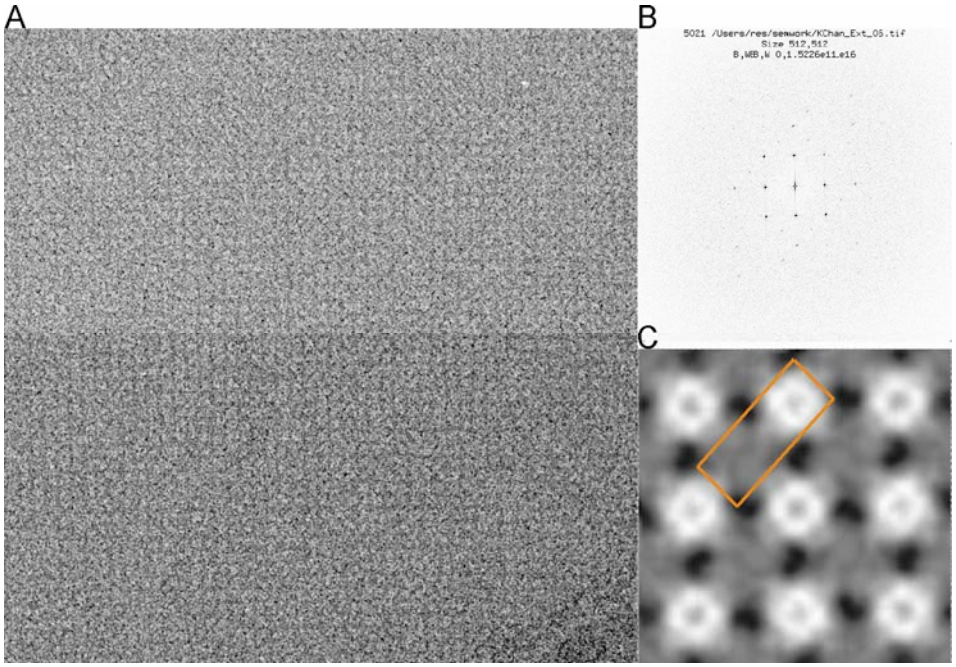

Figure 3.37: (A) Electron micrograph of negatively stained mlCNG crystal reconstituted in *E.coli* polar lipids at LPR 1 in 10 mM MES pH 6.0. The mlCNG particles are arranged in a square lattice.
(B) Power spectrum, showing diffraction spots.
(C) 2D projection map showing dark stained particles and bright particles arranged in alternate rows. 2 x 2 unit cell arrangement is shown in the oreange outlined box, in which the dark stained particles represent the bottom view while the bright particles with a dark centred spot represent the top view. The unit cell has a dimension of 118 Å x 120 Å, and the angle between the crystal lattices is 89.3 deg. All the images shown here are inverted images of the original picture.

Attempts to crystallize mlCNG channel by partial reconstitution was attempted by using different concentrations of either DMPC or *E.coli* polar lipids at 25^{o}C. The channel crystallized in three different buffer conditions; 10 mM MES pH 6.0, 10 mM HEPES pH 7.0, and 10 mM Tris pH 8.0 in *E.coli* polar lipids. Crystals were found in three different protein to lipid ratios; 0.5, 1, and 1.5. A negatively stained image of the crystal is shown in Figure 3.37 A. Figure 3.37 C shows a 2D projection map of alternate rows of dark and bright particles. The dark particles represent the bottom view while the bright particles with a dark centre represent the top view. The reason to believe that the bright particles with a dark centre represent the bottom view is because it is stained with uranyl acetate which can enter the large water filled cavity located in the intracellular side of a channel. In the top view the pore region is too small too accommodate a particle as large as uranyl acetate and is therefore evenly stained and bright.

4 Discussion

4.1 Crystallization of the mlCNG protein

Structure at atomic resolution provides invaluable information of a protein. To perform structural studies on the mlCNG protein, I opted for X-ray diffraction and electron diffraction. For both diffraction techniques, obtaining a protein crystal is a pre-requisite. Crystal growth is facilitated by ordered arrangement of the molecules, proteins in this case. Heterogeneity of any sort (degraded products or aggregated particles) can hamper molecule contacts, and hence crystallization. Studies on conditions used for crystallization revealed that the mlCNG protein tends to aggregate with time. DLS studies indicated an increase in particle size and reduction of protein concentration with time under all conditions tested. Aggregation of protein was reduced under low pH. The presence of cleaved products was identified by MS. Results from DLS experiments and MS together suggests that sample was heterogeneous. This may have been one of the reasons why the protein did not have crystallize in detergents.

Membrane proteins are solubilized using detergents. However, detergents do not mimic well the lipidic environment. Excessive delipidation may lead to instability of the protein and hence aggregation. In some recent reports lipid facilitated protein crystallization. Long *et al* (2005 a and b) crystallized an eukaryotic K^+ channel in the presence of detergents and lipids. In another example Guan *et al* (2005) showed that Lac Y, which is unstable in detergents, crystallized in the presence of lipids. I did not try crystallizing the mlCNG protein in the presence of a mixture of lipids and detergents; instead, I performed crystallization trials by partially reconstituting the protein in lipids.

The mlCNG protein crystallized in the presence of cAMP under several conditions which included several lipid-to-protein ratios (LPR) and a broad pH range. Reconstitution in lipids seems to be a stabilizing factor for the protein. This is because the mlCNG protein crystals were obtained at three different pH 6.0, 7.0 and pH 8.0 in MES, HEPES and Tris buffers, respectively. In HEPES and Tris buffers, mlCNG was shown to aggregate when solubilized in detergents alone.

Under all crystal conditions, the mlCNG protein arranges in a square lattice in a head-to-tail fashion. The unit cell of the mlCNG protein crystal grown in MES buffer with a LPR of 1 has a dimension of 120 x 118 Å, and the angle between the lattices is 89.3 deg. The

crystals diffract up to ~ 15 Å. While I was writing this thesis, the crystal structure of the mlCNG protein was reported in the presence of cAMP by Chiu *et al* (2007). Similar to the crystals I obtained their protein crystal also shows mlCNG arranged in a square lattice in a head-to-tail fashion and diffracts upto ~ 16.3 Å. A model, built on the structure from the 6 TM domain eukaryotic K^+ channel (Long *et al* 2005 a and b) and the monomeric form of CNBD (Clayton *et al*, 2004) well dock in to the single-particle and the lipid-reconstituted protein. The structure indicates that the S1-S4 is arranged parallel to the lipidic membrane (Figure 4.1). Another interesting feature is that the CNBDs are well separated from one another and are not involved in any interfacial contact. These results are in line with the data on ligand binding and activation kinetics, i.e. that the CNBDs in mlCNG do not interact with each other; thus the dimer observed in the X-ray crystal structure does not represent the biological unit.

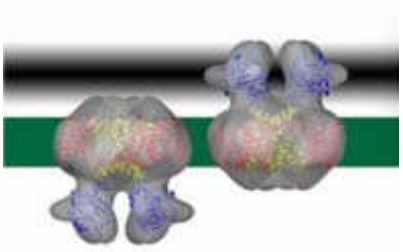

Figure 4.1: This figure is adapted from Chiu *et al* 2007. 3D reconstruction of single particles from the crystal of mlCNG protein. The figure shows a head-to-tail arrangement of mlCNG protein in grey. The membrane is shown in green. The model was generated by docking the structures of Kv 1.2 (PDB entry 2A79), shown in red (S1-S4) and yellow (S5-S6), and the cAMP containing structure of the cyclic nucleotide binding domain of mlCNG (PDB entry 1VP6).

The next important step would be to improve crystal quality to obtain a better resolution of the structure. Combining powerful techniques like electron diffraction and AFM, it should be possible to obtain a reasonably good resolution of the mlCNG protein using 2D crystallization technique.

4.2 Studies of ligand binding

I studied ligand binding in a cyclic nucleotide-activated K^+ channel and its isolated CNBD. I followed the approach developed by Kraemer *et al* 2002, who used a fluorescent analog of cAMP, 8-NBD-cAMP. On binding 8-NBD-cAMP the fluorescent

intensity of the fluorophore increases 7 fold. The binding affinity of cyclic nucleotides was derived from competition experiments where 8-NBD-cAMP-saturated protein is challenged with increasing concentrations of cNMPs. The binding isotherm is derived for a single subunit. The binding constants K_D (Table 4) derived from the measurements indicate that the full length channel and the CNBD have a similar binding affinities for the cyclic nucleotides, cAMP and cGMP. This indicates that in the full-length channel, the CNBDs do not interact with each other.

Table 4: Summary of binding constants.

	CNBD	**R348A**	**mlCNG**	
	8-NBD-cAMP fluorescence	**8-NBD-cAMP fluorescence**	**8-NBD-cAMP fluorescence**	**Rb^+-flux assay**
Ligand	K_D (nM)	K_D (μM)	K_D (nM)	$K_{1/2}$ (nM)
cAMP	67.8 ± 8.7 (7)	18.5 ± 4.3 (7)	81.6 ± 17.5 (6)	60-100[a,b]
8-NBD-cAMP	22.0 ± 10.9 (11)	7.3 (1)	15.9 ± 2.7 (5)	
cGMP	300.4 ± 15.4 (7)	22.3 ± 5.7 (6)	320.7 ± 25.5 (6)	600[a]

a, Nimigean et al, 2004; b, Clayton et al, 2004

Comparison of the results obtained from ligand-binding experiments with that of channel activation (Nimigean *et al*, 2004) reveals that the K_D of cAMP-binding coincides with the $K_{1/2}$ of channel activation by cAMP, and the K_D of cGMP binding is 2 fold lower than $K_{1/2}$ of cGMP activation. Both results suggest that binding and gating in the mlCNG channel is non-cooperative. A corollary is that the binding event is not affected by intersubunit contact and that binding sites in the tetrameric channel act independently of each other.

The results of my experiment suggest that only a small binding energy is required for activation of the protein. It would seem that some of the binding energy is used for the gating transition and that the binding affinity of the channel therefore, should be lower than that of the isolated CNBD. However, our results indicate that the main conformational change for the closed–open transition occurs in the CNBD and the linker themselves and that the gating step is energetically less demanding. Similar observations were also made for the nucleotide exchange factor EPAC by Kraemer *et al* (2002). In their study the CNBD of EPAC and the full-length EPAC both had similar binding

constants, indicating that the conformational change during activation may be energetically less demanding. On the other hand, as the mlCNG protein is not present in its native state, and is solubilized in detergent; gating of the channel may have been affected resulting in a K_D similar to the isolated CNBD.

It will be interesting to unveil the structural basis for the high cAMP affinity to of the mlCNG protein. The K_D is determined by two factors k_{on} (on-rate) and k_{off} (off-rate).

K_D is the ratio of k_{off} / k_{on}. A low K_D can be attributed to

1. Low k_{off}
2. High k_{on}
3. Combination of both.

By using pre-steady-state kinetic, it should be possible to study the rate constants of ligand binding. Preliminary experiments on studying pre-steady-state kinetics (Peuker 2007) using caged cyclic nucleotides and flash photolysis suggests that the low K_D may arise due to high on-rates. Further experimentation using flash photolysis and rapid mixing-techniques certainly would enlighten our understanding of ligand-binding dynamics.

Most studies of ligand binding have not used eukaryotic CNG channels. The molecular basis that determines affinity and selectivity is not well understood; ligand binding has been inferred from electrophysiological measurements (Gordon and Zagotta, 1995a, b; Varnum et al, 1995). Several residues in the CNBD and some mutations at sites distant from the CNBD affect cyclic-nucleotide binding (Kaupp and Seifert, 2002). I measured ligand binding on the CNBD mutant R348A. Mutation of this residue results in a CNBD protein that crystallizes without cAMP. This residue is a crucial determinant of cNMP-binding to the CNBD of HCN 2 channel (Zagotta *et al*, 2002), and of the wild-type CNBD of mlCNG protein. The Arg residue stacks on top of the purine ring and interacts with the amino group of cAMP directly. The CNBD in CNG channels lacking this particular residue. This indicates that the Arg residue may be one of the determinants of ligand selectivity and sensitivity. The K_D values derived for R348A are in micromolar range (Table 4), i.e. ~ 400 fold lower than for the wild-type. Furthermore, the R348A mutant shows similar binding affinities for cAMP and cGMP, indicating that ligand selectivity and sensitivity both are affected. Mutation experiments on HCN and CNG

channels have revealed several other residues crucial for cNMP selectivity. Residues in CNGA1 that have been attributed to control selectivity of cGMP over cAMP are T560 (Altenhofen *et al* 1991), D604, F533 and K596. Recent studies on HCN2 mutants provide structural and functional aspects of ligand selectivity. HCN2 binds both cAMP and cGMP, the crystal structure of the CNBD of HCN 2 has been solved in presence of both ligands. HCN contains Thr in position analogous to T560 of CNGA1. Mutation of another residue I665D (analogous to D604 in CNGA1) results in exclusively cGMP binding to the CNBD of HCN2 channel.

4.3 Structural changes in CNBD on cAMP binding

Structural studies on CNBD were performed using optical spectroscopic techniques, namely CD Spectroscopy and Fluorescence Lifetime Spectroscopy. On one hand, I studied the global changes of Secondary structure elements (SSE) of the CNBD upon cAMP binding; on the other hand, I studied local changes in the CNBD arising due to ligand binding.

CD spectroscopy shows that the SSE of the CNBD remained unchanged after refolding and unfolding. The large differences that were observed between the two states reflected the change in the SSE of the protein on binding cAMP. CD spectroscopy is highly sensitive to helical structures. A helical structure has 3 times the absorption coefficient in comparison to β-sheets (Figure 2.5). The results indicate an increase of helicity on ligand binding. The difference in the helicity between the cAMP-free state and the bound state is contributed by eight amino-acid residues (~ 5.7 %). A similar difference is observed by comparing the deconvoluted data of the liganded state and the unliganded state (Table 1). The pronounced difference of the CD spectra of the liganded and the unliganded state, which is contributed by few residues, offer an interesting perspective to study the dynamic changes in SSE by pre-steady state experimentation. Recent studies show that using continuous-flow mixing in combination with CD spectroscopy it is possible to study dynamic changes associated with the SSE of proteins (Hoffmann *et al* 2007).

Another interesting facet with regards to structural changes observed in the CNBD protein is the change in Trp fluorescence on cAMP binding. A single Trp located in the C-linker region contributes to the gating mechanism of the channel. On binding of

cAMP, the average lifetime of Trp shortens due to fluorescence quenching by a nearby Phe (^{223}FVRNW^{227}). The crystal structure reveals that the Trp moves closer to a nearby Phe (the only amino acid capable of quenching Trp fluorescence; for a list of amino acids which are shown to quench Trp fluorescence please refer to Chen *et al* 1996 and Lackowicz, 2nd Edn, pp 446-485) on the C-linker region. In the ligand-bound state, the distance between the two residues is 3.5 Å and in the ligand-free state it is separated by 8 Å.

Furthermore, the decrease of the average lifetime of Trp fluorescence is dose-dependent phenomenon. It fits well with the binding isotherm and K_D of 80 nM was obtained. Although these results were fit with a binding isotherm, changes in Trp fluorescence is an indirect measure of binding because the residue is located in the C-linker region and not in the binding domain. Quenching due to cAMP can be ruled out because the shortest distance between cAMP and Trp is 23 Å. FRET can also be ruled out, because there is no overlap between the spectrum of cAMP (maxima at 258 nm) and the red-shifted emission spectra (maxima 340 nm) of Trp emission of CNBD. Taken together the results obtained from ligand binding, Trp fluorescence, and the results from activation kinetics (Nimigean *et al* 2004) all indicate that binding may be directly coupled to gating without involving any allosteric factor.

4.4 Binding and Gating

Several models were proposed to comprehend the relation between ligand binding and gating in CNG channels. One of the influential models dealt with a closed ligand-bound channel which requires an allosteric transition to open. This model was inspired from the Del-Castillo and Katz scheme.

$$C \xleftrightarrow{2K} C \xleftrightarrow{K/2} C \xleftrightarrow{L} O$$

where *K* is the binding constant, and *L* is the allosteric transition factor.

It was assumed that the binding affinity for different CNG channels is similar, but they differ from each other with respect to promoting the channel open. This idea was later challenged by Li and Lester (1999). They showed with single-channel measurements on CNGA2 that binding affinities of cNMPs differed by a factor of 1000, while the allosteric

factor *L* differed by a factor of 2 only. Furthermore, they also showed that the second binding event was crucial in promoting the channel open.

A recent study by Biskup *et al* (2007) provides a detailed view of ligand binding and channel activation. Using a combination of electrophysiology and fluorimetry they show that the binding sites in CNGA2 are not equivalent and both positive and negative cooperativity exist between the subunits of the channel. These authors like Li and Lester conclude that the second binding event is crucial in promoting the channel open, and the subsequent binding events stabilize the open state by driving the channel away from the second binding event.

Binding the ligand closely follows its activation, raising the possibility that the binding of a single ligand may result in mlCNG activation. I cautiously interpret the results on ligand binding to mlCNG activation reported by Nimigean *et al* (2004). This is because the activation kinetics of the channel shows a slow response. The response is slower than that observed for the K^+-ion transporter valinomycin.

This may be due to:

1. Low open probability of the channel
2. The mlCNG protein may require an additional activation factor. e.g. another bacterial channel KcsA requires low pH on the extracellular side for activation (Heginbotham *et al* 1999).

Although it remains unclear from mlCNG activation kinetics, a homologous channel mmCNG (see 3.1.0, mm stands for *Magnetospirillum magnetotacticum*, the source form which the CNG gene was cloned from) K^+-selective inward rectifier(Kuo *et al* 2007). The activation showed no cooperativity and the $K_{1/2}$ was observed in the submicromlar range. It is reasonable to assume that mlCNG, which is homologous to mmCNG, shows a similar response (see Appendix for amino acid sequence).

Bacterial CNG channels may represent a new class of CNG channels. The properties of the bacterial CNG channel lie between CNG and HCN channels. Some of the properties of the bacterial channel with respect to its eukaryotic counterparts are:

1. All three channel types (CNG, HCN and pro-CNG) carry a 6 TM domain and a C-terminal CNBD.

2. Like the HCN channels, bacterial CNG channels carry the K^+ selective pore motif. Bacterial CNG channels exclusively conduct K^+ (Nimigean *et al* 2004, Kuo *et al* 2007), while the HCN channels carry a mixed current of monovalent ions (Kaupp and Seifert, 2001).

3. The binding affinity of cNMPs to mlCNG is similar to that observed for the isolated CNBD of HCN2 (Winkhaus 2007).

4. The mlCNG protein carries an Arg residue at position 348, which is homologous to R632 in HCN 2. The crystal structure of the CNBD of both HCN2 and mlCNG show that the Arg stacks over the purine ring of cAMP and also interacts with the N6 position. CNBD from the CNG channels lack Arg at this position. The mutant R348A has K_D values similar to the $K_{1/2}$ of CNG channels.

5. Like HCN channels, the activation kinetics of mlCNG and mmCNG show no cooperativity. Unlike the HCN channels which are activated by hyper-polarization, mmCNG is an inward rectifier.

6. Rapid activation and slow deactivation kinetics of mmCNG are similar to eukaryotic CNG channels.

7. Unlike both the eukaryotic counterparts where the C-terminal domain of one subunit interacts with the neighbouring domain, no such interaction occurs in bacterial CNG channels.

4.5 Perspectives

My study focussed on answering the question, how does ligand binding in CNG channel cause channel activation?

I have answered a small fraction of the question, and have obtained leads to answering the remaining:

1. At the moment mlCNG crystals diffracts up to ~ 15 Å. Improving crystal quality and with the aid of powerful techniques such as AFM and cryoelectron microscopy, it should be possible to obtain a structure at good resolution.

2. Reconstituted channel serves as starting material in ssNMR studies. Using this technique it should be possible to obtain the structure of the channel at atomic resolution.

3. FT-IR measurements on cAMP free mlCNG protein is an ongoing project in collaboration with Prof. J. Heberle's group at the University of Bielefeld.

4. Using flash photolysis and rapid-mixing techniques, it should be possible to study rate constants in ligand binding assay.

5. Rapid-mixing experiments in combination with CD spectroscopy allows to study dynamic changes in the SSE of CNBD protein.

6. Activation kinetics has been reported from mlCNG channel reconstituted in liposomes. They show a slow activation response and may not represent its physiological activity. Electrophysiological measurements like that performed on mmCNG would reveal more on the activation kinetics of the channel and will also hold the key in understanding ligand binding to channel activation.

5 References

Aggarwal,S.K., and MacKinnon,R. (1996). Contribution of the S4 segment to gating charge in the *Shaker* K^+ channel. Neuron *16*, 1169-1177.

Altenhofen,W., Ludwig,J., Eismann,E., Kraus,W., Bönigk,W., and Kaupp,U.B. (1991). Control of ligand specificity in cyclic nucleotide-gated channels from rod photoreceptors and olfactory epithelium. Proc. Natl. Acad. Sci. USA *88*, 9868-9872.

Berman,H.M., Ten Eyck,L.F., Goodsell,D.S., Haste,N.M., Kornev,A., and Taylor,S.S. (2005). The cAMP binding domain: an ancient signaling module. Proc. Natl. Acad. Sci. U. S. A *102*, 45-50.

Birnboim,H.C., and Doly,J. (1979). A rapid alkaline extraction procedure for screening recombinant plasmid DNA. Nucleic Acids Res. *7*, 1513-1523.

Biskup,C., Kusch,J., Schulz,E., Nache,V., Schwede,F., Lehmann,F., Hagen,V., and Benndorf,K. (2007). Relating ligand binding to activation gating in CNGA2 channels. Nature *446*, 440-443.

Blundell,T.L., and Johnson, L.N. (1976) Protein crystallography, pp- 58-82, New York : Academic Press.

Bradford,M.M. (1976). A rapid and sensitive method for the quantitation of microgram quantities of protein utilizing the principle of protein-dye binding. Anal. Biochem. *72*, 248-254.

Bradley,J., Bönigk,W., Yau,K.-W., and Frings,S. (2004). Calmodulin permanently associates with rat olfactory CNG channels under native conditions. Nature Neurosci. *7*, 705-710.

Chen,S., Wang,J., and Siegelbaum,S.A. (2001). Properties of hyperpolarization-activated pacemaker current defined by coassembly of HCN1 and HCN2 subunits and basal modulation by cyclic nucleotide. J. Gen. Physiol. *117*, 491-503.

Chen,Y., and Barkley,M.D. (1998). Toward understanding tryptophan fluorescence in proteins. Biochemistry *37*, 9976-9982.

Chiu,P.-L., Pagel,M.D., Evans,J., Chou,H.-T., Zeng,X., Gipson,B., Stahlberg,H., and Nimigean,C.M. (2007). The structure of the prokaryotic cyclic nucleotide-modulated potassium channel MloK1 at 16 Å resolution. Structure *15*, 1053-1064.

Clayton,G.M., Silverman,W.R., Heginbotham,L., and Morais-Cabral,J.H. (2004). Structural basis of ligand activation in a cyclic nucleotide regulated potassium channel. Cell *119*, 615-627.

Craven,K.B., and Zagotta,W.N. (2004). Salt bridges and gating in the COOH-terminal region of HCN2 and CNGA1 channels. J. Gen. Physiol. *124*, 663-677.

Craven,K.B., and Zagotta,W.N. (2006). CNG and HCN channels: Two peas, one pod. Annu. Rev. Physiol. *68*, 375-401.

Del-Castillo,J., and Katz,B. (1957). Interaction at end-plate receptors between different choline derivatives. Proc. R. Soc. Lond B Biol. Sci. *146*, 369-381.

DiFrancesco,D., and Tortora,P. (1991). Direct activation of cardiac pacemaker channels by intracellular cyclic AMP. Nature *351*, 145-147.

Doyle,D.A., Morais Cabral,J., Pfuetzner,R.A., Kuo,A., Gulbis,J.M., Cohen,S.L., Chait,B.T., and MacKinnon,R. (1998). The structure of the potassium channel: Molecular basis of K^+ conduction and selectivity. Science *280*, 69-77.

Gauss,R., Seifert,R., and Kaupp,U.B. (1998). Molecular identification of a hyperpolarization-activated channel in sea urchin sperm. Nature *393*, 583-587.

Gordon,S.E., and Zagotta,W.N. (1995b). Localization of regions affecting an allosteric transition in cyclic nucleotide-activated channels. Neuron *14*, 857-864.

Gordon,S.E., and Zagotta,W.N. (1995a). Subunit interactions in coordination of Ni^{2+} in cyclic nucleotide-gated channels. Proc. Natl. Acad. Sci. USA *92*, 10222-10226.

Greenfield,N., Davidson,B., and Fasman,G.D. (1967). The use of computed optical rotatory dispersion curves for the evaluation of protein conformation. Biochemistry *6*, 1630-1637.

Greenfield,N., and Fasman,G.D. (1969). Computed circular dichroism spectra for the evaluation of protein conformation. Biochemistry *8*, 4108-4116.

Grueter,B. (2006). Bindungsstudien an einem bakteriellen zyklisch Nukleotid-gesteuerten Ionenkanal. Universitaet zu Koeln.

Heginbotham,L., and MacKinnon,R. (1992). The aromatic binding site for tetraethylammonium ion on potassium channels. Neuron *8*, 483-491.

Kaneko,H., Putzier,I., Frings,S., Kaupp,U.B., and Gensch,T. (2004). Chloride accumulation in mammalian olfactory sensory neurons. J. Neurosci. *24*, 7931-7938.

Kaupp,U.B., Niidome,T., Tanabe,T., Terada,S., Bönigk,W., Stühmer,W., Cook,N.J., Kangawa,K., Matsuo,H., Hirose,T., Miyata,T., and Numa,S. (1989). Primary structure and functional expression from complementary DNA of the rod photoreceptor cyclic GMP-gated channel. Nature *342*, 762-766.

Kaupp,U.B., and Seifert,R. (2002). Cyclic nucleotide-gated ion channels. Physiol. Rev. *82*, 769-824.

Kaupp,U.B., and Seifert,R. (2001). Molecular diversity of pacemaker ion channels. Annu. Rev. Physiol. *63*, 235-257.

Kraemer,A., Rehmann,H.R., Cool,R.H., Theiss,C., de Rooji,J., Bos,J.L., and Wittinghofer,A. (2001). Dynamic interaction of cAMP with the Rap guanine-nucleotide-exchange factor Epac1. J. Mol. Biol. *306*, 1167-1177.

Kuo,M.M., Saimi,Y., Kung,C., and Choe,S. (2007). Patch clamp and phenotypic analyses of a prokaryotic cyclic nucleotide-gated K+ channel using Escherichia coli as a host. J. Biol. Chem. *282*, 24294-24301.

Lackowicz JR (1999) Principles Fluorescence Spectroscopy 2nd edn,pp 446–485. New York, NY, USA: Kluwer Academic/Plenum.

Lackowicz JR (1999) Principles Fluorescence Spectroscopy 2nd edn,pp 487–514. New York, NY, USA: Kluwer Academic/Plenum.

Laemmli,U.K. (1970). Cleavage of structural proteins during the assembly of the head of bacteriophage T4. Nature *227*, 680-685.

Li,J., and Lester,H.A. (1999). Single-channel kinetics of the rat olfactory cyclic nucleotide-gated channel expressed in *Xenopus* oocytes. Mol. Pharmacol. *55*, 883-893.

Li,J., Zagotta,W.N., and Lester,H.A. (1997). Cyclic nucleotide-gated channels: structural basis of ligand efficacy and allosteric modulation. Q. Rev. Biophys. *30*, 177-193.

Liu,D.T., Tibbs,G.R., Paoletti,P., and Siegelbaum,S.A. (1998). Constraining ligand-binding site stoichiometry suggests that a cyclic nucleotide-gated channel is composed of two functional dimers. Neuron *21*, 235-248.

Long,S.B., Campbell,E.B., and MacKinnon,R. (2005b). Voltage sensor of Kv1.2: structural basis of electromechanical coupling. Science *309*, 903-908.

Long,S.B., Campbell,E.B., and MacKinnon,R. (2005a). Crystal structure of a mammalian voltage-dependent Shaker family K+ channel. Science *309*, 897-903.

McKay,D.B., and Steitz,T.A. (1981). Structure of catabolite gene activator protein at 2.9 Å resolution suggests binding to left-handed B-DNA. Nature *290*, 744-749.

McPherson,A., Malkin,A.J., and Kuznetsov,Y.G. (1995). The science of macromolecular crystallization. Structure. *3*, 759-768.

Nimigean,C.M., Shane,T., and Miller,C. (2004). A cyclic nucleotide modulated prokaryotic K^+ channel. J. Gen. Physiol. *124*, 203-210.

Novak, K.D. (2006). Charakterisierung eines zyklisch Nukleotid-gesteuerten Ionenkanals aus *Mesorhizobium loti* .Universitaet zu Koeln.

Peuker,S. (2007)**.** Untersuchungen zur Bindungskinetik zyklisch Nukleotid-gesteuerter Ionenkanaele. Universitaet zu Koeln.

Rehmann,H., Prakash,B., Wolf,E., Rueppel,A., de Rooij,J., Bos,J.L., and Wittinghofer,A. (2003). Structure and regulation of the cAMP-binding domains of Epac2. Nature Struct. Biol. *10*, 26-32.

Riggs,P. (1994). Expression and purification of maltose-binding protein fusions. In Current Protocols in Molecular Biology, F.M. Ausubel, R. Brent, R.E. Kingston, D.D. Moore, I.G. Seidman, J.A. Smith, and K. Struhl, eds. Greene Publishing Ass. & Wiley Int.), p. 16.6.1-16.6.14.

Robinson,R.B., and Siegelbaum,S.A. (2003). Hyperpolarization-activated cation currents: from molecules to physiological function. Annu. Rev. Physiol. *65*, 453-480.

Santos,N.C., and Castanho,M.A. (1996). Teaching light scattering spectroscopy: the dimension and shape of tobacco mosaic virus. Biophys. J. *71*, 1641-1650.

Schaffer,S., Weil,B., Nguyen,V.D., Dongmann,G., Gunther,K., Nickolaus,M., Hermann,T., and Bott,M. (2001). A high-resolution reference map for cytoplasmic and membrane-associated proteins of Corynebacterium glutamicum. Electrophoresis *22*, 4404-4422.

Seifert,R., Scholten,A., Gauss,R., Mincheva,A., Lichter,P., and Kaupp,U.B. (1999). Molecular characterization of a slowly gating human hyperpolarization-activated channel predominantly expressed in thalamus, heart, and testis. Proc. Natl. Acad. Sci. USA *96*, 9391-9396.

Seoh,S.A., Sigg,D., Papazian,D.M., and Bezanilla,F. (1996). Voltage-sensing residues in the S2 and S4 segments of the Shaker K+ channel. Neuron *16*, 1159-1167.

Shabb,J.B., Buzzeo,B.D., Ng,L., and Corbin,J.D. (1991). Mutating protein kinase cAMP-binding sites into cGMP-binding sites. J. Biol. Chem. *266*, 24320-24326.

Shi,N., Ye,S., Alam,A., Chen,L., and Jiang,Y. (2006). Atomic structure of a Na^+- and K^+-conducting channel. Nature *440*, 570-574.

Su,Y., Dostmann,W.R.G., Herberg,F.W., Durick,K., Xuong,N.-H., Ten Eyck,L., Taylor,S.S., and Varughese,K.I. (1995). Regulatory subunit of protein kinase A: Structure of deletion mutant with cAMP binding domains. Science *269*, 807-813.

Tränkner,D., Jägle,H., Kohl,S., Apfelstedt-Sylla,E., Sharpe,L.T., Kaupp,U.B., Zrenner,E., Seifert,R., and Wissinger,B. (2004). Molecular basis of an inherited form of incomplete achromatopsia. J. Neurosci. *24*, 138-147.

Varnum,M.D., Black,K.D., and Zagotta,W.N. (1995). Molecular mechanism for ligand discrimination of cyclic nucleotide-gated channels. Neuron *15*, 619-625.

Weitz,D., Ficek,N., Kremmer,E., Bauer,P.J., and Kaupp,U.B. (2002). Subunit stoichiometry of the CNG channel of rod photoreceptors. Neuron *36*, 881-889.

Weber, K., and Osborn, M. (1969). The reliability of molecular weight determinations by dodecyl sulfatepolyacrylamide gel electrophoresis. *J Biol Chem* **244**, 4406-4412.

Weitz,D., Zoche,M., Müller,F., Beyermann,M., Körschen,H.G., Kaupp,U.B., and Koch,K.-W. (1998). Calmodulin controls the rod photoreceptor CNG channel through an unconventional binding site in the N-terminus of the β-subunit. EMBO J. *17*, 2273-2284.

Wen,J., Arakawa,T., and Philo,J.S. (1996). Size-exclusion chromatography with on-line light-scattering, absorbance, and refractive index detectors for studying proteins and their interactions. Anal. Biochem. *240*, 155-166.

Whitaker,G.M., Angoli,D., Nazzari,H., Shigemoto,R., and Accili,E.A. (2007). HCN2 and HCN4 isoforms self-assemble and co-assemble with equal preference to form functional pacemaker channels. J. Biol. Chem. *282*, 22900-22909.

Whitmore,L., and Wallace,B.A. (2004). DICHROWEB, an online server for protein secondary structure analyses from circular dichroism spectroscopic data. Nucleic Acids Res. *32*, 668-673.

Winkhaus,F. (2007) Quantitative Bestimmung der Ligandenbindung von HCN2-Schrittmacherkanälen.Universitaet zu Koeln.

Wuthrich,K. (1998). The second decade--into the third millenium. Nat. Struct. Biol. *5 Suppl*, 492-495.

Yellen,G. (1998). The moving parts of voltage-gated ion channels. Q. Rev. Biophys. *31*, 239-295.

Zheng,J., and Zagotta,W.N. (2004). Stoichiometry and assembly of olfactory cyclic nucleotide-gated channels. Neuron *42*, 411-421.

Zhong,H., Molday,L.L., Molday,R.S., and Yau,K.-W. (2002). The heteromeric cyclic nucleotide gated channel adopts a 3A:1B stoichiometry. Nature *420*, 193-198.

Zhou,L., Olivier,N.B., Yao,H., Young,E.C., and Siegelbaum,S.A. (2004). A conserved tripeptide in CNG and HCN channels regulates ligand gating by controlling C-terminal oligomerization. Neuron *44*, 823-834.

6 Appendix

6.1 Sequence alignments of the pro-CNG channels

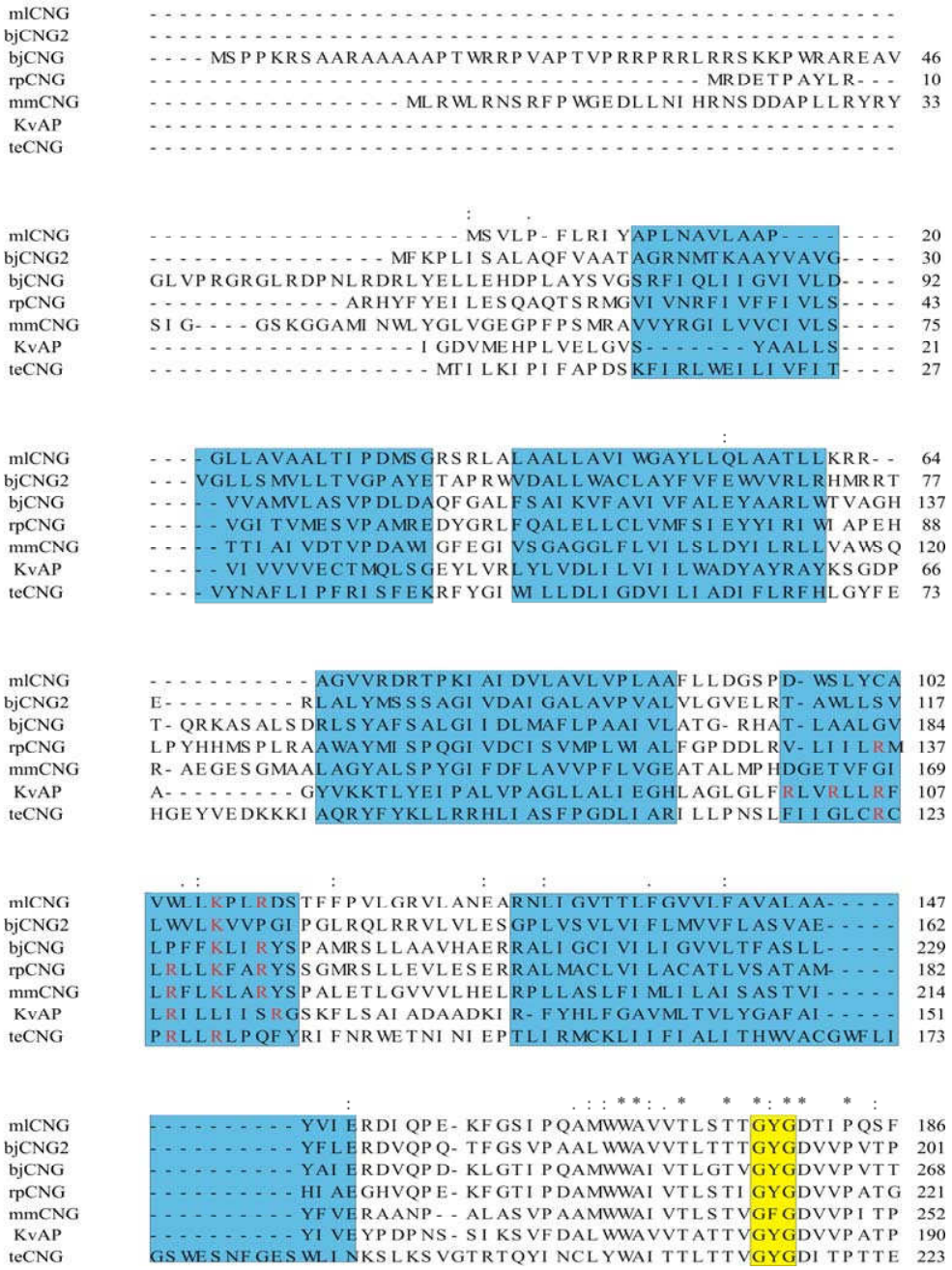

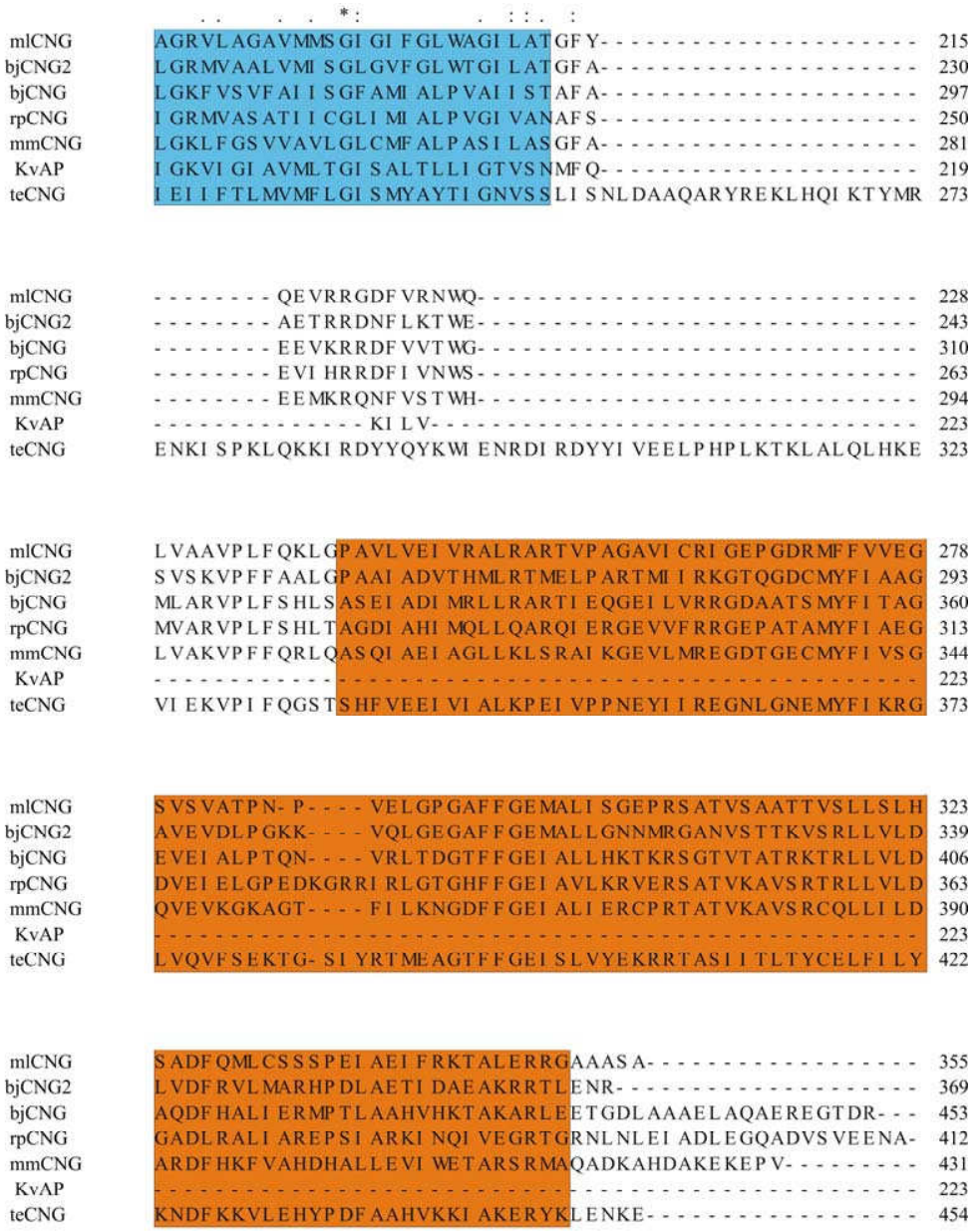

Figure 6.1: Sequence alignment of the prokaryotic CNG channels and a 6 TM K+-selective channel KvAP. The CNG channels have been named according to the source from which the channel was cloned from. Specific name of the bacterium is mentioned in parentheses. mlCNG (*Mesorhizobium loti*), bjCNG (*Bradyrhizobium japonicum*), rpCNG (*Rhodopseudomonas palustris*), mmCNG (*Magnetospirillum magnetotacticum*), and teCNG (*Trichodesmium erythraeum*). The transmembrane segments are shown in blue, the Arg marked in red corresponds to positive charges in S4 domain, the selectivity filter is marked in yellow and the CNBD is marked in orange.

6.2 Sequence alignment of CNBDs from several cNMP binding proteins

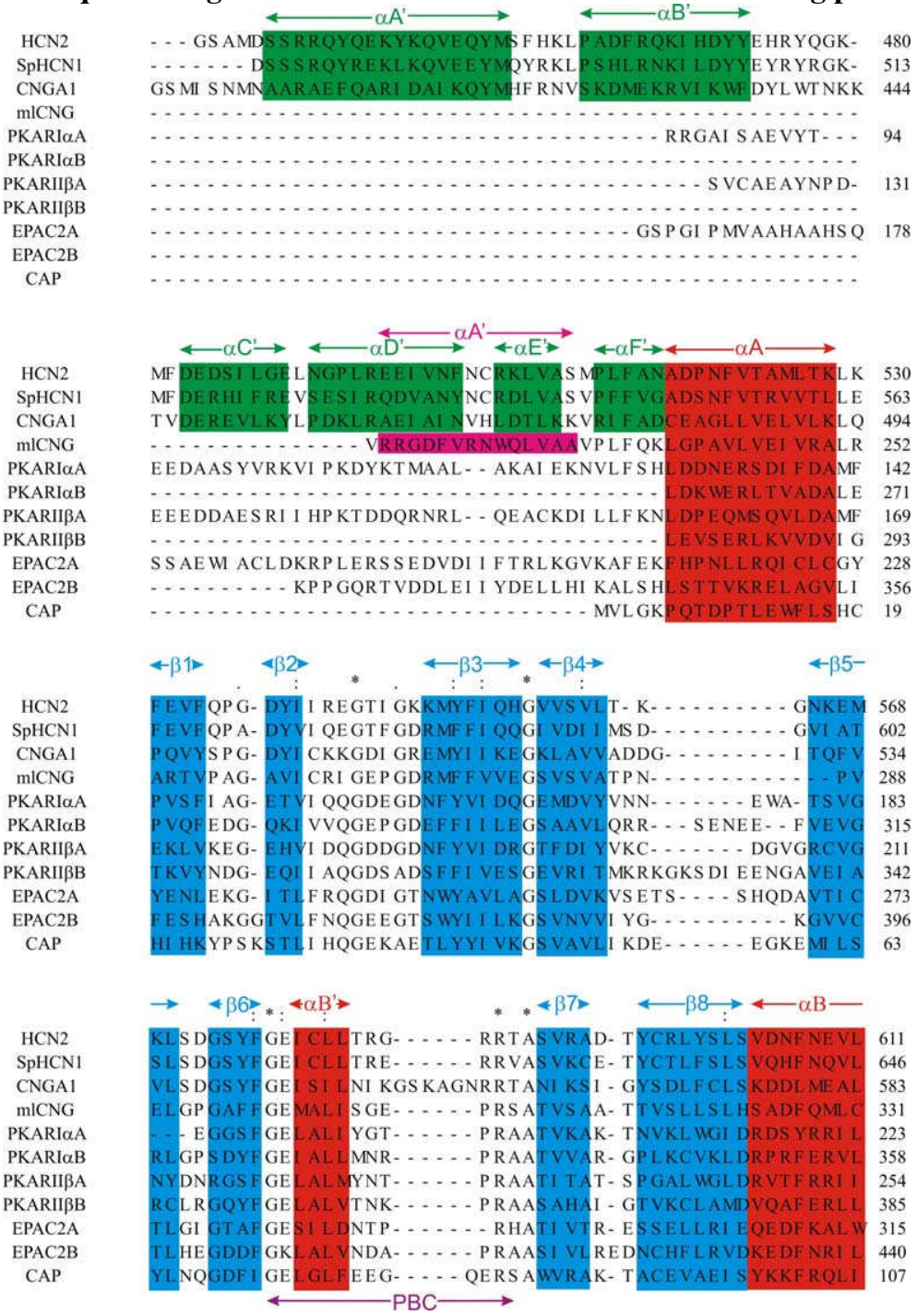

Figure 6.2 Sequence alignment of CNBDs from several cNMP binding proteins: HCN2 (PDB entry 1Q43), SpHCN1 (PDB entry 1Q43), CNGA1, mlCNG (PDB entry 1VP6), PKARIα (PDB entry 1NE6), PKARIβ (PDB entry 1CX4), EPAC (PDB entry 107F), and CAP (PDB entry 2CGP). PKA and EPAC carry two CNBDs; in the sequence alignments the second CNBD is assigned as B. The residues in blue box correspond to β-sheets of the CNBD, the residues in red box correspond to helices of CNBD, the residues in green box correspond to helices of the C-linker region of eukaryotic channels, the residue in the pink box correspond to C-linker region of mlCNG protein.

6.3 Theoretical tryptic digestion of the mlCNG protein

Table 5: Detailed description of theoretical tryptic digestion of the mlCNG protein, and the mass of the monoisotopic residues.

	Residues	**Monosiotopic mass (+1)**	**Sequence**
1	1 - 8	962.550	<MSVLPFLR> I
2	9 - 36	2778.559	R <IYAPLNAVLAAPGLLAVAALTIPDMSGR> S
3	37 - 38	262.152	R <SR> L
4	39 - 62	2509.553	R <LALAALLAVIWGAYLLQLAATLLK> R
5	63 - 63	175.120	K <R> R
6	64 - 64	175.120	R <R> A
7	65 - 69	501.315	R <AGVVR> D
8	70 - 71	290.146	R <DR> T
9	72 - 74	345.214	R <TPK> I
10	75 - 110	4008.244	K <IAIDVLAVLVPLAAFLLDGSPDWSLYCAVWLLKPLR> D
11	111 - 120	1138.590	R <DSTFFPVLGR> V
12	121 - 127	772.432	R <VLANEAR> N
13	128 - 152	2649.538	R <NLIGVTTLFGVVLFAVALAAYVIER> D
14	153 - 158	729.378	R <DIQPEK> F
15	159 - 189	3344.641	K <FGSIPQAMWWAVVTLSTTGYGDTIPQSFAGR> V
16	190 - 219	3127.648	R <VLAGAVMMSGIGIFGLWAGILATGFYQEVR> R
17	220 - 220	175.120	R <R> G
18	221 - 225	593.305	R <GDFVR> N
19	226 - 238	1513.853	R <NWQLVAAVPLFQK> L
20	239 - 249	1165.731	K <LGPAVLVEIVR> A
21	250 - 252	359.241	R <ALR> A
22	253 - 254	246.157	R <AR> T
23	255 - 264	1043.567	R <TVPAGAVICR> I
24	265 - 271	743.369	R <IGEPGDR> M
25	272 - 307	3738.855	R <MFFVVEGSVSVATPNPVELGPGAFFGEMALISGEPR> S
26	308 - 342	3726.836	R <SATVSAATTVSLLSLHSADFQMLCSSSPEIAEIFR> K
27	343 - 343	147.113	R <K> T
28	344 - 348	589.331	K <TALER> R
29	349 - 349	175.120	R <R> G
30	350 - 355	447.220	R <R> G

7 Publications and Achievements

Publications during my Ph.D. study

1. Cukkemane A. A., Gensch T., Seifert, R.,Kaupp U.B. (2007). Functional characterization of a prokaryotic cyclicnucleotide-gated ion channel. *European Biophysical Journal* (36):S148

2. Cukkemane A. A., Grüter B., Novak K.,Gensch T., Bönigk W., Gerharz T., Kaupp U.B., Seifert, R. (2007). Subunits actindependently in a cyclic nucleotide-activated K^+ channel. *EMBO Reports* (8) 749-755

Awards

Poster prize in the category of Ion channels at the European biophysics Congress (EBSA) 2007, London

Acknowledgements

This report represents an ambitious undertaking and I would like to sincerely thank Prof U.B.Kaupp for allowing me to work under his able guidance. I'm sincerely grateful to Prof G. Bueldt, Ms. A.Eckert, Mr. R.Esser, Dr. T.Gensh, Dr. R.Seifert, Dr. H.G.Koerschen, Dr.W.Boegnik, Dr.A.Baumann, Dr.F.Mueller, Dr. I. Weyand, Dr. P.J.Bauer and Dr. J.Granzin for their motivation & unstinted support. All their help & cooperation in the hours of need was unforgettable.

Words are insufficient to express my gratitude to Dr. T.Gensch (''KOPF HOCH''), and Dr. R.Seifert. Without their help my study would have been impossible.

I thank Prof. A. Engel and his group in Basel in helping me with the crystallography work. I am grateful to Dr. H.W.Remigy and Dr. M. Chami for the guidance and support with my work in Basel

I would like to thank Prof.M.Bott for permitting me to perform mass spectrometry experiments in his lab. Double thanks to Jens (now Dr. Schweitzer) for all the help and the great time we had while performing the experiments together.

I would like to thank Prof.K.W.Koch and Dr.J.Y.Hwang in helping me out by providing useful tips in completing my thesis work.

Many thanks to Dr J. Buitenhuis, Dr.Z.Zhang and Fd bacteriophage for bringing us together on one working platform.

I am grateful to have a bro-in-arm in Sebastian Peuker, who is now the master of ligand binding experiment.

I am grateful to my friends from INB-1 and INB-2 them being, Nachiket Kashikar, Baerbel Grueter, Kerstin Novak, Fredrieke Winkhaus, Luru Dai, Luis Alvarez, Timo Struenker, Dagmar Harzheim, Kathrina Debowski, Sandra Hackelberg, Mathias Buerk, Julia Schneider, Arnaud Legendre, Anja Mataruga, Gabriel Knop, Frank Thiel, Astrid Loogen, Nadine Jordan, Sabine Balfanz, Norman Goodwin, Arne Brombas, Arne Franzen, Christoph Artzweiler, Joachim Schmitz, Doris Hoeppner-Heitmann, Ingo Gregor, Joerg Enderlein, Iris von der Hocht, Thomas Dertinger, Jana Kriegsmann, Illona Ritter, Christian Baeken, Renu Batra-Safferling, Marcus Safferling, Oliver Weiergraeber, Anne Zuber, Ruslan Efremov, Dagmar Kaschuba, Hans Fried, Claus Fuetterer, Annett Duemmler, Sebastian Wachten, Anja Bruehl, Miriam Kraehling, Daniel Portz, Hans-Dieter Grammig, Andreas Helten and Qui Van for their constant help, affection & cooperation.

I am highly obliged to Dr.N.Rao, Dr.J.Pai and Mr. G.Lincks, to have given me an opportunity to work at the Research centre.

Umpteen thanks to all my teachers who have had a profound impact in my life and have moulded and guided me into the world of science. The teachers include my parents, Dr. M.G.Watve, Dr.S.K.Paknikar, Dr.B.D.Bhole, Mr.V.G.Kshirsagar, Dr.R.L.Deopurkar, Dr.A.Lohia, and Dr.S.A.Bapat. And as your student I would like to seek your blessings all through out my life.

Above all, I am lucky to have my parents and my brother Abhilekh who have been by my side throughout my PhD study. Words in one paragraph will not be sufficient to express the support I have received. I keep seeking your blessings to drive me ahead. I am also very lucky in having a lovely fiancée Nivedita, whom I shall be marrying soon and her family by my side.

And last but not the least I thank and apologies all my other teachers and friends whose name I missed out.
SORRY.

Jül-4270
April 2008
ISSN 0944-2952